Experimental Studies on Flow Structures Behind Bluff Bodies and Suppression of Vortex Street

Amir Teimourian

Submitted to the
Institute of Graduate Studies and Research
in partial fulfillment of the requirements for the degree of

Doctor of Philosophy
in
Mechanical Engineering

Eastern Mediterranean University
December 2016
Gazimağusa, North Cyprus

Approval of the Institute of Graduate Studies and Research

Prof. Dr. Mustafa Tümer
Director

I certify that this thesis satisfies the requirements as a thesis for the degree of Doctor of Philosophy in Mechanical Engineering.

Assoc. Prof. Dr. Hasan Hacışevki
Chair, Department of Mechanical Engineering

We certify that we have read this thesis and that in our opinion it is fully adequate in scope and quality as a thesis for the degree of Doctor of Philosophy in Mechanical Engineering.

Assoc. Prof. Dr. Hasan Hacışevki
Supervisor

Examining Committee

1. Prof. Dr. Kahraman Albayrak

2. Prof. Dr. Şenol Başkaya

3. Prof. Dr. Fuat Egelioğlu

4. Assoc. Prof. Dr. Hasan Hacışevki

5. Asst. Prof. Dr. Murat Özdenefe

ABSTRACT

One of the most significant features of flow around bluff bodies is the formation of vortices in the downstream wake. Such unsteady wake could incur unsteady loading where the vortex-induced vibration can have destructive effects on the structure of sky scrapers, cooling towers, chimneys and bridges which civilization relies on.

In this study vortex shedding in the wake region of single and dual bluff bodies have been investigated, and possible passive flow control method have been employed to suppress formation of vortex street in the wake region downstream the bluff bodies.

In this study the effects of entrainment of fluid through perforated surface on suppression of vortex street behind Perforated Square Cylinder have been studied experimentally. Wake region have been investigated in terms of coherent flow structure, time averaged properties and effectiveness of different perforations. The quantitative measurements revealed that the perforated surfaces are only effective within width interval of y/D= ±1.0. It was observed that in the near wake region up to approximately 1.5D downstream the wake, the shedding phenomenon has been suppressed significantly. It was also demonstrated that velocity profiles and flow structure affected by different perforated surfaces, and as a result coherent structures have been diminished considerably.

In addition, interacting wakes of two inclined flat plates in tandem arrangement have been studied experimentally. The effects of gap ratio (g/D) between the plates together with angle of attack (α) on the flow structure in the wake region, incoherent and coherent time averaged properties profiles have been investigated. Different set of experiments have been conducted for gap ratios 0.5 and 1.5 between the plates, replicating single and dual body vortex shedding mode. In addition, various angle of

attack (45-75 degree) have been studied to probe the effects of inclination on the wake region in terms of shedding frequency and Strouhal number variation. The results revealed that Strouhal number decreases as angle of attack increases. Moreover, increasing gap ratio affects the flow structure and as gap ratio increases, incoherent Turbulent Kinetic Energy production in the downstream wake have been decreased.

Keywords: Vortex Shedding, Suppression, incoherent and coherent flow structure, Perforated Square Cylinder, Inclined flat plate, Interacting wake, Tandem arrangement

ÖZ

Cisimlerin etrafındaki akışların en belirgin özelliklerinden biri da cismin gerisinde oluşan girdaplardır. Böyle düzensiz dalgalı titreşimlere neden olarak yüksek yapılarda, bacalarda, soğutma kulelerinde ve köprülerde düzensiz yüklemelere ve yıkıcı etkilere sebep olabilmektedir. Bu çalışmada tek ve çift cisimlerin arkalarında oluşan dalgalardaki girdaplar araştırılmış ve pasif control metodları uygulanarak girdap oluşumunun engellenmesi araştırılmıştır.

Bu çalışmada ayrıca delikli kare silindir üzerine akışın dolması ve arkasındaki girdap oluşumu incelenmiştir. Dalga alanı koherent akış yapıları ve zaman ortalamalı akış özellikleri incelenmiştir. Ölçümler açığa çıkarmıştır ki delikli yüzeylerde genişlik oranı Y/D=1.0 olan silindirler etkili olmaktadırlar. Ayrıca yakın dalga bölgelerinde 1.5D mesafesine kadar olan yerlerde girdap oluşumu gözle görülür şekilde bastırılmaktadır. Hız profilleri ve akış yapılarının değişik delikli yüzeylerde etkilendikleri ve sonuç olarak koherent yapıların yok olduğu tesbit edimliştir. Ek olarak eğimli iki düz plakanın etkileşimi deneysel olarak incelenmiştir. İki plakanın arasındaki boşluk oranının (g/D) atak açısı (α) ile birlikte dalga bölgelerindeki akış yapıları, koherent ve incoherent zaman ortalamalı özellikleri incelenmiştir. Değişik deney setleri için boşluk oranları 0.5 ve 1.5 arasında olan plakalar yapılmış, tek ve çift gövdeli girdap modları gözlemlenmiştir. Ayrıca atak açısı 45-75 dereceler arasında çalışılmış ve meyilin dalga bölgesinde girdap frekansı ve Strouhal numarasının değişimi araştırılmıştır.

Neticeler göstermiştir ki atak açısı arttıkça Strouhal sayısı düşmektedir. Ayrıca boşluk oranının artması ile akış yapılarının etkilendiği ve turbulent kinetic enerjisi üretiminin akış arkasında ilerledikçe azaldığı gözlemlenmiştir.

Anahtar kelimeler: Girdap, Bastırma, İnkoherent ve koherent akış yapısı, Delikli kare silindir, Meyilli düz plaka, ardışık düzenleme.

To.....

Mamani & Boosha

ACKNOWLEDGMENT

I would like to thank my supervisor Assoc. Prof. Dr. Hasan Hacışevki, not only for his scientific oversight of my research but also for the friendly manner in which he would resolve all my problems. He has inspired me to become an independent researcher and helped me to realize the power of critical reasoning.

My parents, Mamani and Boosha, receive my deepest love for their dedication and many years of unconditional support. You have been a source of inspiration throughout the years for me, and you show me the path toward success. I am indebted to you forever.

There are no proper words to convey my deepest gratitude for Tara for her understanding and love during the past years. Your support and encouragement was in the end what made this dissertation possible. I am blessed to have you in my life. I will always remember our memorable moments on top of the summits.

Hanifa, you always supported me and have my back without any question. I will never forget our amazing trips from AL10 to NW and then to popular destination of W1. I had the best of time and Mind the Gap Please.

Gaya, also receive my special thanks for her non-stop greed of games & treats!

TABLE OF CONTENTS

LIST OF TABLES

LIST OF FIGURES

NOMENCLATURE

CCA	Constant current anemometer
CTA	Constant temperature anemometer
D	Square cylinder/ Flat Plate Width [mm]
g	Gap between two plates in tandem arrangement [mm]
HWA	Hot wire anemometer
MSE	Mean square error
R_w	Wire resistance [Ohm]
R_e	Reynolds Number (uD/ν)
SN	Single normal probe
S_t	Strouhal Number (fD/U_∞)
S_t'	Modified Strouhal Number (fD'/U_∞)
u	Stream-wise direction velocity [m/s]
$\bar{u}$	Time mean velocity component [m/s]
u'	Incoherent velocity component [m/s]
$\tilde{u}$	Coherent velocity component [m/s]
v	Transverse direction velocity [m/s]
x	Stream-wise direction
y	Transverse direction

α	Angle of Attack
f	Vortex shedding frequency [Hz]
ν	Kinematic viscosity [m^2 / s]
< >	Phase averaging

Chapter 1

INTRODUCTION

1.1 Vortex shedding phenomenon

Many researchers have been attracted by the problem of flow past bluff bodies because of their vast number of applications in engineering and industry. As the fluid pass the body, the streamline pattern around the bluff body and the wake region is disturbed and such disturbances greatly influenced by the shape, orientation of the body and velocity of the fluid. The term bluff body or non-streamline body is a term to describe geometries such as flat plate, rectangular or circular cylinders. While bluff bodies such as flat plate with sharp edges exhibit fixed separation point, the separation point for the case of rounded edges bluff bodies can move to be adjusted with flow structure. Despite these dissimilarities, flow around bluff bodies feature a common flow structure development in the wake region. The wake flow is characterized by time-averaged velocity, flow structures and velocity fluctuations.

One of the most significant features of flow around these bodies is the formation of vortices in the downstream wake. Such unsteady wake could incur unsteady loading where the vortex-induced vibration can have a destructive effects on the structure of the sky scrapers, cooling towers, chimneys and bridges which civilization relies on. This phenomenon is not only the main concern during design stages of industrial systems but also during serviceability stages. Therefore, to investigate the unsteady loading phenomena different geometries and arrangements such as tandem, staggered

or several other arrangements have been studied, resembling different engineering applications in civil or aerospace industry for instance (H Hacışevki & Teimourian, 2015; H. Hacışevki & Teimourian, 2016; Irwin, 2008; Zdravkovich, 1997).

In this study suppression of Vortex Street behind bluff bodies have been studied experimentally by employing passive flow control theory. Wake region have been investigated in terms of coherent and incoherent flow structures, and time averaged properties. The effectiveness of the employed method and suppression of the vortex street in the wake region have been investigated.

1.2 Historical Review

The majority of natural flows and industrial applications are considered as turbulent flow and are very complicated. Jet streams in the upper troposphere or water current below the surface of the oceans in case of natural flows or wakes of ships, car and aircraft in case of engineering application are all turbulent flow. However, despite the observations of variety of turbulent flows, it is not easy to state a precise definition for turbulence. Instead it is possible to define turbulent flow in terms of its characteristics (Tennekes & Lumley, 1972).

The behavior of fluid flow around structures have been observed for centuries by large number of scientists. Perhaps the ancient Greek scientist Archimedes is the first scientist to publish his observation on fluid flow.

Moreover, Leonardo da Vinci is one of the pioneers on the flow visualization and observing characteristics of the turbulent flow 5 centuries ago. The classic sketch of turbulent flow past a bluff body provided one of the earliest references to the importance of vortices. Three centuries later Osborne Reynolds proposed an

averaging method to express turbulent flow properties such as velocity components in terms of summation of mean and fluctuating components known as Reynolds-averaging.

Finally, Vincenc Strouhal a Czech scientist revealed the relation between periodic flow of wire and the velocity passing over it (Frisch, 1995; Yunus & Cimbala, 2006). Therefore, for periodic vortex shedding phenomenon behind bluff bodies, the frequency at which vortices are being shed and free stream velocity are expressed in terms of a dimensionless number called Strouhal Number.

1.3 Literature review on Vortex Shedding from Bluff bodies

Vortex shedding phenomenon from bluff bodies have been investigated on geometries and arrangements having different engineering applications in the field of civil engineering, wind engineering and the aerospace engineering. The unsteady loading behavior in the wake region which formed by vortex shedding requires great consideration and as a result attracted many researchers. Such fluctuating forces are the main concern during design stages of industrial systems where the vortex-induced vibration can have a destructive effects on the structure.

Zdravkovich (M. M. Zdravkovich, 1987; Zdravkovich, 1969, 1972, 1977; M. Zdravkovich, 1987; Zdravkovich, 1988, 1996, 1997) is one of the pioneers in investigation of vortex shedding phenomena and describing the formation of Karman vortex street behind bluff bodies. Zdravkovich conducted many extensive research on so called simple bluff body geometries but with many applications in industry.

He (Zdravkovich, 1969) reported that in the laminar wake of a circular cylinder, instability of shear layers together with concentration of vorticity leads to formation

of Karman vortex street.

Although the existence of the Karman vortex street in the wake of bluff bodies had been studied vastly during those years, the appearance of such phenomenon in the wakes of two cylinders in tandem arrangement at the similar velocities had been pushed aside. Then, Zdravkovich (Zdravkovich, 1972, 1977) conducted a comprehensive study and review on the vortex shedding phenomenon from circular cylinders in tandem and staggered arrangements. He observed the existence of vortices being rolled up in the wake region behind the cylinders. His observation showed that for a gap greater than 4D between two cylinders, the vortices are always formed in the wake behind the downstream cylinder. Zdravkovich (1996) also presented an overview of the mechanism of vortex formation phenomenon for different modes at low speed and high speed.

1.3.1 Vortex Shedding from square cylinder

In the context of square cylinder, Okajima (1982), A. Saha, Muralidhar, and Biswas (2000); A. K. Saha (2013), H Hacışevki and Teimourian (2015), Sohankar, Mohagheghian, Dehghan, and Manshadi (2015) and many other researchers conducted extensive researches on vortex shedding phenomenon. They have investigated different features of vortex shedding behind square cylinders and reported wake flow structure, Strouhal number variation and other aerodynamic parameters. These studies provided valuable insight to shedding phenomenon and flow behavior behind such bluff body.

Since the fluctuating forces are derived by the wake structure, therefore any endeavor for suppression of the vortex street to reduce such destructive feature is regarded. For this purpose various passive and active flow-control methods have been employed by

engineers to protect the structures against the damaging fluid forces acting on the bluff bodies. Sakamoto, Tan, Takeuchi, and Haniu (1997), Alam, Moriya, Takai, and Sakamoto (2002), Malekzadeh and Sohankar (2012), Igarashi and Terachi (2002) and Igarashi (1997) investigated passive flow control by employing a control plate or rod upstream of a square cylinder as a mean of controlling the vortex shedding.

They all reported considerable reduction on the mean and the fluctuating forces acting on a square cylinder, and while drag force on the square cylinder is significantly reduced, the fluctuating lift is suppressed as well.

Sakamoto et al. (1997) conducted a systematic experiment to study the effect of employing a control plate on aerodynamic forces, flow structure and frequency of shedding in the wake of a square cylinder. They employed control plates with various width at locations up to 3D upstream of the square cylinder. They observed that employing a control plate resulted in suppression of Karman vortex formation and consequently a reduction in aerodynamic forces with a 95% and 80% reduction in lift and drag fluctuations.

Igarashi (1997) performed an experimental investigation on drag force variation acting on a square cylinder by using an upstream rod. It was observed that a critical gap ratio between rod and square cylinder exists where the vortex shedding phenomenon from the upstream rod disappears. It was also observed that for gap ratio less than the critical ratio, the Strouhal number decreases while for gap ratio higher than the critical ratio the Strouhal number increases. Moreover, a maximum 70% reduction in drag coefficient have been reported. Igarashi and Terachi (2002) performed similar study and investigated the drag force of a flat plate normal to flow

by using an upstream rod. However, they reported the maximum reduction of approximately 30% of the total drag coefficient compared to the drag without the control rod.

Alam et al. (2002) investigated the suppression of aerodynamic forces acting on two tandem square cylinder with employing an upstream control plate. It was observed that for a certain range of control plate location, fluid forces acting on both cylinders decreases significantly. Moreover, it was revealed that in case of locating the control plate at gap ratios between 1.50 to 1.90, vortex street from the upstream cylinder were suppressed. In addition it was observed that in case of gap ratio more than 6D, downstream cylinder has no effect on upstream cylinder.

Malekzadeh and Sohankar (2012) investigated the reduction of the fluid forces acting on a square cylinder in laminar flow regime numerically. The employed passive control by using an upstream control flat plate. They conducted experiment for Reynolds number in a range 50 to 200 for different control plate width located at different distances upstream of the square cylinder. The numerical simulation suggested that a control plate with a width of 0.5 of the square cylinder located 3 width of the square cylinder in upstream, resulted in maximum reduction of the drag with the minimum reduction of the heat transfer.

On the other hand, Çuhadaroğlu, Akansu, and Turhal (2007), Çuhadaroğlu and Turan (2009), Çuhadaroglu (2009), Turhal and Çuhadaroğlu (2010) and Sohankar, Khodadadi, and Rangraz (2015) employed active control method with injection of fluid through the surface of the square cylinder to reduce the destructive effect of vortex shedding phenomenon.

Çuhadaroğlu et al. (2007) conducted an experimental study to investigate the injection effects on pressure coefficient and drag coefficient of a perforated square cylinder at high Reynolds number between Re =10,000 and 24,000. Different configuration of injection have been employed, through front, top and rear surfaces of the cylinder, for instance. The result revealed that injection through the rear face decreases the drag force. However, Injection of fluid through the front faces demonstrate opposite results and causes an increase in drag force.

Moreover, injection through the other faces have been demonstrated negligible effects. Turhal and Çuhadaroğlu (2010) experimentally studies variation of pressure coefficient, drag coefficient and Strouhal number of a perforated square cylinder (horizontal and diagonal) with having fluid injected through various surfaces at high Reynolds number between Re =10,000 and 24,000. The result shows that in case of a diagonal square cylinder surface injection through the top-rear, rear and all surfaces reduces the drag coefficient. However, only injection through all surfaces of a horizontal square cylinder can causes a reduction in drag coefficient.

Numerical study on control of fluid flow of by injection through the surfaces of a square cylinder which have been reported by Sohankar, Khodadadi, et al. (2015), is one of the latest studies in this context. The simulations demonstrated that in case of fluid injection through the front surface, Strouhal number decreases by increasing the injection parameter, while fluid forces fluctuation increases. On the other hand, injection of fluid through the rear face causes a reduction in Strouhal number and drag coefficient.

1.3.2 Vortex Shedding from flat plate

1.3.2.1 Single Normal Flat Plate

Since the subject of the flow over flat plate has been an important matter of debate, many researches have been intended to investigate the flow over single flat plate normal to flow. Mazharoğlu and Hacışevki (1999), Kiya and Matsumura (1988) and Bearman (1971) performed experimental studies whereas Narasimhamurthy and Andersson (2009), A. K. Saha (2007) and Najjar and Vanka (1995) have numerically investigated the wake structures behind a flat plate.

Table 1.1. Selected experimental studies of flow past single flat plate

Researchers	Reynolds	Turbulence intensity	Blockage ratio	Inclination angle	Measurements
Kiya and Matsumura (1988)	2.3×10^4	0.20%	6.70%	90	St, U
Wu, MIAU, Hu, and Chou (2005)	1.8×10^3-2.7×10^4	0.70%	21%	90	St, U
Leder (1991)	2.8×10^4	0.50%	7.30%	90	St, U
Mazharoğlu and Hacışevki (1999)	3.2×10^4	0.5-0.8%	6%	90	St, U
Bearman (1971)	4.8×10^4 - 2.14×10^5	0.20%	--------	90	C_P, C_D, U
Lam and Leung (2005)	5300	0.01	3.70%	20-30	St, U
Deri et al. (2014)	200000	1%	7.40%	10	U
Lam (1996)	30000	1%	5%	30	St, U
J. M. Chen and Fang (1996)	3.5×10^3-3.2×10^4	0.50%	13%	0-90	St, U

Kiya and Matsumura (1988) and Mazharoğlu and Hacışevki (1999) observed maximum turbulent kinetic energy at center of coherent structure corresponding to the edges of the flat plate. Moreover, Mazharoğlu and Hacışevki (1999) revealed that the coherent shear stress alternates twice per cycle due to transverse coherent velocity lagging behind stream wise coherent velocity by a quarter of a cycle. It was found that shearing stress is contributed mostly to incoherent fluctuation with frequency half of the shedding frequency (Kiya & Matsumura, 1988). Some selected experimental investigations of flow past single flat plate are summarized in table 1.1

with measured data reported by the researchers.

1.3.2.2 Single Inclined Flat Plate

As discussed to this point the vortex shedding phenomenon with its periodic nature alternates from one edge to the other edge of bluff body. However, the shedding phenomenon from inclined flat plates is slightly different in nature from former mechanism. Therefore, some researchers have been fascinated by inclined bodies rather than bluff bodies normal to flow.

Norberg (1993), Hogan and Hall (2010) and Snarski (2004) investigated wake flow and vortex shedding phenomenon behind inclined rectangular and circular cylinders. It was observed that inclining the cylinder resulted a more disordered vortex shedding in the wake region (Hogan & Hall, 2010). Moreover, at small angle of inclination multiple shedding frequencies has been experienced by Norberg (1993) in the wake region of a rectangular cylinder.

Lam (1996), Lam and Leung (2005) and Lam and Wei (2010) have been devoting a great deal of time on investigating the vortex shedding behind an inclined flat plate and describing its mechanism from such geometry.

Lam (1996) studied shedding phenomenon and wake region behind an inclined plate experimentally. The plate inclined at 30 degree at high Reynolds number of 30000 and wake flow measurements have been conducted by employing laser Doppler anemometer. The phase averaged velocity results demonstrated a highly asymmetric wake behind the inclined plate. Moreover the vortex street comprises of counterclockwise vortices which dominated the wake region. These vortices possess high coherent vorticity and accounted for larger Reynolds stress production.

Lam and Leung (2005) investigated inclined flat plate at three different angle of attacks by means of particle image velocimetry measurements. They observed a train of vortices in the wake region alternating from leading to trailing edge resembling vortex street pattern and the vortices were conveted downstream at 80% of free stream velocity. However, these two train of vortices formed by different formation mechanism. As a result, trailing edge vortices have higher vorticity peak at center comparing to leading edge vortices and production of Reynolds stresses are higher in nearby regions. Figure 1.1 illustrated the schematic diagram of vortex shedding form inclined flat plate proposed by Lam and Leung (2005). From the figure kelvin-Helmholtz instability and trailing edge vortices are clearly apparent.

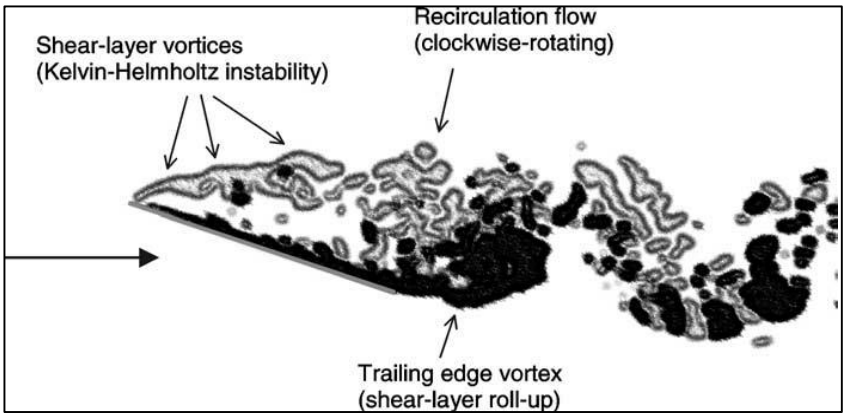

Figure 1.1. Schematic diagram of vortex formation behind an inclined flat plate (Figure taken from Lam and Leung, 2005)

Vortex shedding from an inclined plate also has been investigated numerically by Lam and Wei (2010). They employed κ-ε turbulent model for simulating flat plate at angle of attack between 20 and 45 degree. Similar to their previous study, the vortex street in the wake were evident where vortex strength of each train of vortices was different. The simulation also revealed that vortex shedding from leading edge occurs at a location near the trailing edge of plate.

J. M. Chen and Fang (1996) studied vortex shedding frequencies from an inclined flat plate with beveled edges at angle of attack between 0 and 90 degree. They have reported that the Reynolds number has no effect on Strouhal number (based on effective width normal) for identical angle of attacks. However, the effects of Reynolds number become notable for inclination angle less than 5 degree.

Yang, Pettersen, Andersson, and Narasimhamurthy (2012) performed two-dimensional and three-dimensional simulation of the wake flow behind an inclined plate. The direct numerical simulation shows that two-dimensional simulation exhibited considerably lower pressure on the aft region of the plate. As a result of such prediction, two-dimensional shows higher aerodynamic force comparing to three-dimensional simulation. On the other hand, the three-dimensional results agrees well with available experimental result for inclined flat plate.

1.3.2.3 Tandem Configuration

In addition to flow structures and vortex shedding from a single bluff body, it is also interesting to investigate these phenomena behind bluff bodies in tandem arrangement. Bluff bodies wake interference in tandem arrangement is among the configurations with having the most engineering applications.

In this context, Zdravkovich (1972), Bentley and Mudd (2003), Hangan and Vickery (1999), Zhang and Melbourne (1992), Baxendale, Grant, and Barnes (1985) and Pinarbasi, Pinar, Akilli, and Ince (2015) investigated the vortex shedding phenomenon behind dual bluff bodies namely tandem arrangement. Bentley and Mudd (2003) devoted particular attention to describe the mechanism of vortex shedding together with alternation of vortices and the effect of gap flow on detachment of shear layers for various bluff bodies in the tandem arrangement. They

performed an extended experiment to identify the mechanism of formation of vortex shedding from dual bluff body arrangements. They described the alternation of shedding from one edge to the other edge of bluff body in 6 stages. Zdravkovich (Zdravkovich; 1987) and Sumner (2010; 2004) conducted experimental studies on circular cylinders in tandem arrangement whereas Hangan and Vickery (1999), Chen and Shao (2013) and Carassale et al. (2014) investigated rectangular cylinders in tandem to study the wake formation behind these bluff bodies.

It has been revealed that bluff bodies in close proximity act similar to a "single body" and hence vortices could not roll up inside the gap between the bodies. Therefore, the initiated shear layers from upstream body bypass this dead flow region and form vortices behind the downstream body. However, as the gap ratio between the bodies increases, vortices also roll up inside the gap and for a large enough gap ratio the vortex shedding phenomenon occurs independently from each body. The terms of "single body" shedding mode and also "dual body" shedding mode have been described by Hangan and Vickery (1999), Havel, Hangan, and Martinuzzi (2001), Martinuzzi and Havel (2004), Zdravkovich (1977) and Liu and Chen (2002) in detail.

In the context of normal flat plates in tandem arrangement Nakamura (1996), Hasan Hacışevki (2001), F Auteri, Belan, Gibertini, and Grassi (2008), Franco Auteri, Belan, Cassinelli, and Gibertini (2009), Dianat (2011) and H Hacışevki and Teimourian (2015) have been investigated the vortex shedding and wake interference of the upstream plate on the downstream plate.

Franco Auteri et al. (2009) observed that at low gap ratio between the plates namely g/D=0.9, the recirculating flow in the gap region between plates and downstream of

aft plate were existed and evident. However, the weak recirculating flow in gap region rotates in opposite direction respect to the downstream wake flow and the initiated shear layer from upstream plate bypassed the gap between plate. Such flow field which displays a wide wake in the downstream region corresponds to “single body” shedding mode. On the other hand at higher gap ratio, 1.2 for instance, the flow features a narrower wake with smaller recirculating region in the downstream wake and apparently correspond to “dual body” shedding mode. Thus, the vortices have enough space to roll up inside the gap region with the matching rotation direction to the flow field in the wake region rotation. In figure 1.2 Nakamura (1996) “single body” and “dual body” modes of vortex shedding features were clearly evident at gap ratios g/D=0.5 and g/D=2.0, respectively.

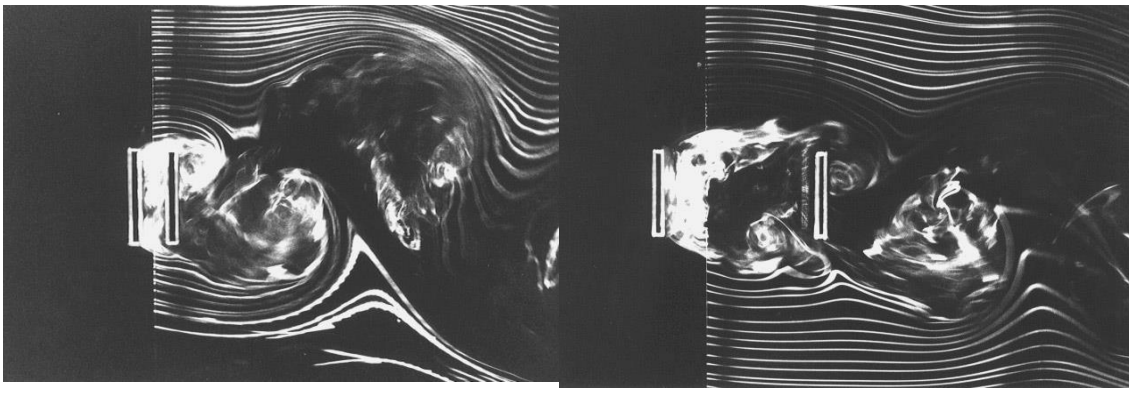

(a) (b)

Figure 1.2. Smoke visualization of flow past two normal flat plates in tandem arrangement (a) g/D=0.5; (b) g/D=2.0 (Figures taken from Nakamura (1996))

Dianat (2011) numerical simulation was also in agreement with findings of smoke visualization of F Auteri et al. (2008), Franco Auteri et al. (2009) and Nakamura (1996). The study employed k-ω turbulent model and clearly depicted that at low gap ratio no vortex rolls up inside the gap between the normal tandem plates. However, at larger gap ratio the onset of vortices rolling up in the gap were evident in the

results of this numerical study. Another distinct feature of flat plates is that the flow field exhibit fixed separation points (F Auteri et al., 2008). Recently, H Hacışevki and Teimourian (2015) have been attempted to identify the wake structures similarity between two tandem flat plates and a square cylinder as the two identical tandem plates resemble a rectangular body without definite top and bottom boundaries. Table 1.2 summarizes available literature on flow past flat plates in tandem arrangement in terms of gap ratio, techniques, measurements and Strouhal number.

The parameter gap ratio between bluff bodies in tandem arrangement act as a main factor on flow field where the flow features such as Strouhal number, considerably depend on this parameter. Igarashi (1981, 1984), F Auteri et al. (2008); Franco Auteri et al. (2009) and D Sumner, Richards, and Akosile (2008) studied this phenomenon for different bluff bodies in tandem arrangement and reported a strong relation between gap ratio and Strouhal number.

F Auteri et al. (2008) reported dependency of vortex shedding frequency or Strouhal number as a function of gap ratio between two flat plates. It was observed that nearby gap ratio g/D=0.9 (critical gap ratio), Strouhal number increases and then decreases rapidly. This phenomenon which exhibit the existence of two distinct flow regimes, has been also observed as double peak in FFT spectrum analysis for that interval corresponding to two different Strouhal number. Hence, due to the observed bistability, the flow structures alternating from one configuration corresponding to value lower than critical gap ratio to another configuration corresponding to value greater than critical gap ratio. It was observed that while Strouhal number remain close to value of single plate for gap ratio below the critical values, it was declined suddenly to a minimum value at gap ratio of 3.5. Moreover, it was revealed that the

large gap ratio flow regime is independent of Reynolds number. However, the critical gap ratio increases with Reynolds number and low gap ratio flow regime is also to some extent Reynolds number dependent.

The investigation on "dual body" mode vortex shedding mechanism revealed that the size of vortices rolled up inside the gap region significantly affect the shedding frequency. Smoke visualizations demonstrated that formation of larger vortex inside the gap for the case of larger gap ratio, resulted a low shedding frequency (F Auteri et al., 2008).

Another interesting flow features of two normal flat plates in tandem is formation of two recirculating region inside the gap between plates and also in the wake behind the aft plate. The study conducted by Franco Auteri et al. (2009) revealed that at low gap ratio between plates, the two recirculating region inside the gap rotates in opposite direction of the two recirculating region in the wake. However, for larger gap ratio these recirculating regions rotate in the same direction as depicted in Figure 1.3.

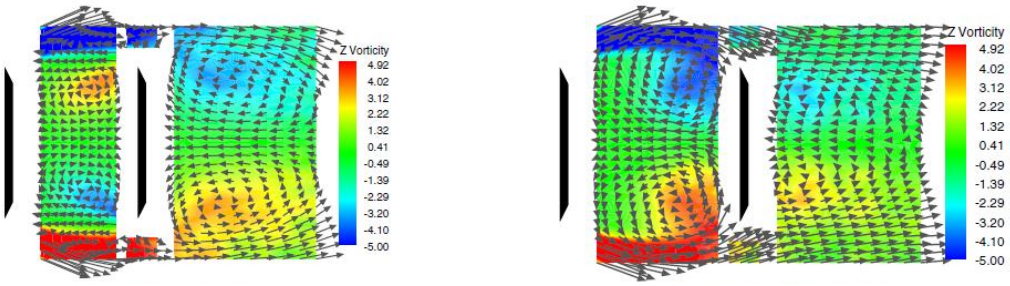

(a) Model 1, *D/c*=0.9 (b) Model 2, *D/c*=1.2

Figure 1.3. Mean velocity vector fields, Z component of the mean vorticity fields [s^{-1}], Re=46800 (Figures taken fromFranco Auteri et al. (2009))

Figure 1.4 depicted variation of Strouhal number against gap ratio in the wake region of two normal flat plates in tandem arrangement from different studies.

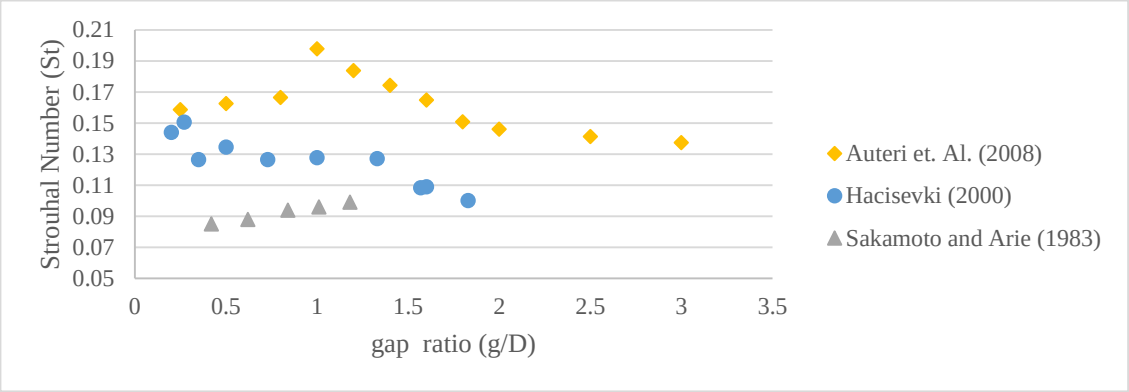

Figure 1.4. Variation of Strouhal number with gap ratio between plates

From the figure it can be concluded that increasing the gap ratio up to certain critical value will increases Strouhal number. However, further increment in gap ratio were resulted a reduction in Strouhal number. This phenomenon could be resulted due to transition from "single body" to "dual body" vortex shedding mode. The critical gap ratio value where Strouhal number changes abruptly has been reported 0. 9 and 1.2 by F Auteri et al. (2008) and Nakamura (1996), respectively.

Table 1.2. Selected studies of flow past flat plates in tandem arrangement

Researchers	Reynolds	Gap ratio	Turbulence intensity	Blockage ratio	Aspect ratio
Franco Auteri et al. (2009)	$8.7 \times 10^3 < Re < 7.5 \times 10^4$	0.9, 1.2	0.20%	10%	7.1
F Auteri et al. (2008)	8340	0.25 - 7.5	0.3	10%	7.1
Nakamura (1996)	1.5×10^4	0.3-2.0	-	1.70%	13.2
Hasan Hacışevki (2001)	3.2×10^4	0.2 - 2.0	0.5-0.8%	6%	14
Dianat (2011)	3.2×10^4	0.3 - 2.0	0.80%	6%	14
H Hacışevki and Teimourian (2015)	3.2×10^4	1.0	0.5%	6%	14

Moreover, F Auteri et al. (2008) also observed that at lower gap ratios between flat plates in tandem the measured Strouhal number was higher than single plate configuration. However, by exceeding the critical gap ratio, Strouhal number abruptly dropped to values lower than the single plate Strouhal number.

1.4 Scope of this work

To sum up, the review shows that even though various passive and active flow control over a square cylinder have been investigated, but there is still a gap in the literature. The previous studies tackled the problem of perforated square cylinder together with an active control theory. Although, the ultimate aim of these studies are suppression of vortex shedding in the wake region of square cylinder, most of the investigations reported variation of aerodynamic parameter such as drag coefficient and pressure coefficient, and very limited results are available in terms of the wake flow structure and Vortex Street. Therefore, the objective of this study is to investigate the effects of perforating a square cylinder on the flow structure and suppression of vortex shedding in the wake region behind the cylinder. Moreover, despite many efforts to describe the vortex shedding mechanism from dual bodies configuration there is still also a gap in the literatures regarding vortex shedding from flat plate geometry. The previous studies either tackled the problem of two normal flat plates in tandem or an inclined single flat plate, and interacting wakes of two inclined tandem flat plates have not been probed. The main reason for this is presumably the lack of practical interest which tackles more specific engineering problems. Therefore, the objective of this study is also to investigate the asymmetric flow structures and vortex formation behind two inclined flat plates in tandem arrangement experimentally.

The Vortex shedding phenomenon and suppression of vortex shedding have been studied by employing triple decomposition technique rather than classical Reynolds decomposition to distinguish the incoherent turbulent flow fluctuation from coherent vortex shedding structure for a better understanding of this phenomena. Downstream wake has been measured quantitatively by employing Hotwire anemometry and phased averaged properties have been presented coherent and incoherent structures of downstream wake have been identified. The effectiveness and suppression of the vortex shedding in the wake region of a perforated square cylinder have been investigated. Finally, the effects of gap ratio between the plates together with angle of attack (alpha) on the downstream wake structure, and the shedding phenomenon for inclined flat plates in tandem have been investigated as well.

In chapter 1 historical review and previous works on vortex shedding phenomenon from bluff bodies have been presented. In chapter 2 some theoretical methods such as triple decomposition and phase averaging have been defined and modified Navier-Stokes equation have been presented. Then, in chapter 3 experimental setup, the EMU subsonic wind tunnel and Hot-wire anemometry have been described. Flow structures and suppression of vortex street behind perforated square cylinder have studied in chapter 4. In addition, interacting wakes of two inclined flat plates in tandem arrangement have been investigated in terms of flow structure, coherent and incoherent structure and also time averaged velocity profiles in chapter 5. Finally some suggestion and future works to improve our understanding of vortex shedding phenomenon have been proposed.

Chapter 2

THEORETICAL DERIVATIONS

2.1 Introduction

In this study vortex shedding phenomenon behind bluff bodies have been investigated by employing the triple decomposition and ensemble averaging technique as proposed by Hussain (1986), Reynolds and Hussain (1972), Cantwell and Coles (1983), Kiya and Matsumura (1988), Perry and Steiner (1987) and Steiner and Perry (1987) . Thus, the turbulent flow (incoherent turbulent fluctuations) and vortex shedding (coherent structure) could be identified and distinguished and resulted in a better understanding of this phenomena.

Moreover, since vortex shedding phenomenon is a classical periodic flow in nature, therefore it is more appropriate to analyze such signal by employing phase averaging technique. Hence only data acquired at the same phase of the signal is analyzed for all periods. In this chapter triple decomposition, ensemble and phase averaging technique have been applied on the momentum equation and modified Navier-Stokes equation have been derived accordingly. As a result of such approach additional stress terms due to coherent structure and incoherent fluctuation can be studied as well. Properties such as coherent and incoherent stresses term, turbulent kinetic energy (TKE) and other terms which are explained in this chapter are examined in detail in the result chapters for different bluff body arrangements.

2.2 Triple Decomposition Technique

As stated previously, Triple decomposition was employed to analyze flow properties such as instantaneous velocity. This technique provides an improved clarification of coherent structure and incoherent turbulent fluctuations by decomposing instantaneous stream wise velocity u as follow:

$$u(\vec{x},t) = \bar{u}(\vec{x}) + \tilde{u}(\vec{x},t) + u'(\vec{x},t) \quad (2.1)$$

Where $\bar{u}$ the time-mean is averaged component, $\tilde{u}$ is the periodic coherent structure and $u'$is the random fluctuation incoherent structure. This definition can be applied for any other velocity components i.e. transverse velocity or product of velocity components such as Reynold normal or shear stresses.

Figure 2.1 illustrates an instantaneous velocity for a periodic signal superimposed with coherent and incoherent random fluctuations.

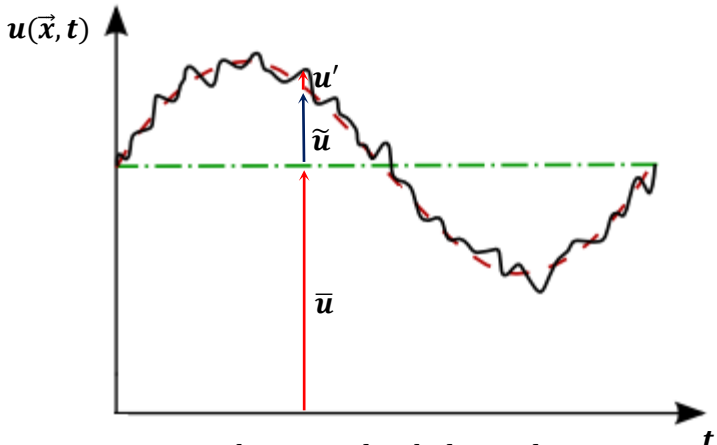

Figure 2.1. Mean, coherent and turbulent velocity components of periodic instantaneous velocity

2.3 Time Averaging and rules

The time mean of incoherent fluctuations u' *and* v' are zero due to their random nature and as a result $\overline{u'} = 0$ and $\overline{v'} = 0$. Moreover, time mean of coherent structure of a periodic vortex shedding are zero, $\overline{\tilde{u}} = 0,$ $\overline{\tilde{v}} = 0$ for instance. Moreover, the readers are referred to (Reynolds & Hussain, 1972) for additional averaging rules applied to derive the modified Navier-Stokes equation. Therefore, Time mean average of any flow property such as velocity is defined mathematically as (Bradshaw, 2013):

$$\bar{u} = \frac{1}{T}\int_0^T u(x,t)dt \tag{2.2}$$

In this study due to periodic nature of shedding phenomenon, $\bar{u}$ is not a function of time.

2.4 Phase Averaging

In order to employ triple decomposition we have to introduce the concept of phase averaging. This is an averaging operation over successive terms taken at exactly same phase during each period. Therefore, the phase average can be defined as follow

$$< u(x,y,t) >= \lim_{N\to\infty} \frac{1}{N}\sum_{n=1}^{N} u(x,y,t+nT) \tag{2.3}$$

where N is the number of cycles used for phase averaging and u is the instantaneous velocity. The phase averaging is the average over large ensemble points having the same phase with respect to the specified wave. Therefore,

$$\tilde{u} = \langle u \rangle - \bar{u} \tag{2.4}$$

That is the phase averaging filters only the coherent oscillations from the instantaneous turbulent motion.

2.5 Derivation of modified Navier-Stokes Equation

The Navier-Stokes momentum equation given in the following equation is formed by four terms

$$\underset{\text{(I)}}{\frac{\partial u_i}{\partial t}} + \underset{\text{(II)}}{u_j \frac{\partial u_i}{\partial x_j}} = \underset{\text{(III)}}{-\frac{1}{\rho}\frac{\partial P}{\partial x_j}} + \underset{\text{(IV)}}{\nu \frac{\partial^2 u_i}{\partial x_j \partial x_j}} \tag{2.5}$$

Applying phase averaging on each term will result

Term (I):

$$\frac{\partial \langle \bar{u}_i + \tilde{u}_i + u_i' \rangle}{\partial t} = \frac{\partial \langle \bar{u}_i \rangle}{\partial t} + \frac{\partial \langle \tilde{u}_i \rangle}{\partial t} + \cancel{\frac{\partial \langle u_i' \rangle}{\partial t}} = \frac{\partial \bar{u}_i}{\partial t} + \frac{\partial \langle \tilde{u}_i \rangle}{\partial t} \tag{2.6}$$

Term (II) from continuity can be written as $\dfrac{\partial (u_j u_i)}{\partial x_j}$

$$\therefore \quad \frac{\partial (u_j u_i)}{\partial x_j} = \frac{\partial}{\partial x_j} \left\langle (\bar{u}_j + \tilde{u}_j + u_j')(\bar{u}_i + \tilde{u}_i + u_i') \right\rangle$$

$$= \frac{\partial}{\partial x_j} \left\langle \bar{u}_j \bar{u}_i + \bar{u}_j \tilde{u}_i + \bar{u}_j \cancel{u_i'} + \tilde{u}_j \bar{u}_i + \tilde{u}_j \tilde{u}_i + \tilde{u}_j \cancel{u_i'} + \cancel{u_j' \bar{u}_i} + \cancel{u_j' \tilde{u}_i} + u_j' u_i' \right\rangle$$

$$= \frac{\partial}{\partial x_j} \left(\bar{u}_i \bar{u}_j + \bar{u}_j \langle \tilde{u}_i \rangle + \bar{u}_i \langle \tilde{u}_j \rangle + \langle \tilde{u}_i \tilde{u}_j \rangle + \langle u_i' u_j' \rangle \right) \tag{2.7}$$

Term (III): $$-\frac{1}{\rho}\frac{\partial \langle \bar{P} + \tilde{P} + P' \rangle}{\partial x_j} = -\frac{1}{\rho}\frac{\partial \langle \bar{P} \rangle}{\partial x_j} - \frac{1}{\rho}\frac{\partial \langle \tilde{P} \rangle}{\partial x_j} - \frac{1}{\rho}\cancel{\frac{\partial \langle P' \rangle}{\partial x_j}}$$

$$= -\frac{1}{\rho}\frac{\partial \langle \bar{P} \rangle}{\partial x_j} - \frac{1}{\rho}\frac{\partial \langle \tilde{P} \rangle}{\partial x_j} \tag{2.8}$$

and Term (IV):

$$\nu \frac{\partial^2 \langle (\bar{u}_i + \tilde{u}_i + u_i') \rangle}{\partial x_j \partial x_j} = \nu \frac{\partial^2 \langle \bar{u}_i \rangle}{\partial x_j \partial x_j} + \nu \frac{\partial^2 \langle \tilde{u}_i \rangle}{\partial x_j \partial x_j} + \nu \cancel{\frac{\partial^2 \langle u_i' \rangle}{\partial x_j \partial x_j}}$$

$$= \nu \frac{\partial^2 \langle \bar{u} \rangle}{\partial x_j \partial x_j} + \nu \frac{\partial^2 \langle \tilde{u} \rangle}{\partial x_j \partial x_j} \tag{2.9}$$

Hence after applying phase averages of each part, the momentum equation can be re-arranged as follow

$$\rho\frac{\partial\overline{u_\iota}}{\partial t}+\rho\frac{\partial\overline{u_\iota u_J}}{\partial x_j}+\frac{\partial\bar{p}}{\partial x_j}-\frac{\partial}{\partial x_j}\left(\mu\frac{\partial\overline{u_\iota}}{\partial x_j}-\rho(\langle\tilde{u}_i\tilde{u}_j\rangle+\langle u'_i u'_j\rangle)-\rho\left(\overline{u_\iota}\langle\tilde{u}_j\rangle+\overline{u_j}\langle\tilde{u}_i\rangle\right)+\langle\tilde{p}\rangle\right)=0 \tag{2.10}$$

Finally, applying time–average rules on the obtained equation will result in the modified Navier-Stokes equation as follows:

$$\rho\overline{\frac{D\overline{u_i}}{Dt}}=-\overline{\frac{\partial\overline{P}}{\partial x_i}}+\frac{\partial}{\partial x_j}\left(\mu\frac{\partial\overline{u_i}}{\partial x_j}-\rho(\overline{\langle\tilde{u}_i\tilde{u}_j\rangle}+\overline{\langle u'_i u'_j\rangle})\right)+\frac{\partial}{\partial x_j}\left(\rho\left(\overline{\overline{u_i}\langle\tilde{u}_j\rangle}+\overline{\overline{u_j}\langle\tilde{u}_i\rangle}\right)+\overline{\langle\tilde{P}\rangle}\right) \tag{2.11}$$

Hence

$$\rho\frac{D\overline{u}}{Dt}=-\frac{\partial P}{\partial x_j}+\frac{\partial}{\partial x_j}\left(\mu\frac{\partial\overline{u}_i}{\partial x_j}-\rho(\overline{\tilde{u}_i\tilde{u}_j}+\overline{u'_i u'_j})\right) \tag{2.12}$$

Therefore, in the modified Navier-Stokes equation derived by triple decomposition for periodic flow, in addition to the Reynolds stress term $u'v'$, there is an additional term $\overline{\tilde{u}_\iota\tilde{u}_J}$ in the Reynolds stress term due to the coherent fluctuation.

Moreover, the Turbulence Kinetic Energy (TKE) can be defined in a similar manner as following equation:

$$\bar{k}=\frac{1}{2}\overline{u'_i u'_i}=\frac{1}{2}(\overline{u'_1u'_1+u'_2u'_2+u'_3u'_3})=\frac{1}{2}(\overline{u'u'+v'v'+w'w'}) \tag{2.13}$$

In this experimental study downstream wake behind the different bluff bodies has been measured quantitatively by employing Hotwire anemometry as described in chapter 3. The wake region have been investigated in terms of coherent velocities, normal and shear stresses and Turbulent Kinetic Energy production, for instance. Detailed investigation coherent structure and suppression of vortex shedding also presented for perforated square cylinder in chapter 4.

Chapter 3

EXPERIMENTAL FACILITY AND DATA ANALYSIS

In order to investigate the turbulent wake flow structure behind the bluff bodies and effectiveness of the employed passive control theory to suppress the vortex shedding several experiments were performed. In this chapter the experimental facilities and set up, measurements techniques and data analysis are described. HWA measurements has been employed to acquire the velocity and fluctuating components in the region of interest in the wake of bluff bodies. HWA working principles, calibration procedure and instrumentation have been also described. Moreover, the traverse mechanism which have been employed to traverse the cross Hotwire probe in the wind tunnel's test section is described as well. The investigated bluff body models and arrangements throughout the experiments are given at corresponding chapters.

3.1 The EMU Subsonic Wind Tunnel

The experiments have been performed at the open type subsonic wind tunnel available in Aerodynamics laboratory of the Mechanical Engineering Department, EMU. The wind tunnel test section dimension is 0.5 x.0.5m and 1.4m long with contraction ratio of 10:1. The tunnel free stream turbulence level is less than 0.8 % at the maximum speed of 30 m/s. The wind tunnel is a suction driven type and the speed is controlled with a 12 kW Danfoss electronic frequency control unit (0 – 50Hz). Figure 3.1 illustrated the schematic diagram of the wind tunnel, traverse mechanism and hotwire anemometry.

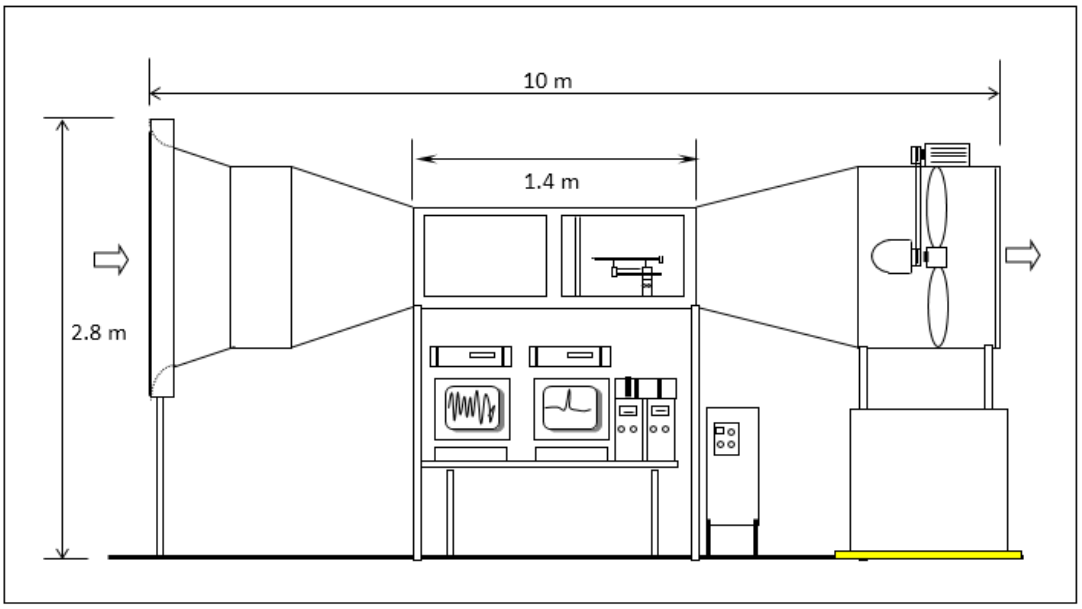

Figure 3.1. Schematic Side view of the Subsonic Wind Tunnel

3.2 Hot-wire Anemometry

Hot wire anemometer (HWA) is one of the widely used technique in turbulent flow measurements which provide a high temporal resolution comparing to other techniques. The temporal resolution which is up to 400 kHz, provide capability of a real time analysis of the flow. Hot wire anemometer is also more affordable compared to other flow measurement systems such as PIV or LDA. Hot wire anemometer measurement principle is based on convective heat transfer from a heated sensing wire or film. For velocity measurement the electrically heated sensor will be exposed to the flow and the sensor maintains at constant temperature with the aid an electronic control unit. Consequently, based on the changes in heat transfer from the sensor, the anemometer measures the corresponding flow velocity.

The technology achievement in the late 1950's leads to development of an accurate technique in flow measurements. This newly developed technique was superior in accuracy and flexibility compare with available flow measurements technique such

as Pitot tube measurements (Bruun, 1996). It can be employed where fast response to the flow changes (high frequency response) are required. However, there are some limitation and drawbacks associated with hot wire anemometer. This method is an intrusive technique since the probe must be placed in the flow with adverse effects. In addition, the sensors are fragile and very susceptible to flows contaminants and requires calibration before and after each experiment for accurate measurements.

There are two types of hot wire anemometer based on their operating methods; Constant Current Anemometer (CCA) mode and Constant Temperature Anemometer (CTA). “Constant current” system operates in a manner to keep the current through the sensing element constant. However, for “constant temperature” operation the element temperature is kept constant by using an electronic control unit to change the electrical current accordingly. As a result the two mentioned methods significantly different in their circuit. In both anemometer systems electronic noises caused by amplifier circuit, resistors in the anemometer bridge and the sensors require special consideration (Brunn, 1995). CTA requires more complex circuit and more expensive comparing CCA, but it is easier to use with low noise problem. Nevertheless, “constant temperature anemometer” (CTA) is satisfying the modern requirements and accepted as standard with more popularity (Bradshaw, 1996).

The probe require frequent calibration due to sensitivity of the sensor to temperature changes together with the effects of available dirt in flow.

3.2.1 Hot Wire probe

Hot-wire and hot-film are the most common probe which are being employed in hot wire anemometer. These sensors facilitate turbulent flow studies and to provide accurate measurements of turbulent flow, it is recommended that dimension of the sensor should be chosen by considering the Kolmogorov length scale of the smallest eddies (Bradshaw, 1996).

The hot wire sensor is made of electrically conductive material and Tungsten, platinum and platinum alloys are among the common material for hot wire production. The hot wire is 5 μm in diameter and 1 mm in length welded to the single and cross probe prongs as illustrated in figure 3.2 and 3.3, respectively.

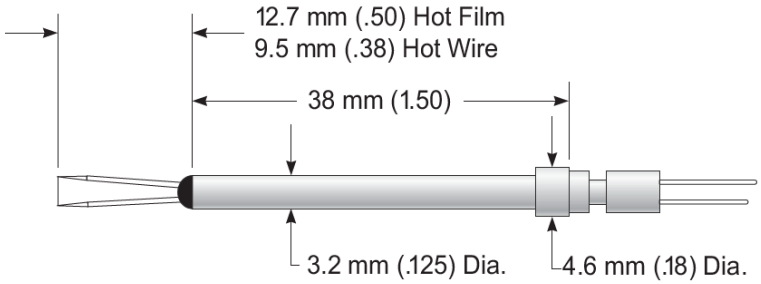

Figure 3.2. Single Hotwire probe Model 1210

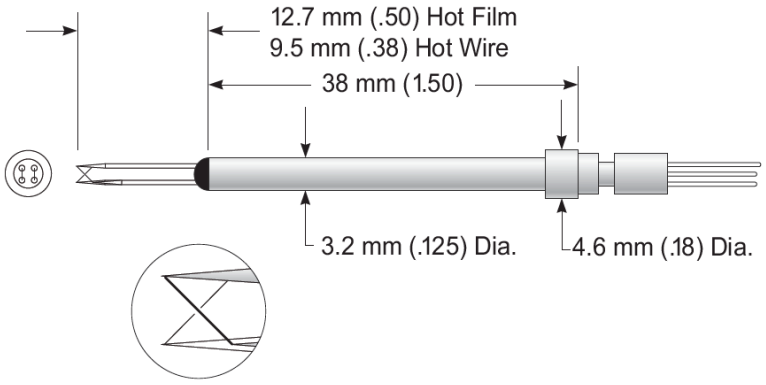

Figure 3.3. Cross Hotwire probe Model 1240

These fragile and highly sensitive wires will be installed on the probe prongs by spot welding or soldering techniques. The length of these prongs are critical and may affect the hot wire system. For instance, long prongs in periodic flows such as vortex shedding may vibrate and may introduce error into the measurements by the HWA. Hot-wire probes facilitate flow field measurements in gas and liquid with high accuracy and response.

3.2.2 HWA PRINCIPLE

As mentioned before the electrical current flows through the wire to maintain the wire temperature. Therefore the dissipated electrical energy from the sensor in form of heat is given by equation 3.1.

$$W_{elec} = I^2 R_w \tag{3.1}$$

Where I is the electrical current through the wire, and R_w is the sensor electrical resistance.

Therefore an equilibrium between the generated thermal energy heat losses to the surrounding is required to keep the wire temperature constant. However the convective heat transfer will varies as the flow velocity changes and leads to a new equilibrium. As stated, the HWA output is correspondent the flow velocity and King's Law is an empirical law describing the non-linear relation between the measure voltage across the wire (E) and flow velocity (V) as follow:

$$E^2 = A + BV^n \tag{3.2}$$

where A, B, and n are the coefficient which obtained from calibration procedure. Therefore a 4^{th} order polynomial curve fit is to be used, which approximates the inverse of the King's law accurately and the output is directly proportional to the effective velocity.

$$V_{eff} = K + A*N + B*N^2 + C*N^3 + D*N^4 \quad (3.3)$$

Where V_{eff} is effective velocity, N is normalized bridge voltage and A, B, C, D and K are the constants that to be determined by calibration procedure. The normalized voltage N is obtained from the following equation:

$$N = \frac{E - E_{min}}{E_{max} - E_{min}} \quad (3.4)$$

Where, E is the Bridge voltage

To generate a look up table which can be used for flow measurements, the fourth order polynomial curve fit have been applied for the normalized voltage to compute velocities. The calibration curve fit for a single probe SN 961171 is shown in figure 3.4. As it can be seen the calibration curve is non-linear, and the calibration have been performed for a velocity range of 0 to 20 m/s for 20 sample data points. The calibration at low velocities, where requires maximum sensitivity treatment, performed with higher sampling density comparing to high velocities.

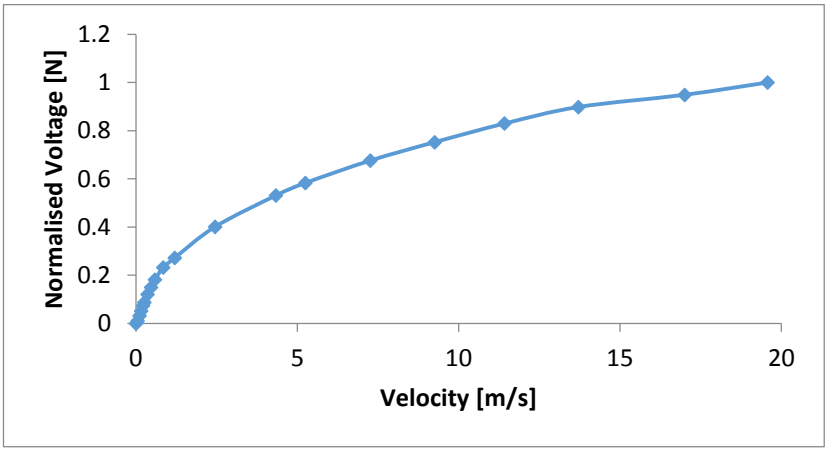

Figure 3.4. Calibration Curve Plot for single probe SN 961171

The look-up table is generated for each probe sensor for the specified flow velocity range which used for calibration. The curve fit and mean square error (MSE) can be

employed to evaluate the accuracy of the calibration. If the MSE is higher than 0.01-0.02 %, the calibration procedure must be repeated to obtain an accurate calibration with proper curve fit and MSE. It should be stated that exceeding the MSE above this range would affect the data acquisition since some other parameter such as positioning effect, soldering and contact resistance have already affected the calibration.

3.2.3 Hot wire instrumentation

In this study the employed HWA is a constant temperature anemometer and consists of a hot-wire probe connected to a Wheatstone bridge (TSI FlowPoint 1500 velocity transducer, CTA bridge) as illustrated in figure 3.5. A DAS-1402 data acquisition card transfer the velocity transducers output to FlowPoint velocity measuring system software.

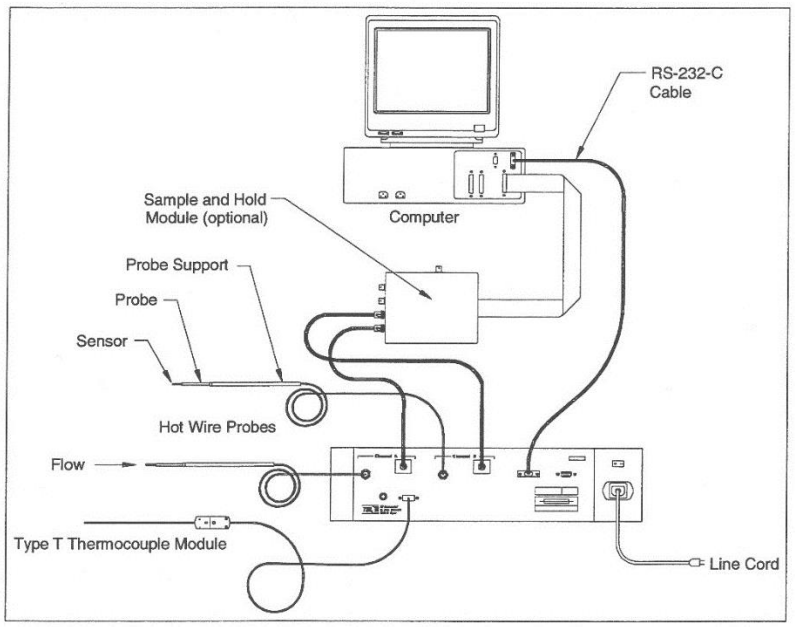

Figure 3.5. Hot wire anemometry system configuration (Figure taken from TSI FlowPoint 1500 Instruction Manual)

The TSI FlowPoint 1500 velocity transducer is the control circuit for the CTA hot-wire anemometry. The special bridges and amplifiers (figure 3.6) with filter circuits of the transducers ensure minimal noise during the data acquisition.

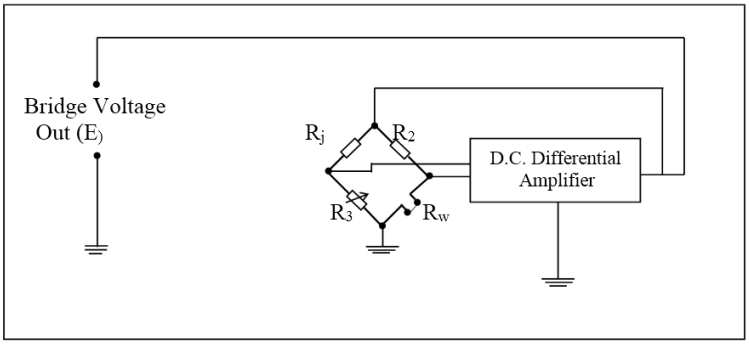

Figure 3.6. Schematic diagram of a thermal anemometer system (Wheatstone bridge)

For this work TSI model 1210-T1.5 type single normal (SN) probes and TSI 1243-T1.5 type x-wire probe have been employed. The sensors were made of tungsten and 3.8 μm in diameter.

3.2.4 Hot Wire calibration

The HWA system requires to be calibrated before each experimental flow measurements. Therefore the voltage-velocity governing relation will be determined by calibration procedure as explained in previous section.

The hot wire probes have been calibrated by employing TSI Model 1125 calibrator which provides the turbulence intensity less than 0.5% to eliminate any error into the calibration constants. The velocity range of the calibrator is between 0.01 to 300 m/s for this model. The calibrator equipped with three chambers for very low velocities (0.001 - 1 m/s), mid-range velocities (0.63 - 15 m/s) and higher velocities (2.5 - 300 m/s) called D3, D2 and D1, respectively.

In order to employ CTA Hotwire system for data acquisition in the experiment, a calibration against known flow velocities are required. Therefore the output voltage would be obtained as a function of the flow velocity.

Due to atmospheric pressure and temperature variation and their effects on the result, for all calibration procedures and data acquisitions the ambient pressure and temperature have been considered for velocity calculations.

The TSI hot wire probes require an ambient condition correction throughout the calibration procedure with considering the temperature (Bearman, 1971) and pressure effects. Therefore, nominal velocities is modified by a correction factor K_{VCF} (TSI Manual):

$$K_{VCF} = \sqrt{\left(\frac{293}{273+T}\right)\left(\frac{P}{760}\right)} \tag{3.5}$$

where T = Atmospheric temperature (C)

P = atmospheric pressure (mm Hg)

In addition to ambient condition correction, it is also required to employ a directional sensitivity correct factor for the calibration with considering the direction of the flow as studied by (Jorgensen, 1971). End flow condition requires that the flow direction and the sensor axis to be in the same direction, whereas for cross flow condition the sensor axis is normal to flow direction. The Hot wire probe response to end flow and cross flow conditions are different. As a result of such directional sensitivity, a cross flow calibrated probe will produce error in measurement if exposed to end flow condition. Therefore, TSI probe were corrected for pitch response by employing correction factor K_{SF} as supplied by the manufacturer.

3.2.5 Hot wire system settings

As discussed in previous section the HWA requires to be calibrated in order to compute a relation between velocity and voltage. The HWA setting such as probe type, probe-cable resistance, sensor resistance, gain, offset can be set within the FolwPoint software. The probe-cable resistance has been determined by employing a short-cut device and additional system's setting are provided by the manufacturer as given in table 3.1.

Table 3.1. Hot wire sensors settings

	Probe resistance	Wire resistance	Operating resistance	Operational temperature
1210-T.15	5.96 Ω	0.28 Ω	11.66 Ω	250 °C
1210-T.15	5.70 Ω	0.24 Ω	11.33 Ω	250 °C
1241-T.15	5.57 Ω	0.19 Ω	1082 Ω	250 °C

3.3 Hot wire probe Traverse Mechanism

The X probe has been mounted on a three-axis traverse mechanism to traverse in the domain of interest during data acquisition as illustrated in figure 3.7. The accuracy of mechanism is ±0.25 mm for traversing in all directions. All the measurements were acquired at the midpoint of the test section in the z-direction and the probe have been traversed in x-y for a domain of 0.5D to 4.0D in the downstream wake region.

Traverse Mechanism Specification:

- 250 x 250 [mm] operation domain in XY plane
- 250 [mm] operation in Z axis
- Accuracy Max. 1600 steps per revolution

The cross Hotwire sensor was mounted on model 1155 probe support 457 mm upstream of the traverse mechanism and the blockage ratio of the mechanism is calculated to be 6 %. Under these circumstances it is accepted that the effect of mechanism on the data measurement system is negligible.

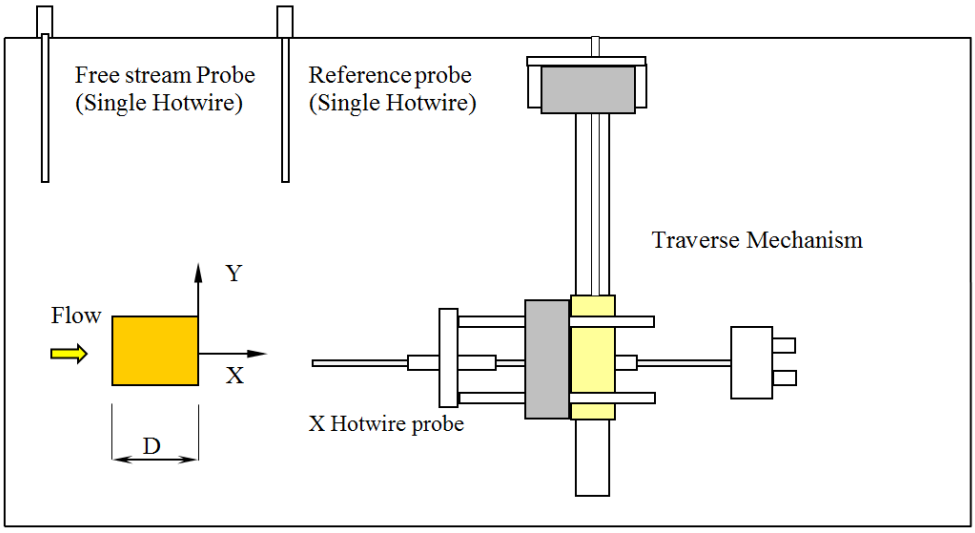

Figure 3.7. Schematic of Hotwire probe traverse mechanism

3.4 Data Analysis Program Code

In this study the acquired velocity data have been analyzed by employing in house FORTRAN codes together with MATLAB/SIMULNIK software. Velocity data have been acquired by employing three velocity transducers. Two individual transducers were dedicated to acquiring free stream velocity and reference velocity signal separately. The last velocity transducer was employed to acquire u and v velocity components from x hotwire probe. Due to noise and distortion of the acquired velocity signal, it is required to clean up/filter the velocity signal.

Therefore, first the acquired velocity data have been converted to a matrix form to perform filtering operation within Matlab/Simulink on the acquired data. FORTRAN

program Convertor1.for has been employed for such reorganizing operation. Then, the velocity signal data have been cleaned up within MATLAB/SIMULINK (figure 3.8) for high and low frequency noises for cut-off value above 0.25 and below 0.40, respectively. After each filtering operation a delay with respect to the original signal have been observed. Therefore, after each filtering operation the delay value have been substituted into the circuit to correct the time shift. Figure 3.9 illustrated a typical filtered and unfiltered velocity signal.

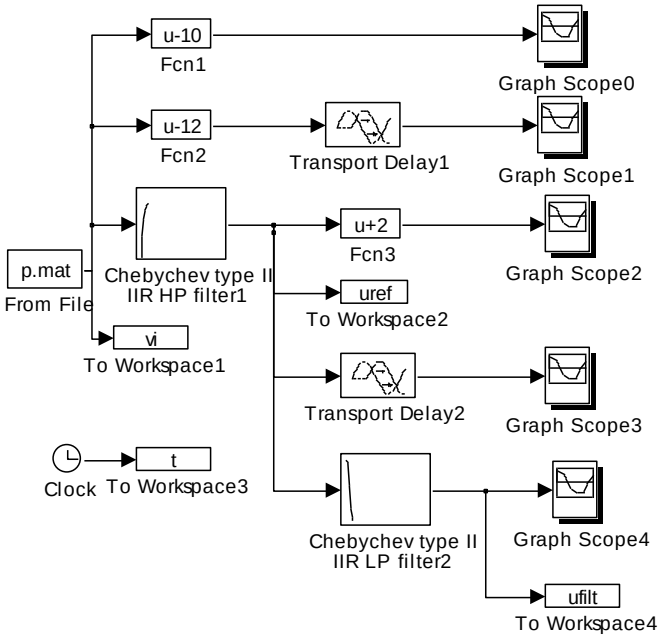

Figure 3.8. Simulink diagram of filtering program

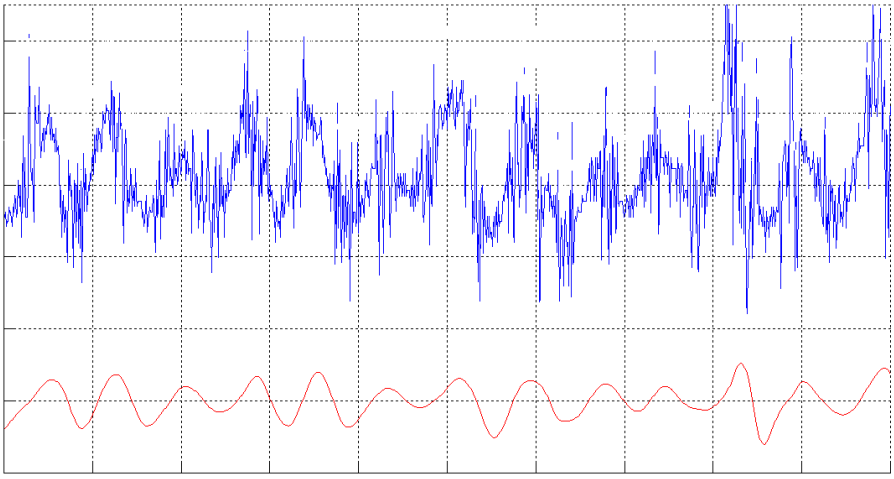

Figure 3.9. Acquired unfiltered and filtered velocity signal

Then, the original velocity signal and the filtered velocity data have been blended by using the FORTRAN program Convertor2.FOR to obtain the zero crossing point from reference signal analysis. Finally the velocity data have been analyzed and velocity properties have been computed by employing ensemble.for program. The phase averaging technique, ensemble averaging and triple decomposition technique have been applied on Navier-Stock equation and ensemble.for program code have been developed based on the modified Navier-Stock equations.

The velocity data have been acquired at sampling rate of 5 kHz for sampling time of 2.048 second with a sampling size of 10 kpts/ch (kilopoints/channel). In this work the flow properties have been analyzed by employing triple decomposition and ensemble averaging techniques as stated in previous chapter. Therefore, after decomposing the instantaneous velocity into three components and applying aforementioned techniques on the Navier-Stokes equation, the modified Navier-Stokes equation derived as:

$$\frac{D\overline{u}_i}{Dt} = -\frac{1}{\rho}\frac{\partial \overline{p}}{\partial x_j} + \nu\frac{\partial^2 \overline{u}_i}{\partial x_i \partial x_j} + \frac{\partial}{\partial x_j}\left(-\langle\overline{\tilde{u}_i \tilde{u}_j}\rangle - \langle\overline{u_i' u_j'}\rangle\right) \tag{2.12}$$

As a result $\langle\overline{\tilde{u}_i\tilde{u}_j}\rangle$ is an extra term contributes to Reynolds stress due to phase averaged product of coherent. Similar to incoherent Reynolds stress term, this coherent Reynolds stress term is a flow dependent property and required extra effort for periodic flow such as vortex shedding phenomenon.

In this study it is required to obtain the dependence of the triple components of the velocity on time (normalized with respect to total period T) during one complete cycle of events. The periodic vortex shedding velocity fluctuation have been selected

as reference signal. Therefore, corresponding to same t/T of consecutive reference cycles, the acquired stream wise and transverse velocity components at the same instant are summed and averaged. This averaging process is repeated for different normalized times during one cycle to construct the variation of different properties $\langle \tilde{u} \rangle$ and $\langle \overline{\tilde{u}} \rangle$ or $\langle \overline{\tilde{v}} \rangle$, $\langle \tilde{u}\tilde{v} \rangle$ and $\langle \overline{\tilde{u}\tilde{v}} \rangle$ etc. The time averaging and phase averaging techniques are applied as defined in section 2.3 and 2.4 and can be applied for all velocity components or products of velocity components.

Moreover, as mentioned earlier the reference signal required to obtain the corresponding phases of each velocity component. Therefore, placing the reference probe at proper location is very essential since improper location of the reference probe will affect the data analysis.

The final consideration is to determine the lowest acceptable number of cycles to perform phase averaging such that the properties were cycle independent. For such purpose a preliminary experiment was performed with number of cycles taken up to 400 cycles. It was observed that for convergence of properties such as normal and shear stress, steady values required at least 150 cycles. Therefore in this study, number of cycles to perform phase averaging was set as 300- 400 cycles.

Chapter 4

SUPPRESSION OF VORTEX STREET BEHIND PERFORATED SQUARE CYLINDER

4.1 Introduction

In this chapter the effect of entrainment of fluid through perforated surface on suppression of Vortex Street behind Perforated Square Cylinder have been studied experimentally. Wake region have been investigated in terms of coherent flow structure, time averaged properties and effectiveness of different perforations. The experiment was conducted at free stream velocity U_∞=10.5 ± 2% m/s with measured turbulence intensity of 0.6% at this speed. A perforated hollow square cylinder with a cross section of 25 mm x 25 mm with corresponding blockage ratio of 5% was selected for the experiment.

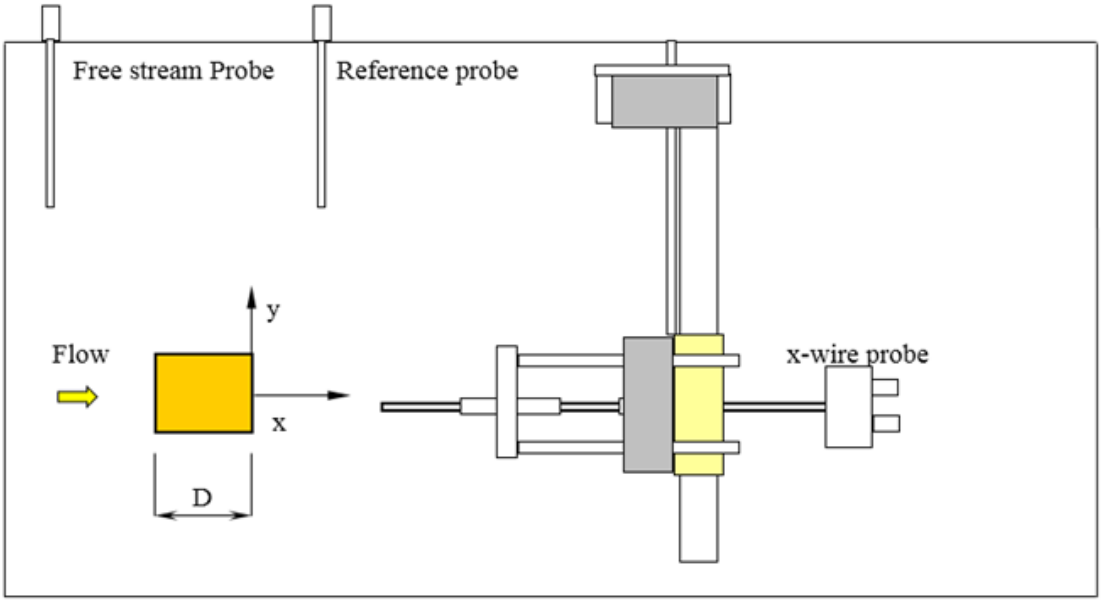

Figure 4.1. Experimental setup

The square cylinder model was constructed from aluminum and four different perforations have been drilled with CNC machine with accuracy ± 0.001 mm. The experimental setup and schematic of perforated square cylinders have been illustrated in figures 4.1 and 4.2, respectively. Each side of square cylinder perforated with 84 holes 2 mm in diameter distributed uniformly on the perforated surface. Reynolds number of the experiment was Re= 18500 (Re=ρUD/μ based on cylinder width) result in turbulent vortex shedding behind the square cylinder in domain of interest (0.5 <x/D< 4.0).

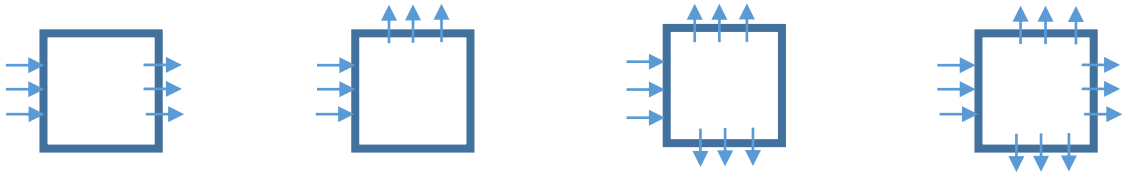

Front-Rear (P0) Front-One face (P1) Front-Two faces (P2) All faces (P3)

Figure 4.2. Schematic of Perforated square cylinders

4.2 Spectral analysis

In order to identify the vortex shedding frequency and quantitative comparison between different perforated square cylinders, Fast Fourier Transform (FFT) have

been implemented on the acquired velocity data. Therefore, the dominant shedding frequency (f) can be observed as a single peak corresponding to Strouhal number in the wake behind the cylinder. The instantaneous velocity acquired at various x/D's downstream in the wake and various transverse direction have been used for frequency spectra determination. Dominant shedding frequency have been found as $f = 43.9\,Hz$ corresponding to Strouhal number s_t =0.104 which is identical to corresponding Strouhal number of the non-perforated square cylinder.

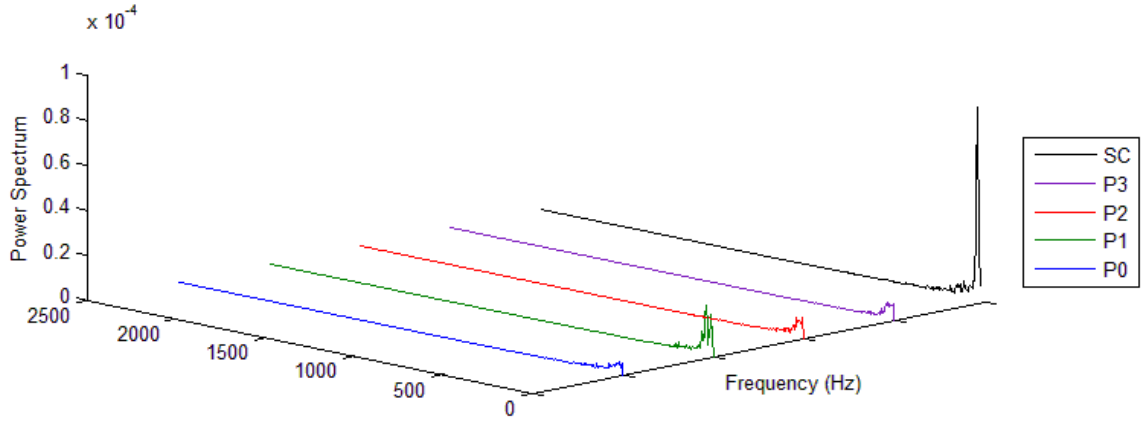

Figure 4.3. Comparison of Power Spectrum Density for different perforated and non-perforated square cylinders

These dominant shedding frequencies have been acquired at positions outside the effective wake width of perforated surface. Similarly, the shedding frequencies obtained by Turhal and Çuhadaroğlu (2010) at similar position for perforated square cylinder with injection demonstrated insignificant alternation in shedding frequency. However, the measurement inside the effective width of perforation were influenced by entrainment of fluid through perforated surfaces. It would be impossible to present all the power spectra's due to space limitation. Therefore, for sake of brevity only a comparison between different perforated square cylinder and a detailed investigation on perforated square cylinder P3 have been presented in figures 4.3 and

4.4, respectively. Power Spectrum Density analysis of transverse velocity for different perforated square cylinders and non-perforated square cylinder measured at x/D=0.5 and y/D=0 (along centerline) in the downstream wake have been demonstrated in figure 4.3.

As it can be seen from the figure, frequency spectra is clearly evident as a single strong peak in the wake of non-perforated square cylinder. In contrary, in the wake region behind a perforated square cylinder no dominant shedding frequency along the centerline is evident. Such observation implied that the vortex shedding have been suppressed by fluid entrainment through the perforated surfaces.

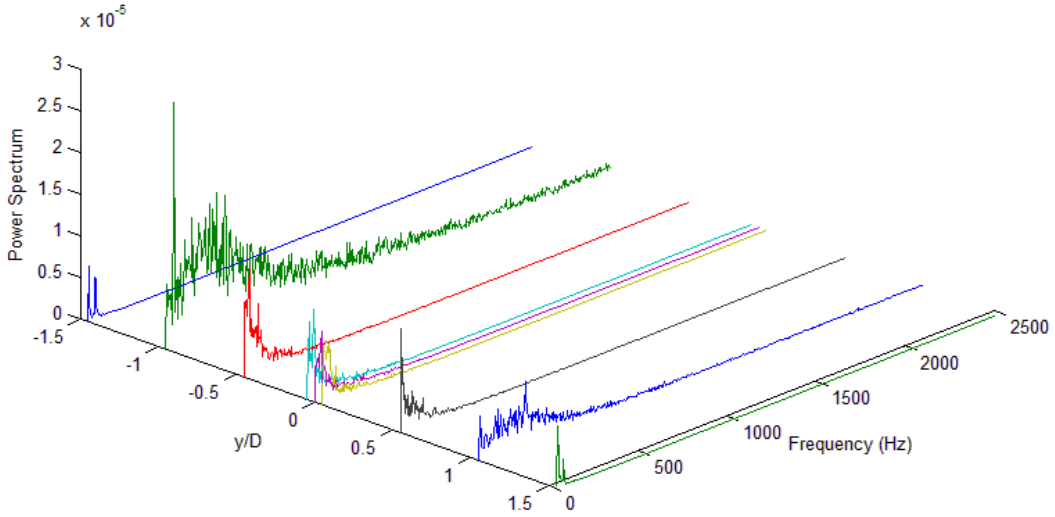

Figure 4.4. Power Spectrum analysis of perforated square cylinder P3 acquired at x/D=0.5 for various traverse direction

In addition, further investigation on Power Spectrum of transvers velocity component acquired at traverse direction interval y/D=±1.5 of perforated square cylinder P3 have been illustrated in figure 4.4. It can be seen that the dominant shedding frequency is clearly evident for the wake region outside of an interval y/D=±0.5. However, inside this interval where the perforated surfaces are effective, the power

spectrum demonstrated evidence of no-single dominant peak with multiple peaks in the spectra. These multiple peaks indicated the secondary vortex formation and suppression of the primary shedding due to entrainment of fluid through the perforated surfaces.

4.3 Phase Averaged Properties

The objective of this study is to investigate the formation of vortex shedding phenomenon in the wake region behind the perforated square cylinders. For that reason, development of vortex street in the wake region behind the perforated square cylinders, have been demonstrated in figures 4.5 to 4.8. For the case of P0 from the phase averaged stream wise velocity <u> contours it can be seen that in the downstream wake region up to approximately x/D=1.5 the vortex shedding has been completely suppressed by the entrainment of fluid into the wake region through the perforated surfaces. In the near wake region of the perforated square cylinder, i.e. x/D=0.5, while within interval y/D=±1 there is no evidence of vortex shedding, some vortices were being rolled beyond the edges of the square cylinder. As the probe moves downstream in the wake some features of vortex shedding have been developed and at x/D=1.5 the contours exhibit patterns corresponding to vortices being shed periodically.

In addition to two peaks beyond the edges of the perforated square cylinder, two low level zone phase drifted by half a period corresponding to edges of the perforated square cylinder are also evident. Eventually, the stream wise phase average velocity contours at x/D=4.0, where perforated surfaces are no more effective, demonstrated a classical vortex shedding and through such development the peaks are drifted more away from the centerline. In contrary, the two low level zones are shifted towards the

centerline behind the perforated square cylinder. Such flow pattern is comparable to stream wise velocity in the wake region of a square cylinder as reported by H Hacışevki and Teimourian (2015). Moreover, comparison of the phase averaged transverse velocity contours demonstrated similar development of Karman Vortex Street in the wake region.

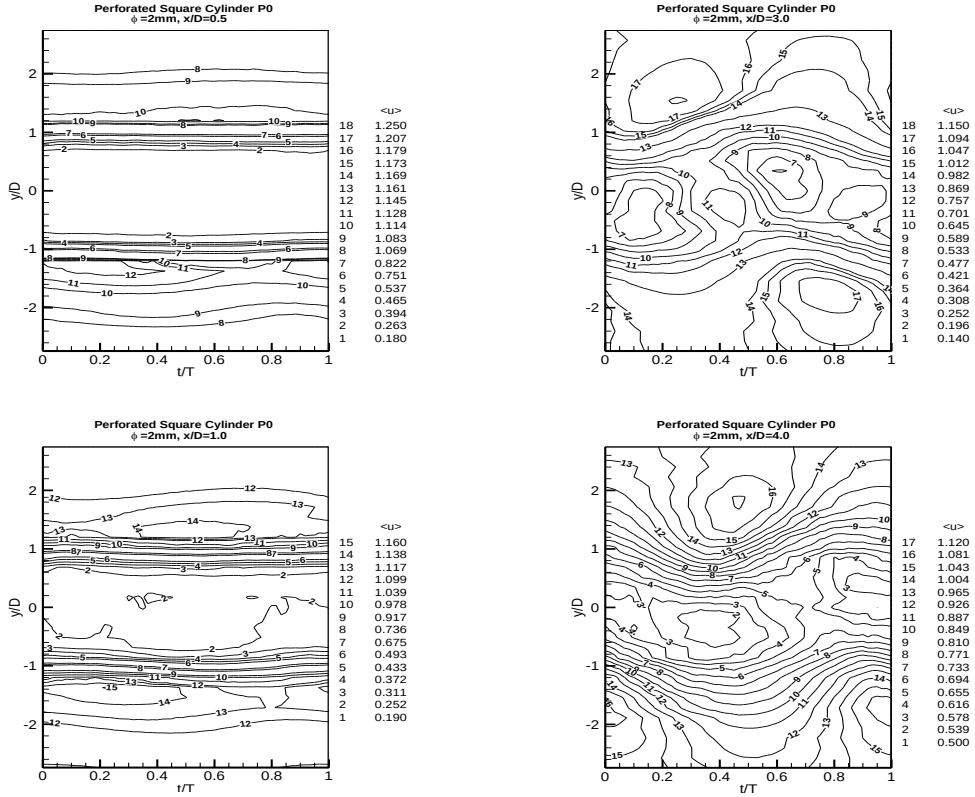

Figure 4.5. Stream wise velocity measured at various x/D in downstream wake of perforated square cylinder P0

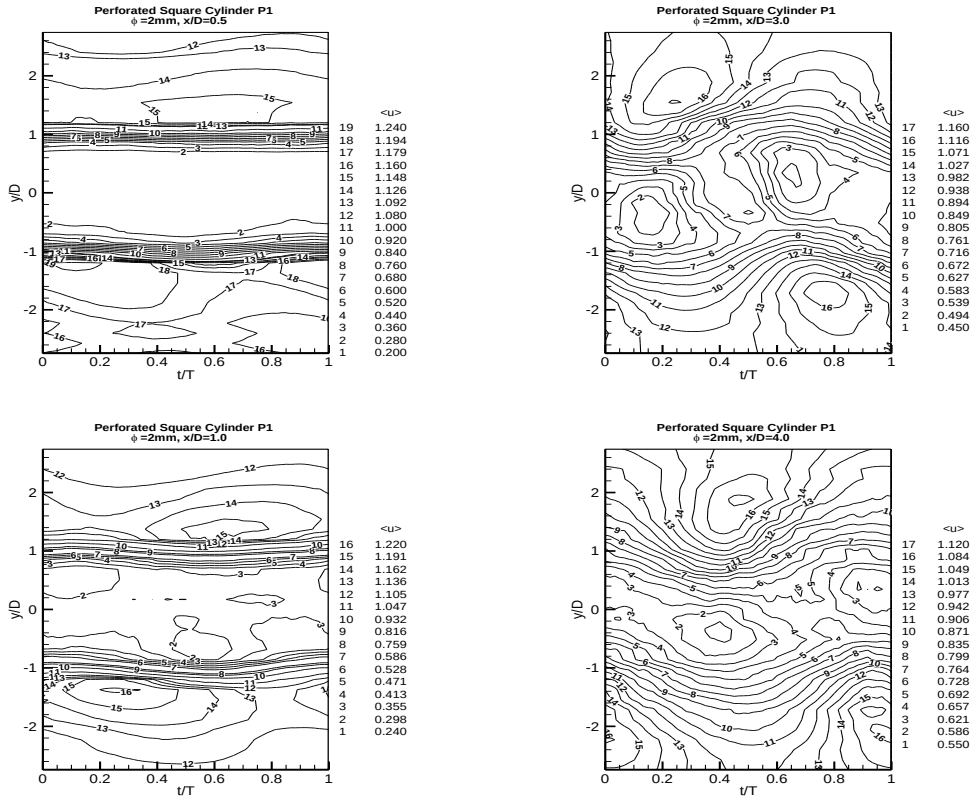

Figure 4.6. Stream wise velocity measured at various x/D downstream of perforated square cylinder P1

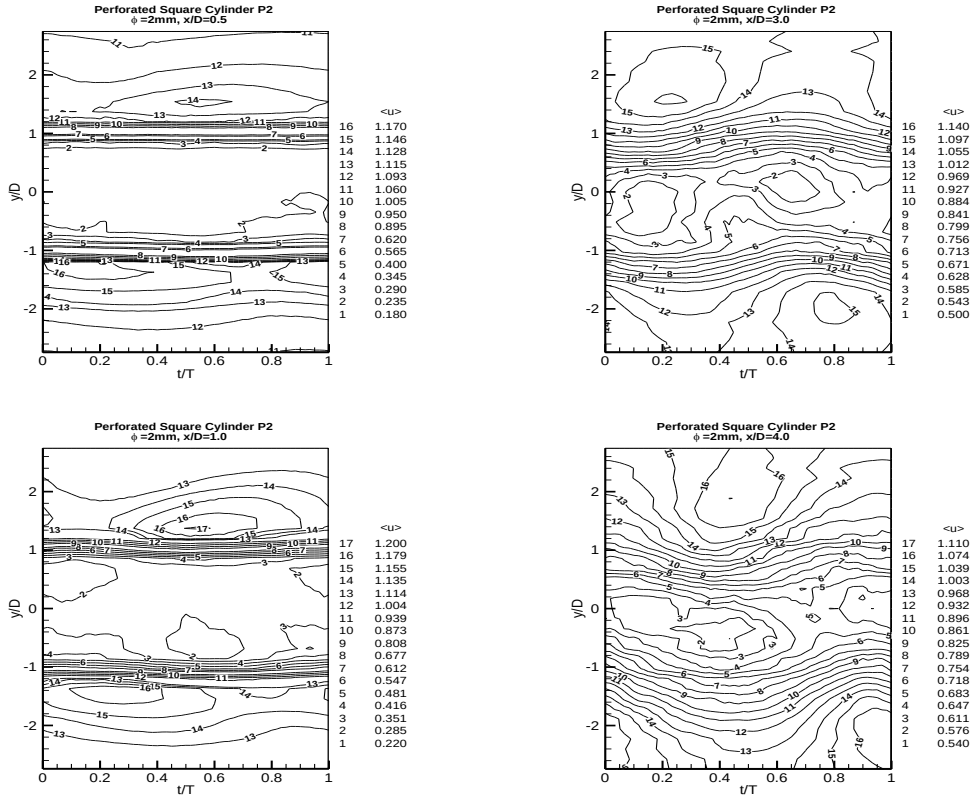

Figure 4.7. Stream wise velocity measured at various x/D downstream of perforated square cylinder P2

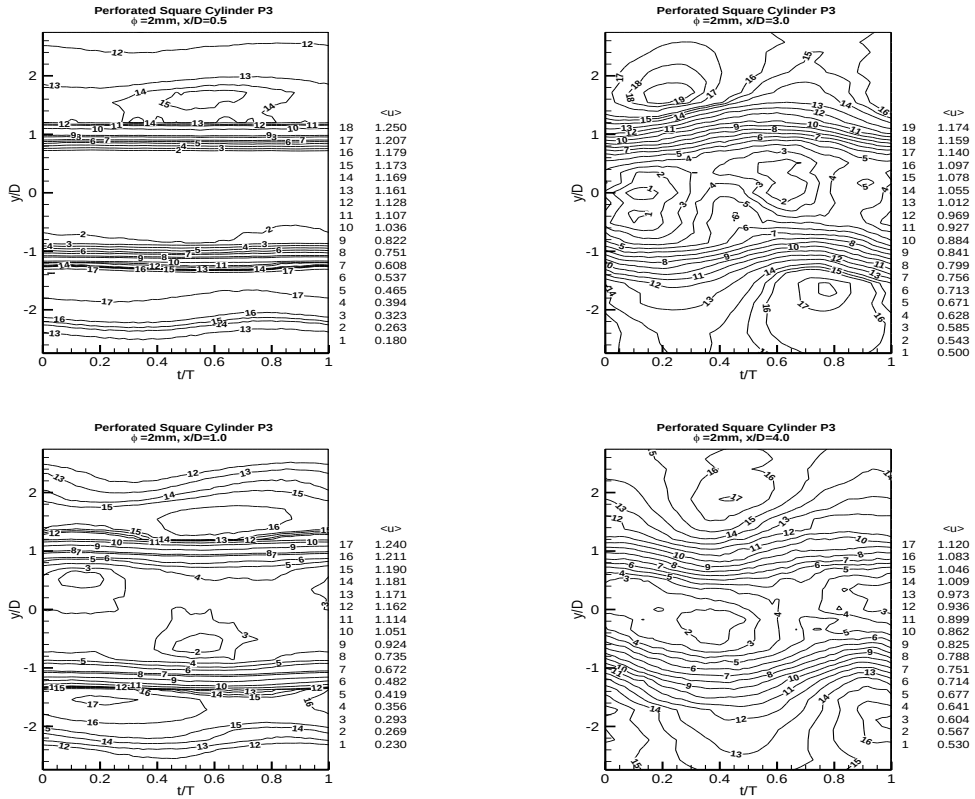

Figure 4.8. Stream wise velocity measured at various x/D downstream of perforated square cylinder P3

Figures 4.9 to 4.12 illustrated transverse velocity component contours acquired at different distances downstream in the wake region. Similar to stream wise velocity component, the peaks are occurring in duration of half a period phase (t/T=0.5). However, a comparison between stream wise and transverse velocity component measured at x/D=4.0 revealed that transverse velocity peaks lag behind stream wise velocity peaks with a phase shift equal ¼ of a cycle. The contours around this peak region imply a remarkable lateral momentum transfer towards the growing vortex on the other edge of the square cylinder. However, such phenomenon has been suppressed by the perforated surface at near wake i.e. x/D=1.0 where the perforated surfaces are effective.

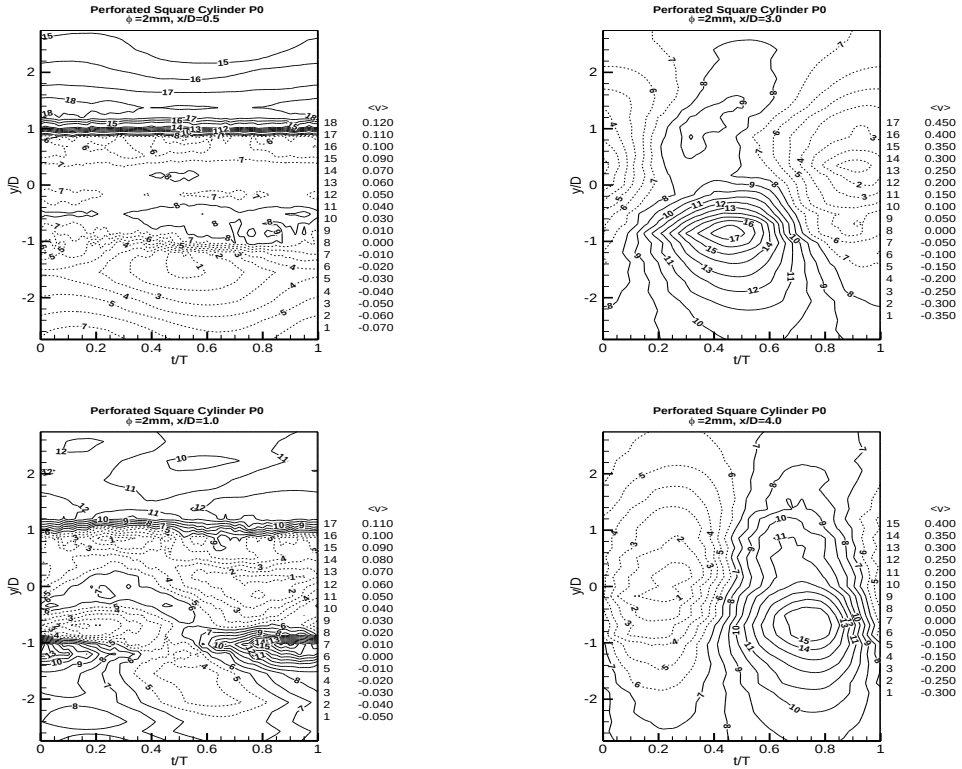

Figure 4.9. transverse velocity measured at various x/D downstream of perforated square cylinder P0

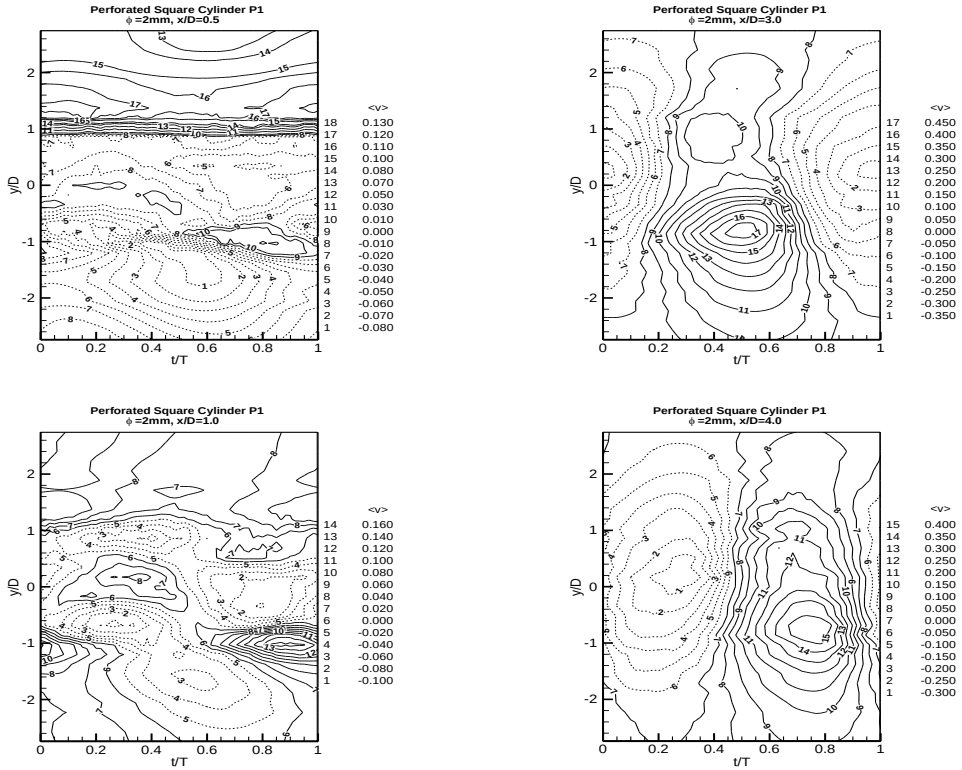

Figure 4.10. transverse velocity measured at various x/D downstream of perforated square cylinder P1

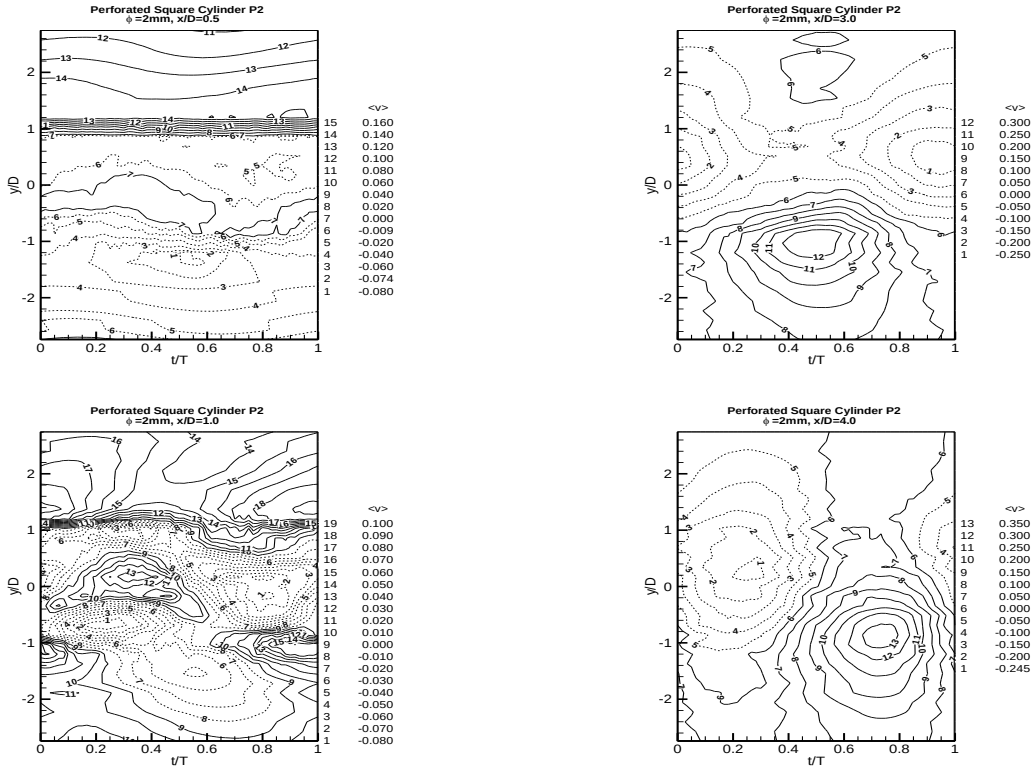

Figure 4.11. transverse velocity measured at various x/D downstream of perforated square cylinder P2

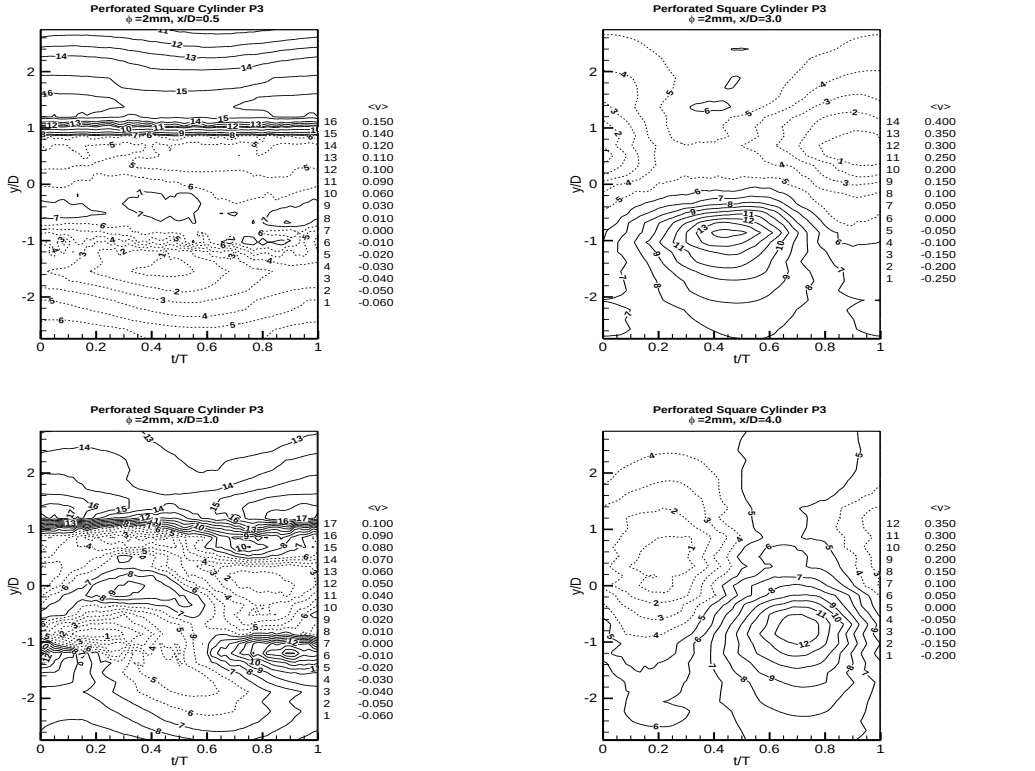

Figure 4.12. transverse velocity measured at various x/D downstream of perforated square cylinder P3

4.4 Coherent structure

Variation of phased averaged coherent velocities $\langle \tilde{u} \rangle$ and $\langle \tilde{v} \rangle$ are illustrated in figures 4.13 to 4.20. As it can be concluded from the figure, development of the coherent structure have been delayed by the entrainment of fluid through the perforated surfaces. It can be that in the near wake region there is no evidence of coherent structures. However, as the probes moves downstream the features of such structures are being developed and more apparent and therefore, the peak magnitude of coherent structure were increased. As it can be seen from coherent stream wise contours, due to such development two alternating peaks corresponding to edges are evident. Moreover, as the coherent structure are gaining momentum, the coherent transverse velocity grows as wide as the wake region.

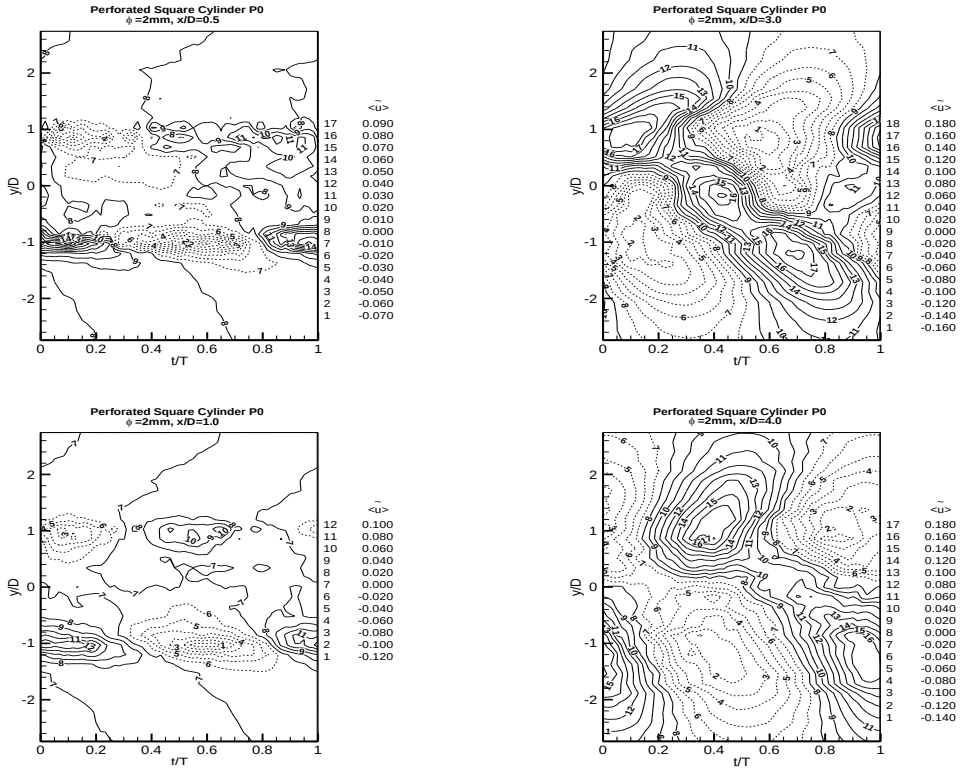

Figure 4.13. Coherent stream wise velocity measured downstream of perforated square cylinder P0

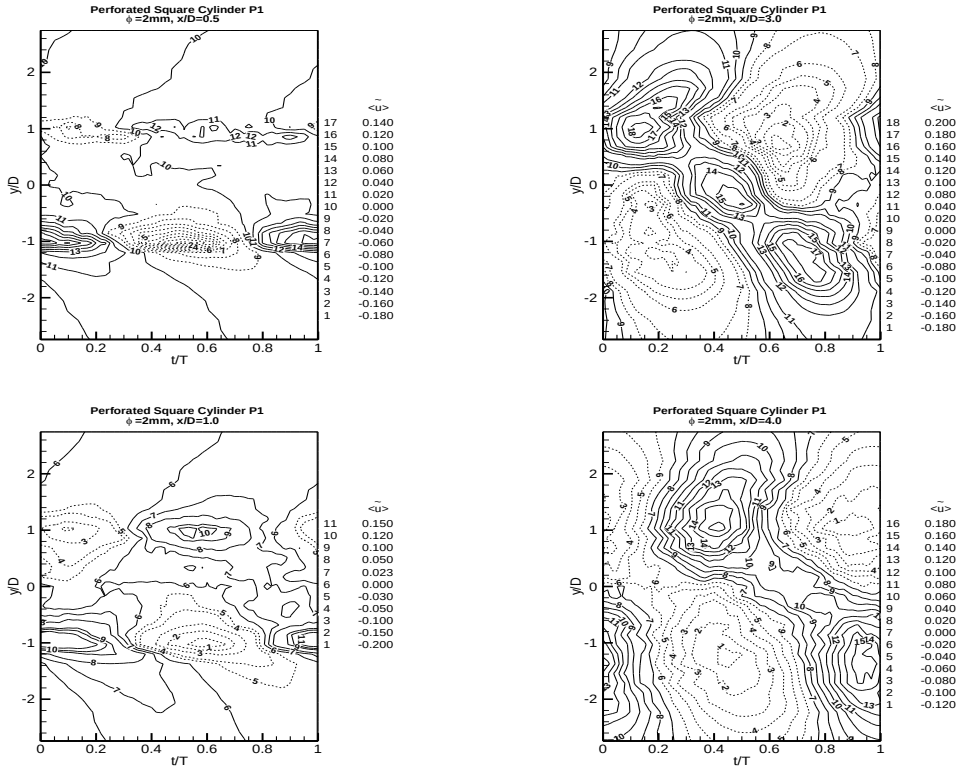

Figure 4.14. Coherent stream wise velocity measured downstream of perforated square cylinder P1

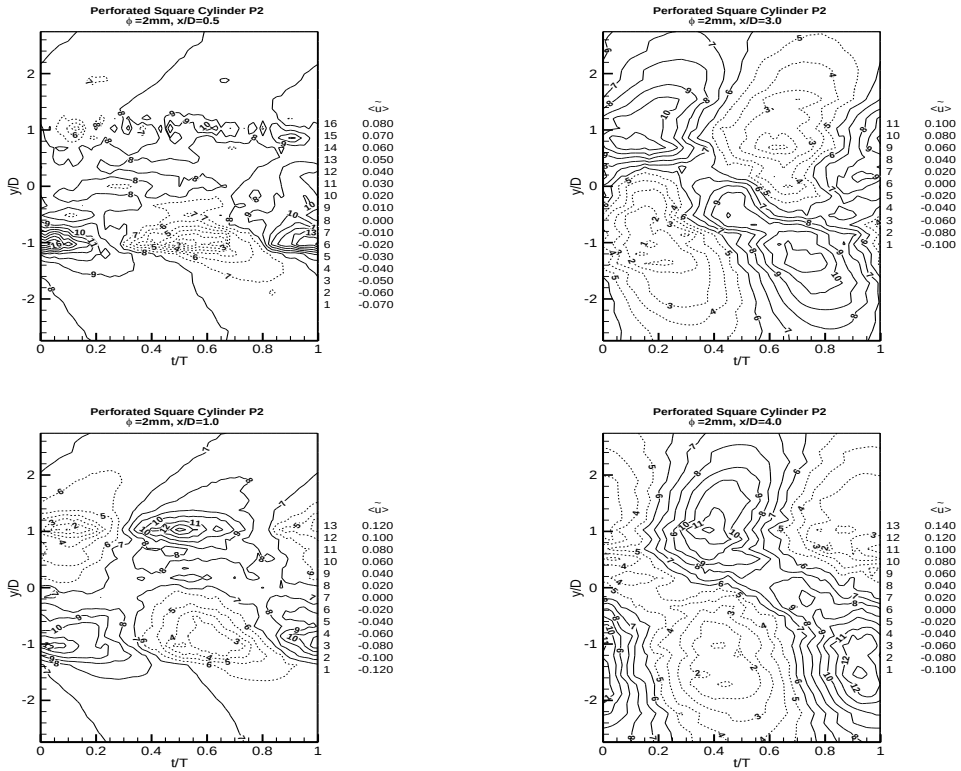

Figure 4.15. Coherent stream wise velocity measured downstream of perforated square cylinder P2

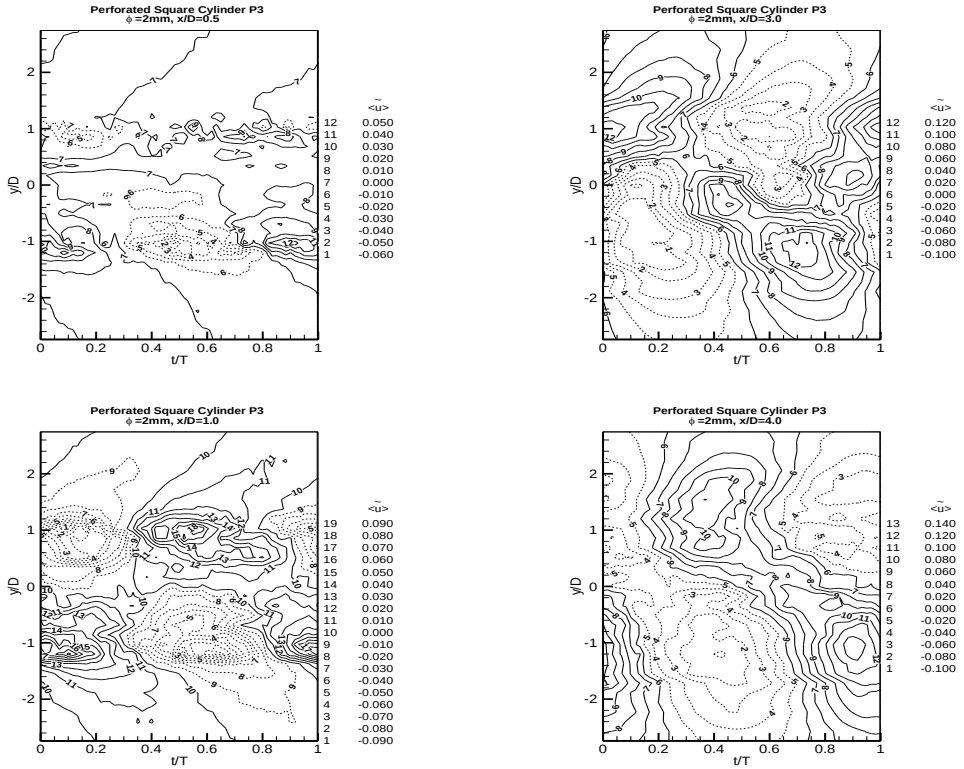

Figure 4.16. Coherent stream wise velocity measured downstream of perforated square cylinder P3

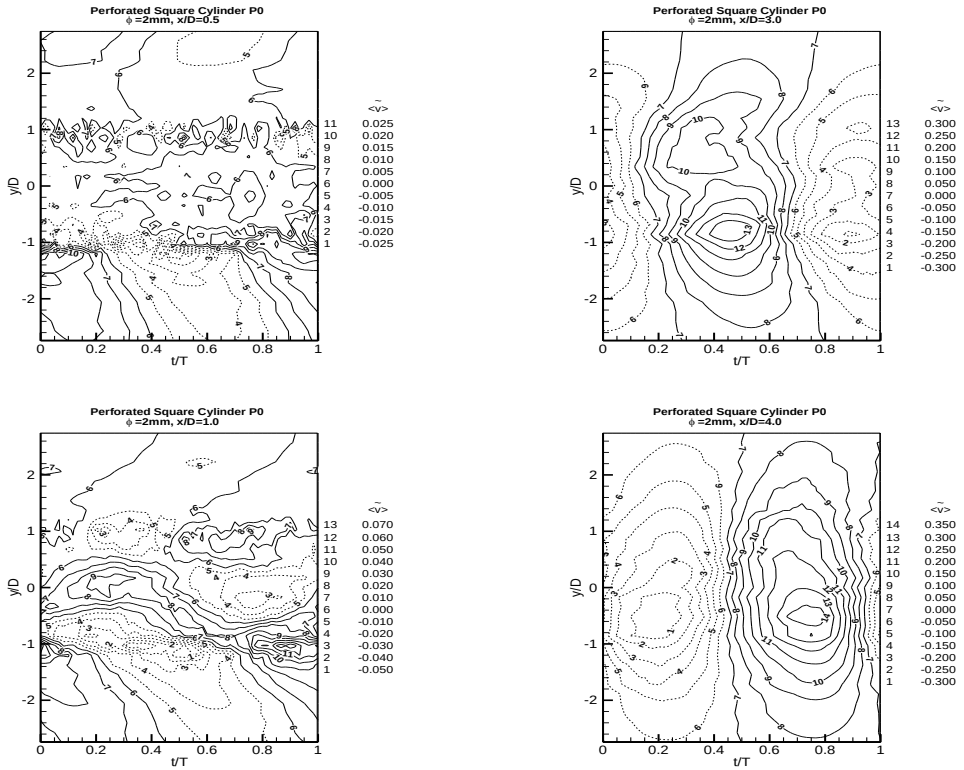

Figure 4.17. Coherent transverse velocity measured downstream of perforated square cylinder P0

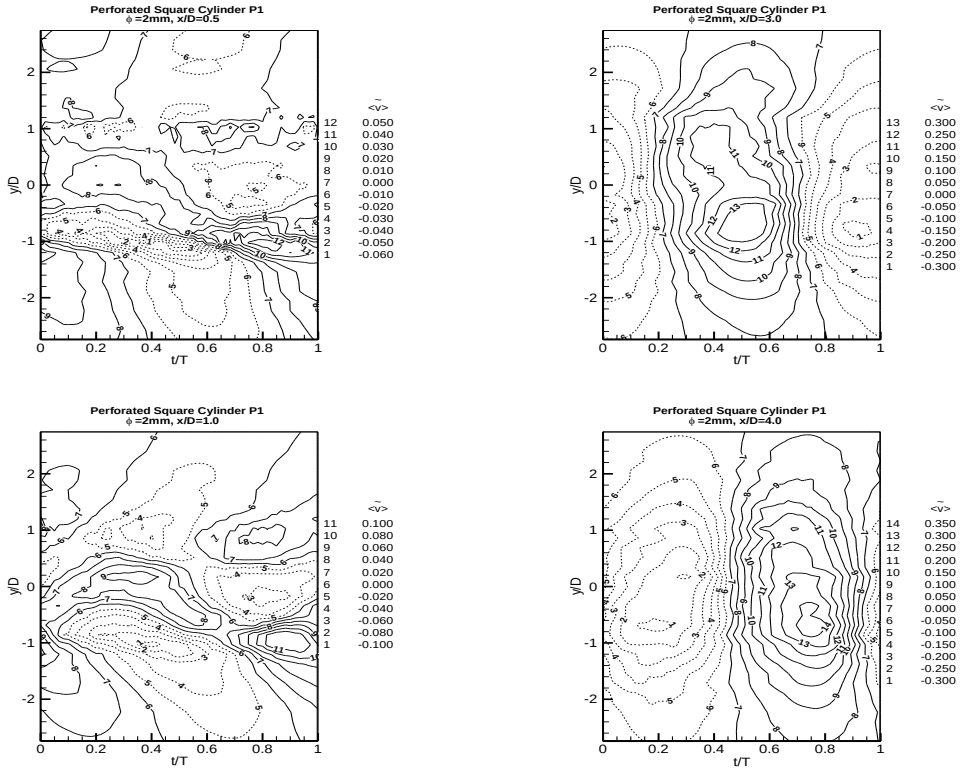

Figure 4.18. Coherent transverse velocity measured downstream of perforated square cylinder P1

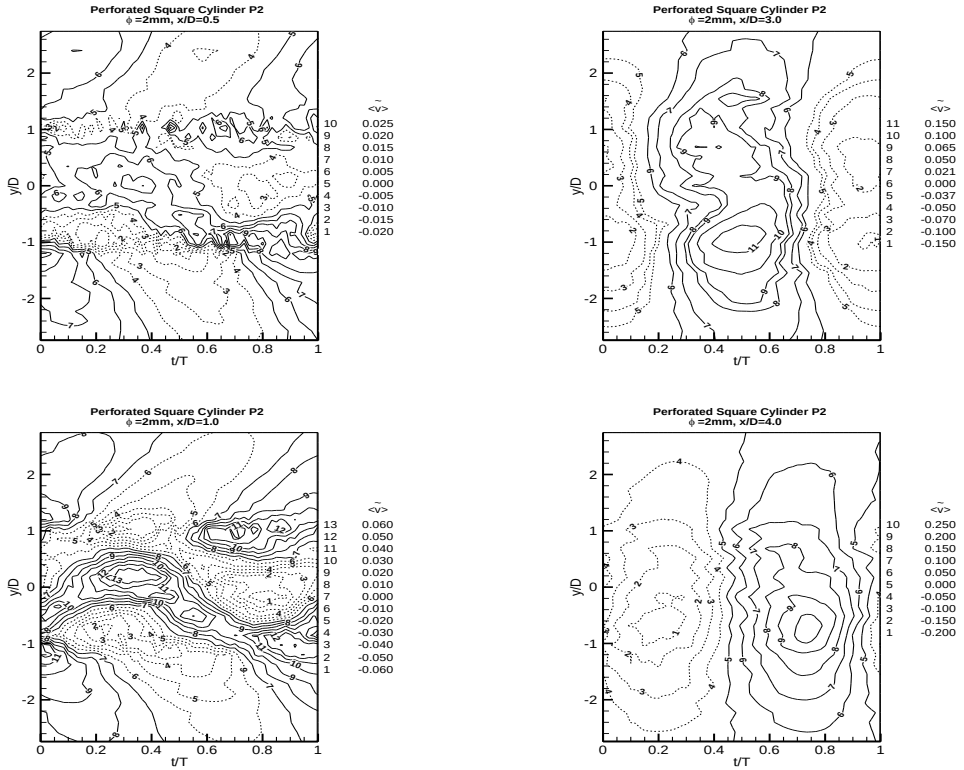

Figure 4.19. Coherent transverse velocity measured downstream of perforated square cylinder P2

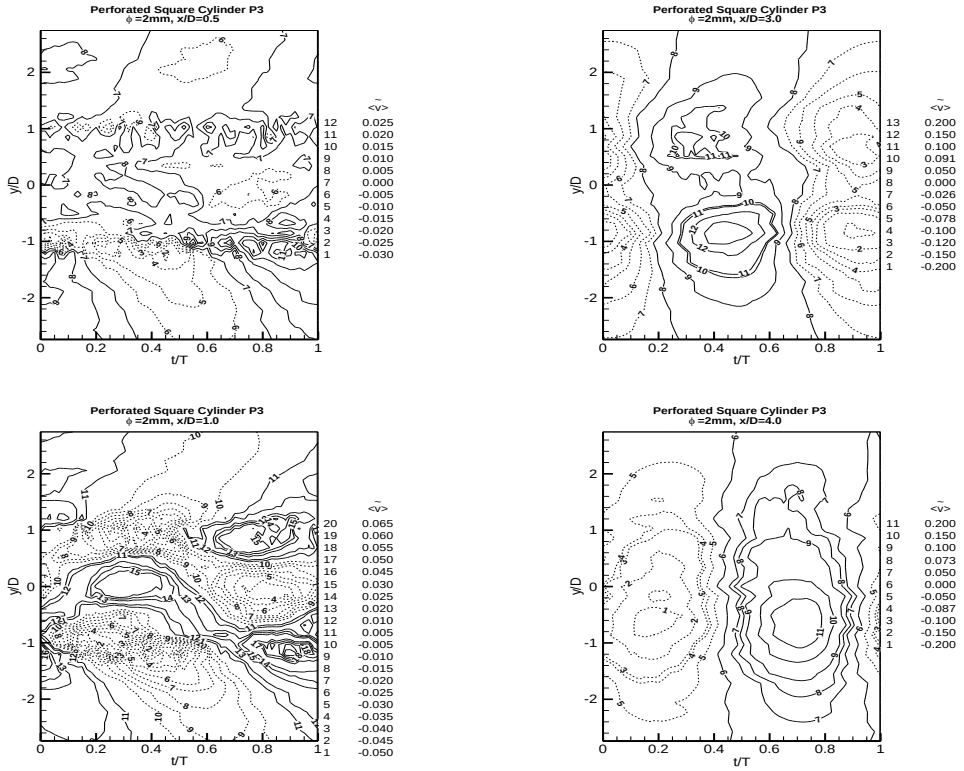

Figure 4.20. Coherent transverse velocity measured downstream of perforated square cylinder P3

As discussed previously, triple decomposition would provide a better illustration of vortex shedding phenomenon. Therefore, to investigate the development of coherent structure of shedding phenomenon, coherent Turbulent Kinetic Energy production in the wake region behind perforated square cylinder P1, have been depicted in figure 4.21.

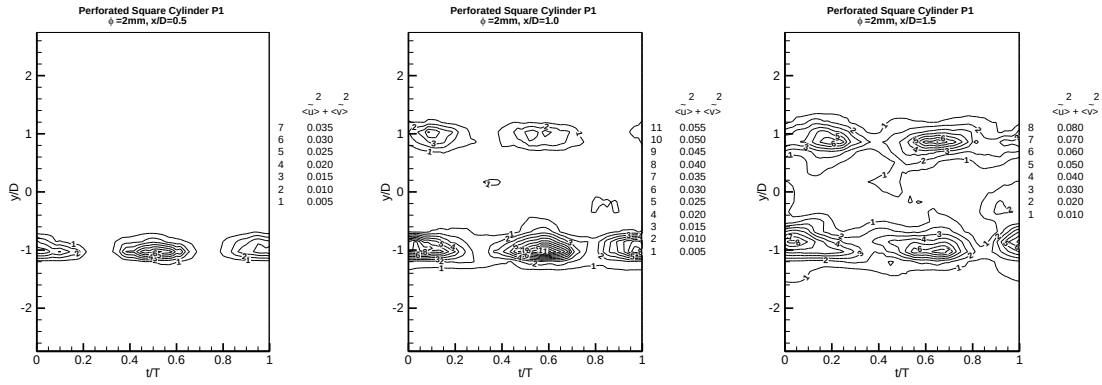

Figure 4.21. Coherent Turbulent Kinetic Energy production in the wake region of perforated square cylinder P1

It can be seen from the figure that at near wake region while coherent structures have been formed beyond the right edge, the wake of left edge showed no evident of coherent structure. As the probe moved downstream, the perforated surface is losing its effectiveness and as result first evident of coherent structure on the left edge was also developed. Farther downstream in the wake (i.e. x/D=4.0) the two coherent structure are combined and formed a larger structure as wide as the wake.

Reduction in coherent TKE production can be a measure of effectiveness of such perforation. As a result the reduction in coherent TKE peak production for P1 (compared with non-perforated square cylinder) varies form 66% to 27% between x/D=0.5 to 1.5 in the downstream wake and beyond the x/D=1.5 the effectiveness drops significantly to approximately 7% at x/D= 3.0. The effectiveness of other perforated surfaces for coherent stream wise and transverse velocities and coherent TKE have been illustrated in table 4.1.

Table 4.1. Reduction in coherent structure peak value for perforated square cylinder

	x/D=0.5			x/D=1.0			x/D=1.5		
	$\langle\tilde{u}\rangle$	$\langle\tilde{v}\rangle$	TKE	$\langle\tilde{u}\rangle$	$\langle\tilde{v}\rangle$	TKE	$\langle\tilde{u}\rangle$	$\langle\tilde{v}\rangle$	TKE
P0	65	86	90	52	73	88	36	56	64
P1	42	64	67	24	54	38	7	16	27
P2	69	86	92	52	73	88	21	50	55
P3	81	86	96	64	77	88	39	63	73

4.5 Time averaged properties

Better understanding of the flow structure also requires to quantify development and decay of flow properties such as stream wise velocity, transverse velocity and turbulent stresses in the downstream wake region. In this section quantitative comparison of time averaged stream wise, time averaged transverse velocity and time averaged turbulent stresses measured at various x/D's in the wake region have

been presented. While, time averaged properties such as stream wise and transverse velocity are normalized with free stream velocity (U_∞), turbulent normal and shear stress are normalized with U_∞^2. Variation of time averaged stream wise and transverse velocity components $\langle \overline{u} \rangle$ and $\langle \overline{v} \rangle$ profile of different perforated square cylinders have been demonstrated in figures 4.22 and 4.23, respectively. From the figures symmetrical and anti-symmetrical variation of $\langle \overline{u} \rangle$ and $\langle \overline{v} \rangle$ profile with respect to wake axis is clearly apparent.

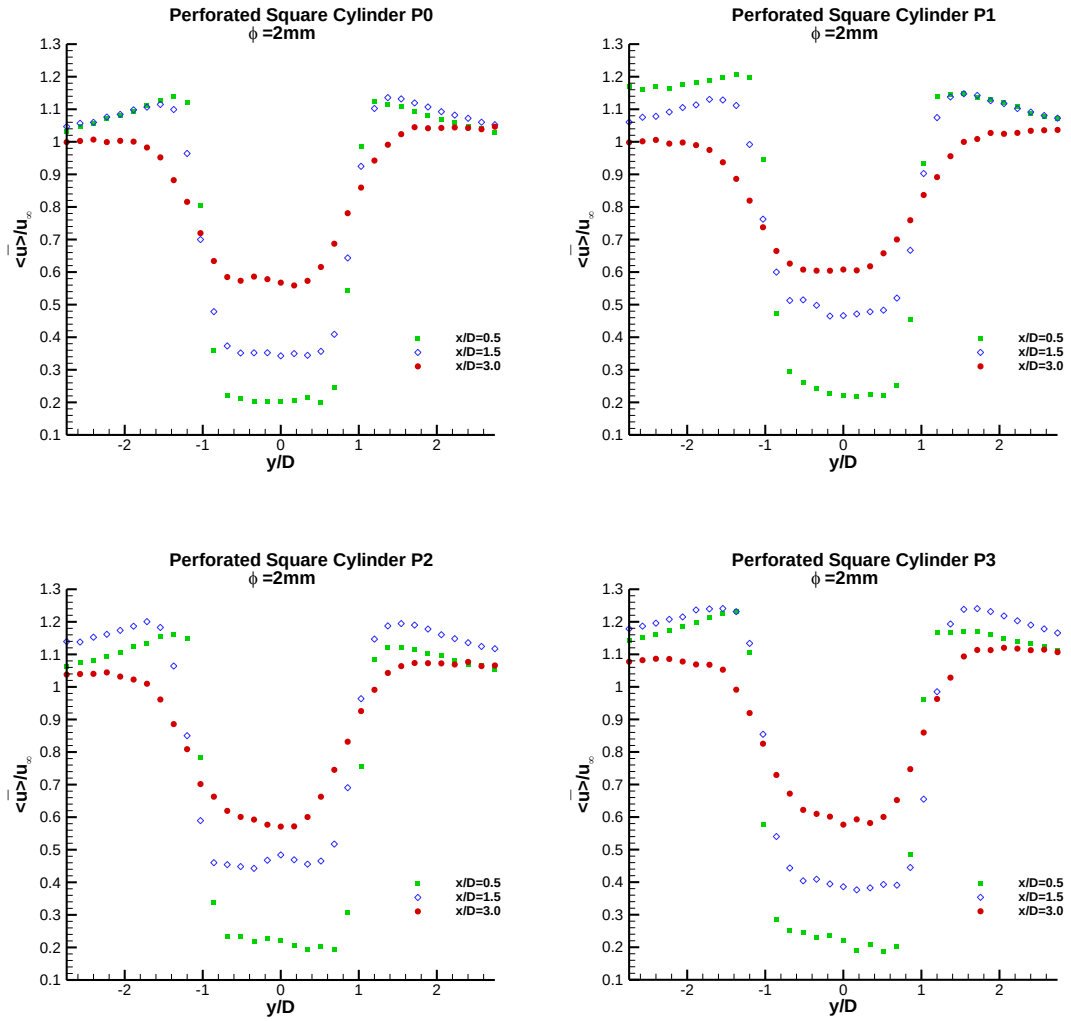

Figure 4.22. Comparison of variation of $\langle \overline{u} \rangle$ for different perforated square cylinders

It can be observed that for the case of perforated square cylinder P1, with no perforated surface in the rear face, the u profile measured at near wake (x/D=0.5),

decreases up to centerline and then increases gradually. However, in case of P0 with a perforated rear face, u profile remains approximately constant with some fluctuation corresponding to the measurement exactly behind the perforations. Moreover, it can be also observed that further downstream the wake, the effect of perforated surfaces were decayed considerably.

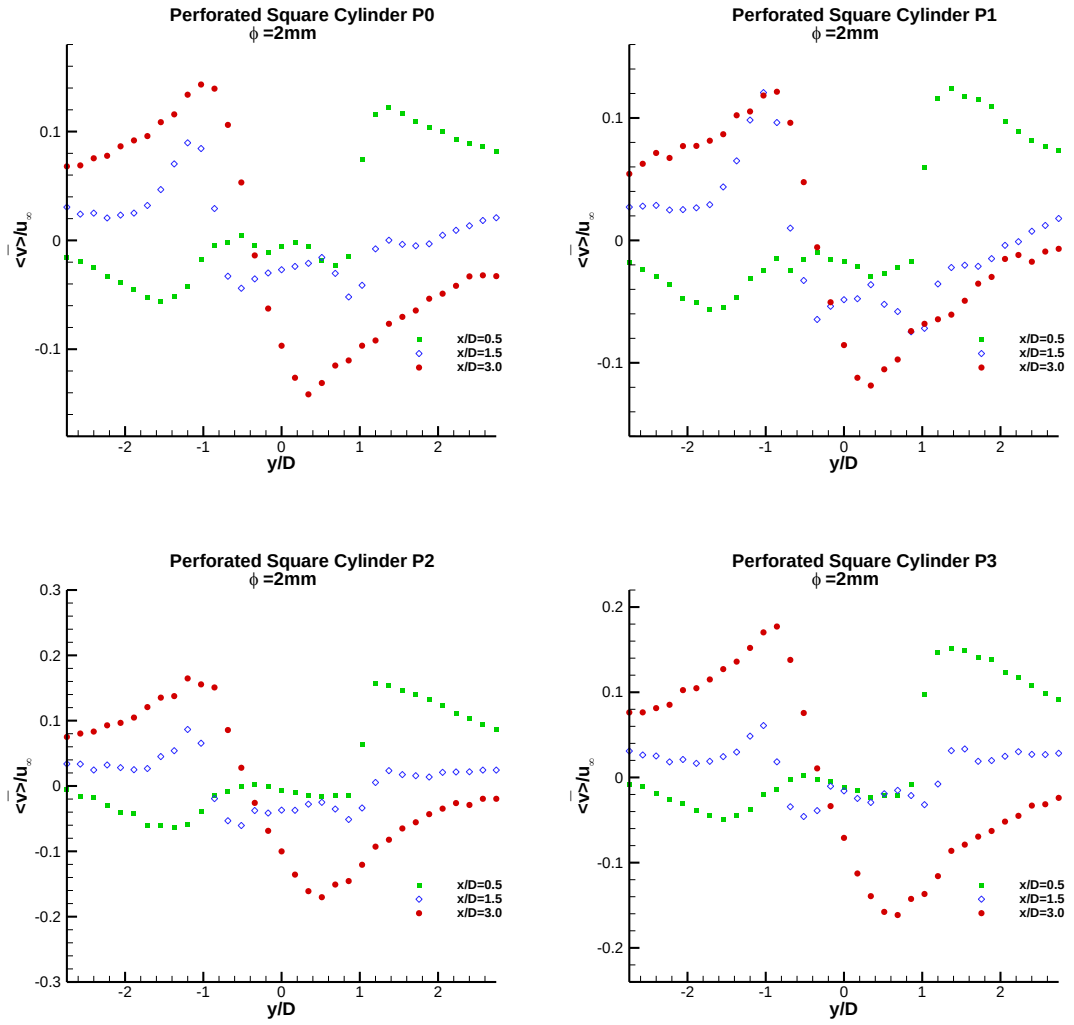

Figure 4.23. Comparison of variation of $\langle \bar{v} \rangle$ for different perforated square cylinders

The effects of perforated surface is more apparent on transverse velocity component plots. It can be observed that within the effective region i.e. x/D=0.5, v profile is affected significantly. The time averaged v profile for P1, which correspond to an antisymmetric perforation, shows that the peak values measure at all x/D's are in the

same order of magnitude. However, other perforated square cylinders with a symmetrical perforation exhibit lower time averaged peak values at near wake measurements.

Time averaged incoherent stream wise and transverse stresses in the downstream wake for different perforated square cylinder measured at x/D=1.0 and 4.0 are illustrated in figures 4.24 and 4.25, respectively. From the figures it can be observed that both stream wise and transverse normal stresses significantly decayed compared with non-perforated square cylinder in the interval of y/D=±1.0 at near wake. However, father downstream the wake at x/D=4.0, incoherent stresses reached to a value close to non-perforated square cylinder.

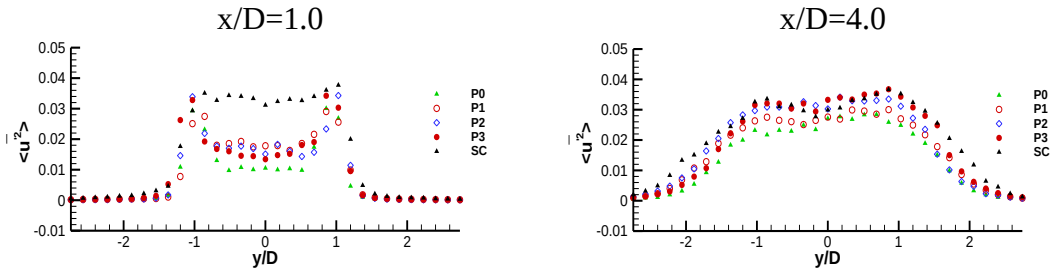

Figure 4.24. Comparison of time averaged incoherent stream wise normal Reynolds stress for different perforations

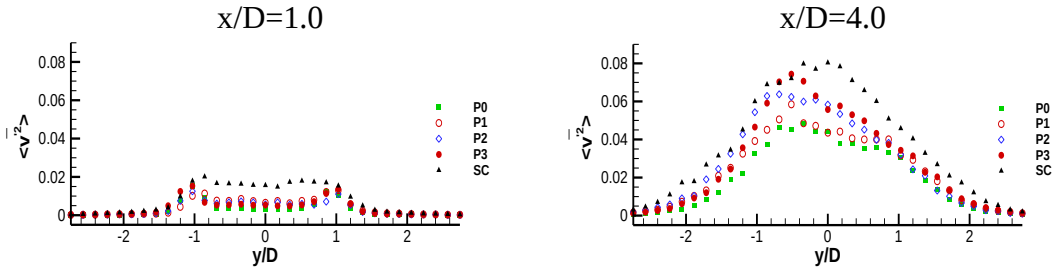

Figure 4.25. Comparison of time averaged incoherent transverse normal Reynolds stress for different perforations

It can be observed that P0 exhibit lowest stream wise and transverse normal stress. Such observation is as a result of direct entrainment of fluid through the perforated

rear side into the wake region together with having the highest entrainment flow rate. Moreover, from figures 4.24 and 4.25 it can be observed that for near wake (x/D=1.0) measurement both stream wise and transverse stresses exhibit double peaks corresponding to the vortex shed from the edges. However, such profile transform gradually to single peak profile as the vortices developed toward the centerline.

In addition, normalized phase averaged turbulent shear stress acquired in the downstream wake of different perforated square cylinder are illustrated in figure 4.26. It can be observed that turbulent shear stresses reaches a positive and negative peak at y/D= -1 and 1, while the sign change of turbulent shear stress along the wake centerline is apparent.

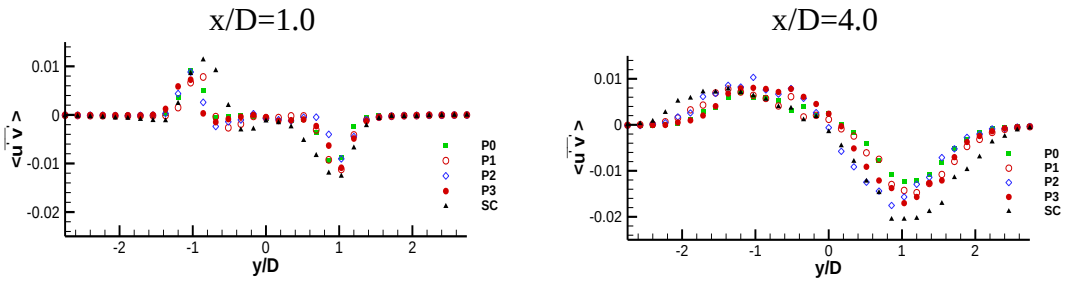

Figure 4.26. Comparison of incoherent time averaged incoherent turbulent shear stress for different perforations

Clearly, insufficient number of phases during one cycle resulted in discrete variation for phase averaging rather than a continuous variation of the properties. However, in this study with employing 60 phases during one cycle, the time mean phase averaged properties over one cycle are zero within accuracy of ±1 %. Such observation has been illustrated in figure 4.27 for coherent stream wise and transverse velocity components.

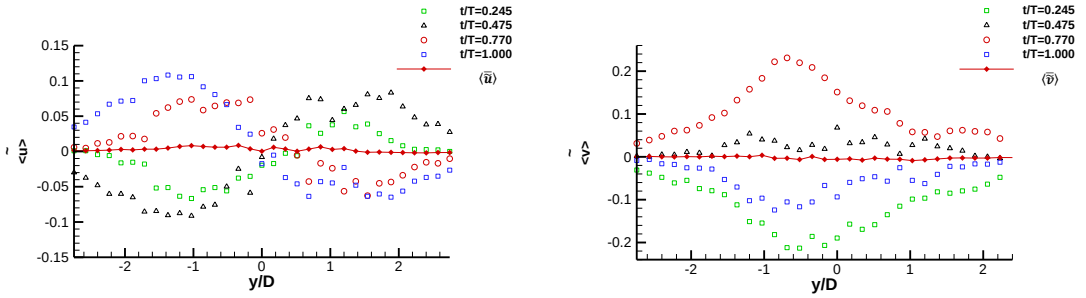

Figure 4.27. Phase averaged coherent velocity components profile measured at x/D=4.0 at various normalized times

4.6 Experimental Uncertainty

The measurement errors by CTA hotwire systems were under influence of calibration equipment, positioning (the alignment of the probe in the experimental set-up), linearization (curve fitting), electrical noise and turbulence intensity of free stream. However, the commercial CTA's have low drift and low noise with negligible effects on uncertainty of measurement. A dedicated calibrator has been employed for the calibration process and therefore the uncertainty due the calibrator would be in order of MSE (Mean Square Error) of the calibrated probes that were in the range of 0.02 – 0.05%. On the other hand, CTA velocity measurement accuracy depends on the turbulence intensity level of the flow. Error in high turbulence intensity (around 35%) wake region for X wire measurements has been reported by Tutu and Chevray (1975) up to 28%. In this work regions with similar level of turbulence intensity and also regions with turbulence intensity 15% or lower have been observed.

Therefore, the error in result such as figure 4.21 might match to a value as reported by Tutu and Chevray (1975) for high turbulence intensity hot wire measurements. However, for u component measurement in high turbulence intensity wake region such as figures 4.5 to 4.8, error is compatible with accuracy of the calibration which is less than 2% in this work.

Chapter 5

INTERACTING WAKES OF TWO INCLINED FLAT PLATES IN TANDEM ARRANGEMENT

5.1 Introduction

In this chapter vortex shedding phenomenon behind two inclined flat plates in tandem arrangement have been studied experimentally. The effects of gap ratio (g/D) between the plates together with angle of attack (α) on the wake flow structure, incoherent and coherent properties have been investigated.

Different set of experiments have been conducted for gap ratios 0.5 and 2.0 between the plates replicating single and dual body vortex shedding mode. In addition, various angle of attack (45-75 degree) have been studied to probe the effects of inclination on the wake region in terms of shedding frequency and Strouhal number variation.

The measurements have been carried out at constant free stream velocity of U_∞=10.75 ± 2% m/s, and corresponding Reynolds number 2.1×10^4 (Re=ρUD/μ based on the flat plate width) with measured free stream turbulence intensity 0.6% at this speed. Two flat plates with cross sectional measurement of 30 mm width by 6 mm thickness made of plexiglass with corresponding blockage ratio between 4 - 6% (for angle of attack between 45 to 75 degrees) were used for the experiments. Szepessy and Bearman (1992) and Cowdrey (1962) investigated the use of end plate to preserve two dimensionality of the flow. Therefore, with employing end plates, the aspect ratio of the investigated plates were 14 which was compatible with Szepessy and Bearman (1992) suggestion of min AR for uniform vortex shedding along the

height of the plates. All the measurements were acquired at the midpoint of the wind tunnel in the z-direction where the flow can be considered as two-dimensional flow.

Figure 5.1 illustrates the schematic of the two flat plates in tandem arrangement, experimental set up and the coordinates. The angle of attack for both plates varies between 45 to 75 degrees and the gap between the two plates g/D varies in the range of 0.5 and 2.0 for this experiments, as illustrated in the figure.

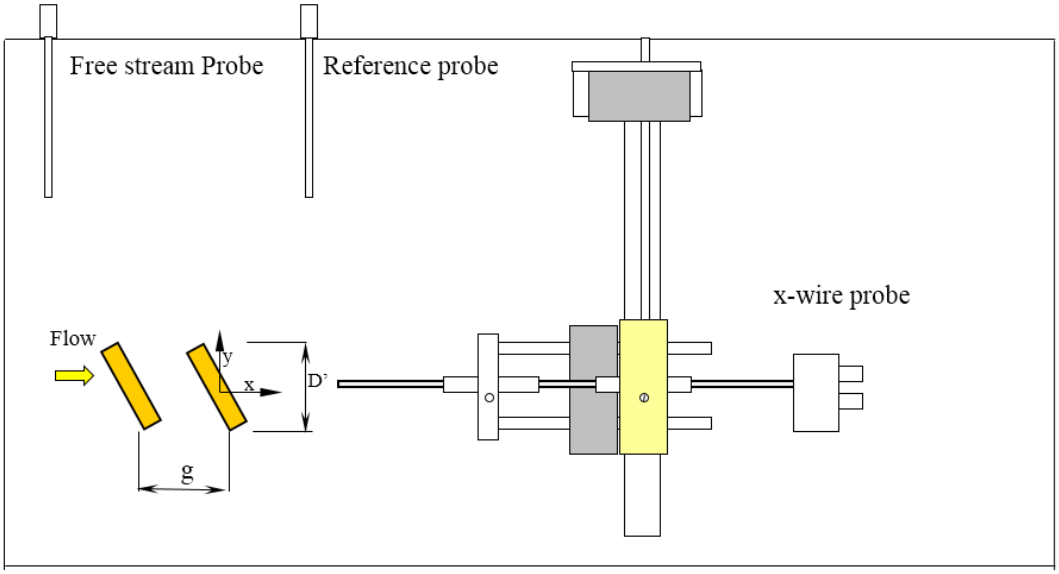

Figure 5.1. Experimental setup and coordinates

The velocity field have been acquired for various x/D between 2.0D to 4.0D ($2.0 \leq x/D \leq 4.0$) downstream the aft plate in the wake region, and to obtain the most distinguishable peak for Fast Fourier Transform analysis, the probe traversed in transverse direction between $y/D = \pm 2.61$.

5.2 Spectral analysis

In order to determine the dominant vortex shedding frequency in the domain of interest Fast Fourier transformation (FFT) has been implemented on the acquired velocity component. As a result, the most powerful spectral peak corresponded to the dominant vortex shedding frequency.

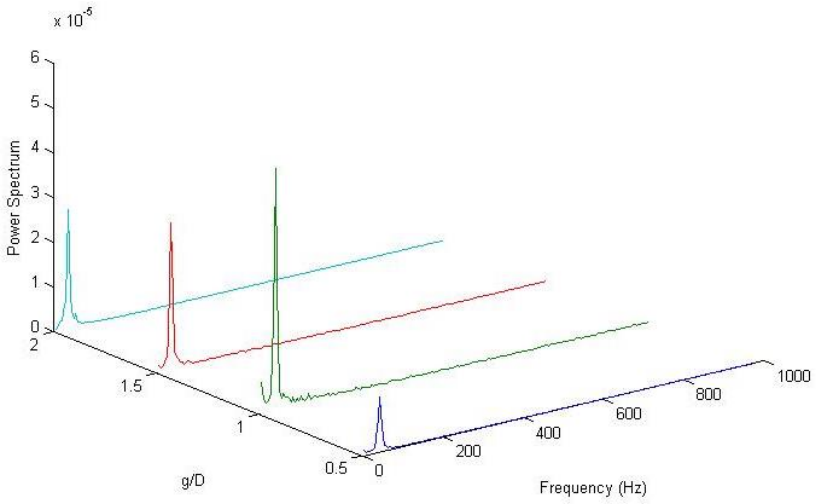

Figure 5.2. Spectral analysis for various g/D at angle of attack 75 and Re =21000.

Spectral analysis of transverse velocity component for various gap ratios between inclined tandem plates at angle of attack 75 and Re =21000 is illustrated in figure 5.2. For all g/D's the dominant shedding frequency is completely apparent as a single peaks with corresponding Strouhal number ($s_t = fD/U_\infty$). Moreover, magnitude of the peaks in the power spectral density graph varies as the g/D between the plates changes.

The computed Strouhal number ($s_t = fD/U_\infty$ based on the plate width) for different angle of attack has been plotted in figures 5.3 and 5.4 for gap ratios 0.5 and 1.5, respectively. From the figures, it can be concluded that Strouhal number decreases as the angle of attack increases.

Moreover, for angle of attack above 75° Strouhal number shows no change or slight changes. Further investigation on other gap ratios between the inclined tandem plates, also demonstrated similar trends for Strouhal number variation.

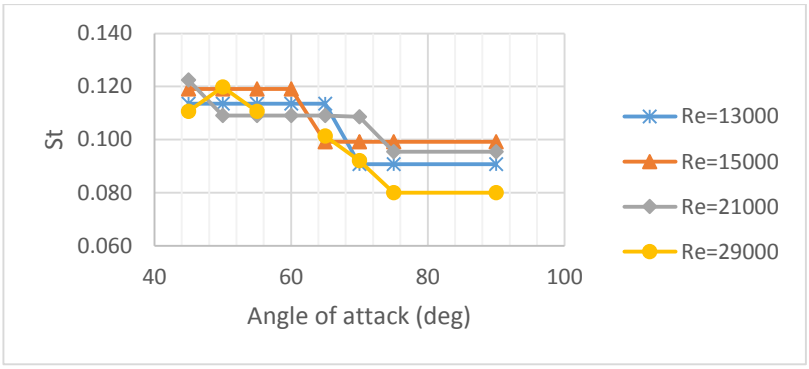

Figure5.3. Strouhal number variation with α for g/D=0.5

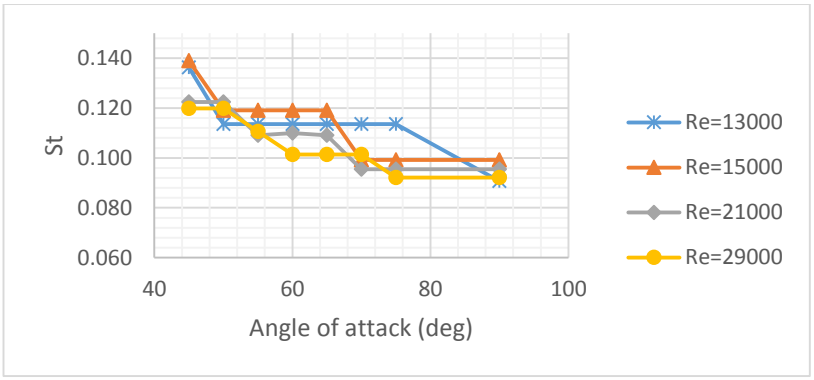

Figure 5.4. Strouhal number variation with α for g/D=1.5

In addition it is also interesting to investigate the Strouhal number of vortex shedding scaled with projected width, D'=D sinα, of the plate normal to flow stream. Knisely (1990) reported that the modified Strouhal number ($s_t{}' = fD'/U_\infty$ based on the plate width) has approximately a constant value. However, as it can be seen from figures 5.5 and 5.6, the reduction in $s_t{}'$ is even more apparent than reduction of s_t.

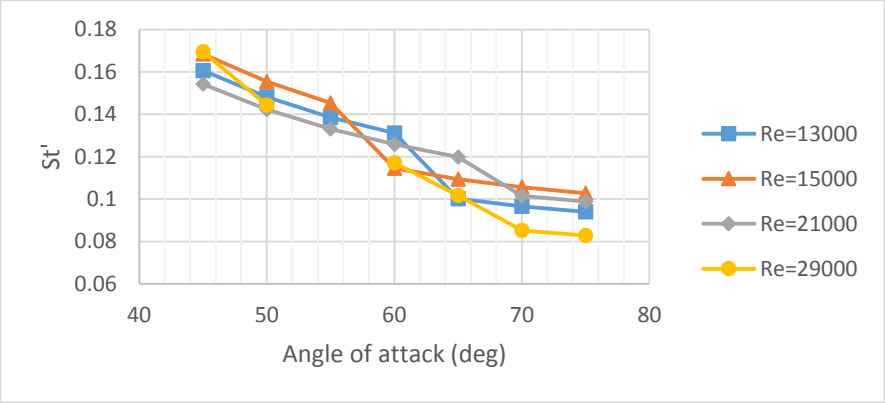

Figure 5.5. Strouhal number variation with α for g/D=5.0

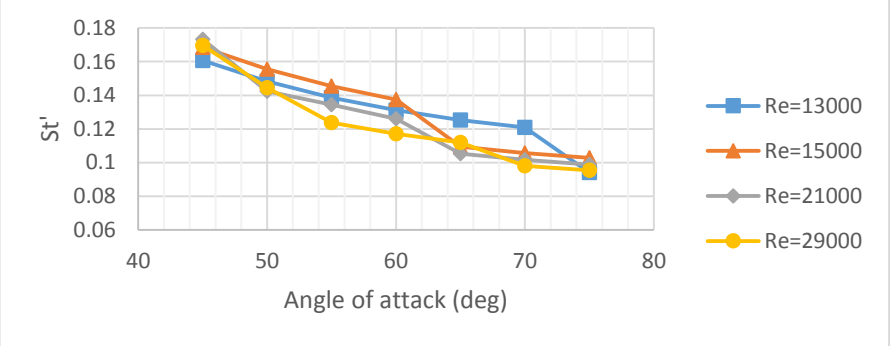

Figure 5.6. Modified Strouhal number variation with α for g/D=1.5

Moreover, variation of Strouhal number with gap ratio for different angle of attack has been investigated. Figures 5.7 and 5.8 illustrate the St Variation for α=75° and 45°, respectively. As it can be seen from the figures, at angle of attack 75° the Strouhal number decreases as the gap between plates increases. However, at angle of attack 45° the Strouhal number initially increases as the gap ratio increases to g/D=1.0 and then for further gap between the plates Strouhal number started to decline.

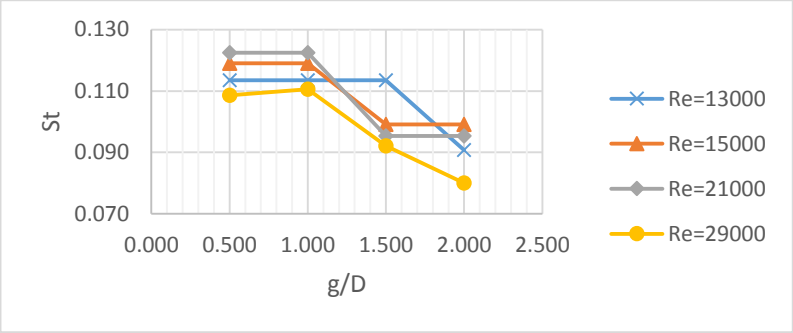

Figure 5.7. Strouhal number variation with gap ratio for α=75°

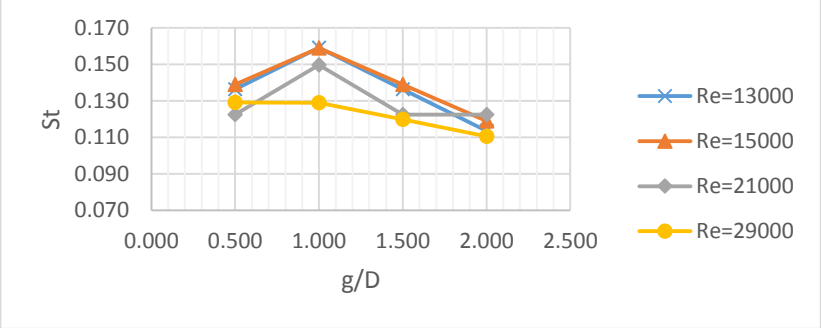

Figure 5.8. Strouhal number variation with gap ratio for α=45°

5.3 Phase Averaged flow structure

One of the objective of this study is to investigate the formation of vortex street in the wake region of two tandem inclined flat plates at high incidence. Development of flow structure and vortex shedding in the wake region behind one single plate and also two inclined plates have been illustrated through figures 5.9 to 5.17. From the figures the vortex shedding phenomenon and the periodic flow patterns for both stream wise and transverse velocity components are completely evident.

One feature of stream wise velocity contours is that two low level zones exist along the centerline downstream of the aft plate. These two low level zone drifted ¼ period from each other. Therefore, such observation implies that the downstream wake behind the aft plate encounters a shedding frequency twice the reference frequency of vortex shedding in stream wise direction. This observation also has been

confirmed by implementing FFT analysis on acquired stream wise data behind the aft plate. Such phenomenon would be as a result of interaction of two shear layers initiated from the edges of the plates. However, the wake regions beyond the edges were encountering normal shedding frequency. In contrary to stream wise velocity data, such variation of Strouhal number has not been observed in transverse direction. Another interesting feature of stream wise contour is that in addition to two low level zones close to the centerline, two peaks exist at the same normalized time (t/T) at the edges of the wake. These alternating peaks correspond to the vortices shed from initiated shear layers of the edges of plates.

The evolution from single body shedding mode to dual body shedding mode is also evident from stream wise contours. For the stream wise measurements at x/D=4.0 it can be seen that the low level zone were formed close to the center line behind the single inclined plate. However these low level regions were offset from the centerline towards the edges for two tandem inclined plate with g/D=0.5. Then, increasing the gap ratio to g/D=1.5 between the plates causes these zones shifted towards the centerline again.

Moreover, comparison of the stream wise and transverse velocity contours demonstrated that although the peaks of stream wise velocity were formed close to the center line, maximum positive and negative magnitude in the case of transverse velocity existed and developed beyond the edges of the plates in the wake region. Remarkably, it was also observed that the peaks in stream wise velocity coincide with changes in transverse velocity direction, which is the evident of formation of Karman Vortex Street. Therefore, as the stream wise velocity reaches its peak, the transverse velocity changes the direction and ¼ period later reaches its peak towards

the centerline. As a result after a vortex is shed, a significant momentum transfer towards the opposite shear layer is observable.

Another significant observation is the development of stream wise and transverse velocity towards downstream in the wake region. As it can be seen from the figures, as the probe move downstream the vortex shedding phenomenon is more apparent from stream wise velocity component and it exhibit more waviness structure. On the other hand, the transverse velocity develops toward the centerline and at x/D=4.0 it become approximately as wide as the wake region.

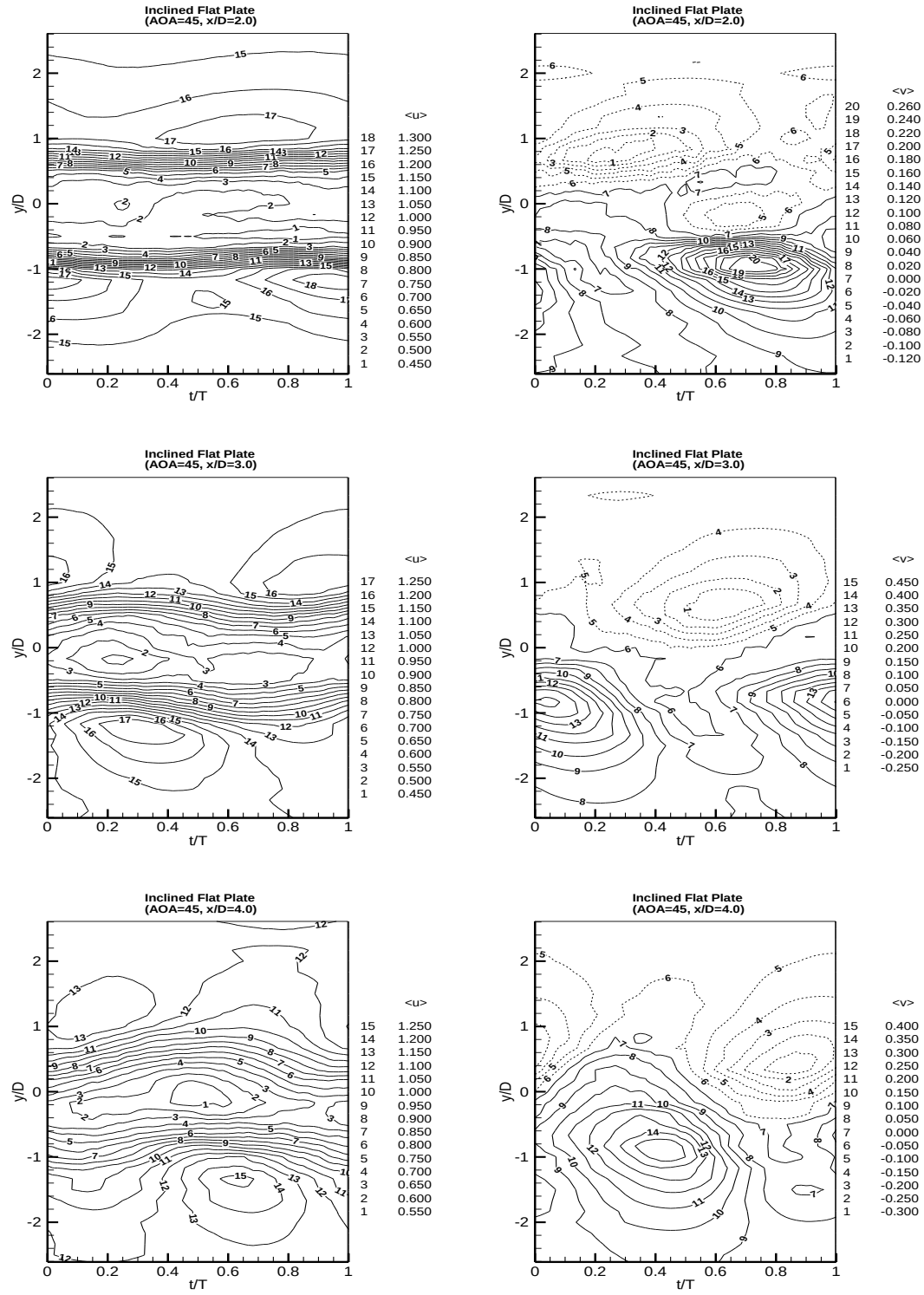

Figure 5.9. Stream wise and transverse velocity measured at various x/D downstream of single inclined flat plat at α=45

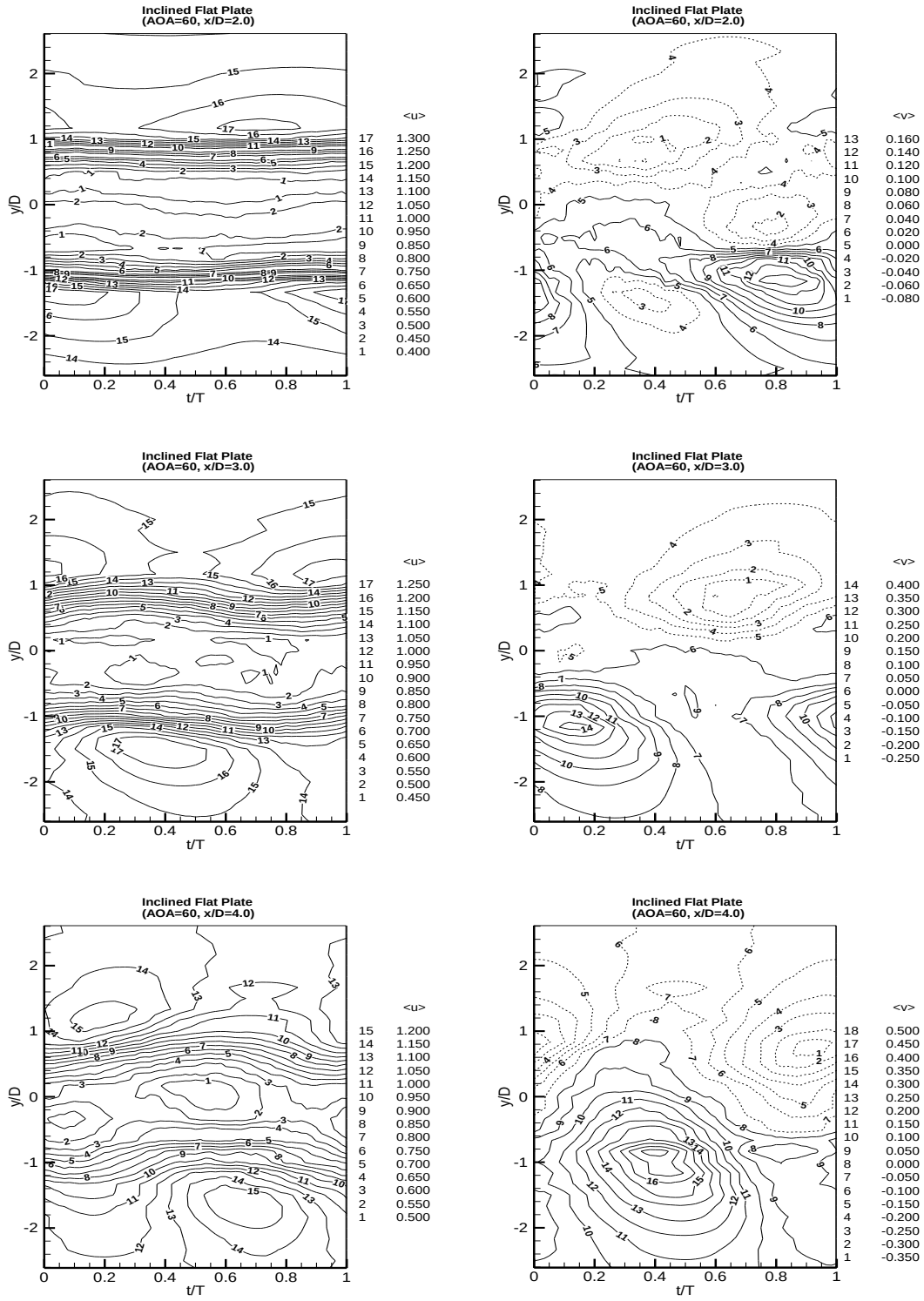

Figure 5.10. Stream wise and transverse velocity measured at various x/D downstream of single inclined flat plat at α=60

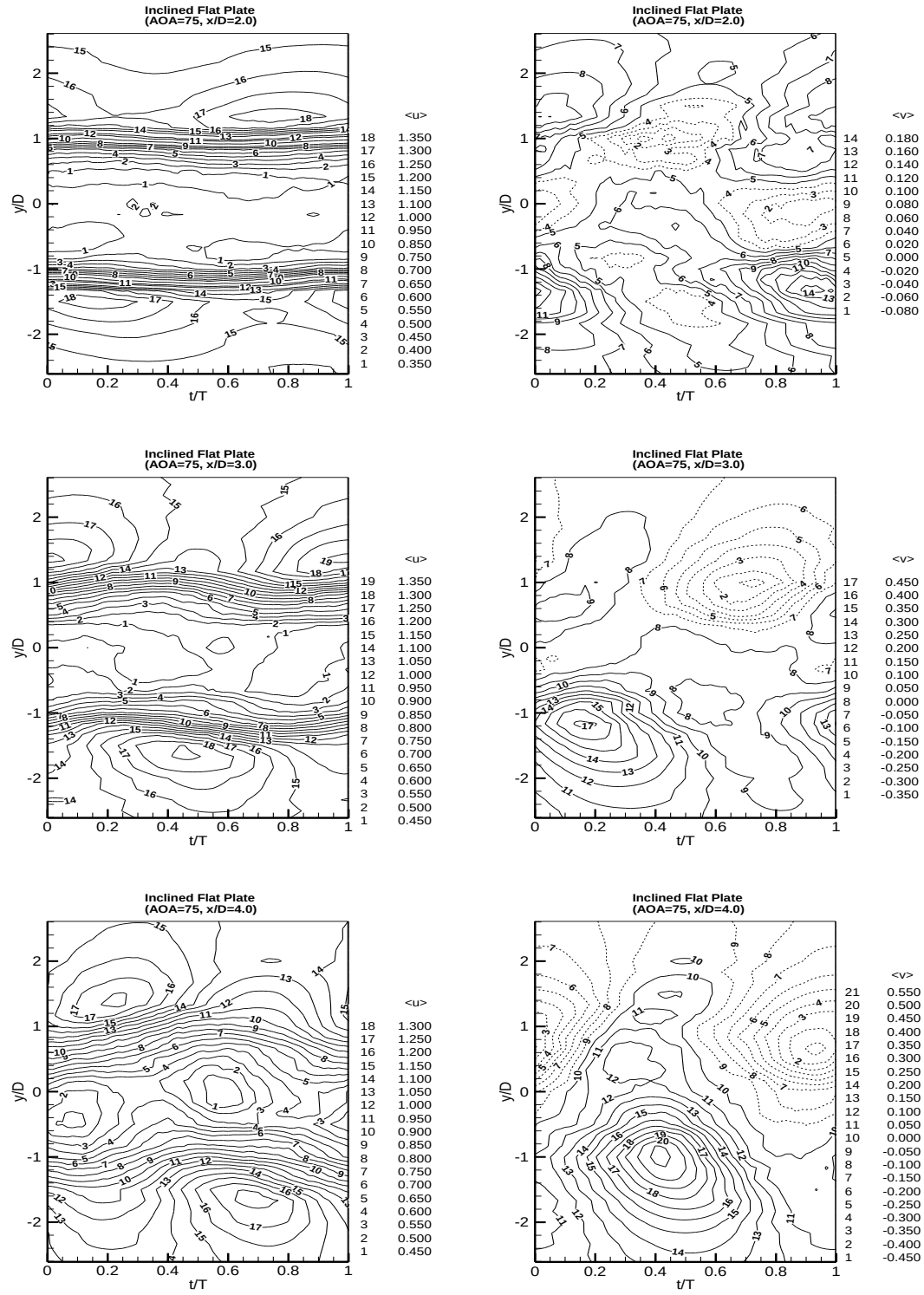

Figure 5.11. Stream wise and transverse velocity measured at various x/D downstream of single inclined flat plat at α=75

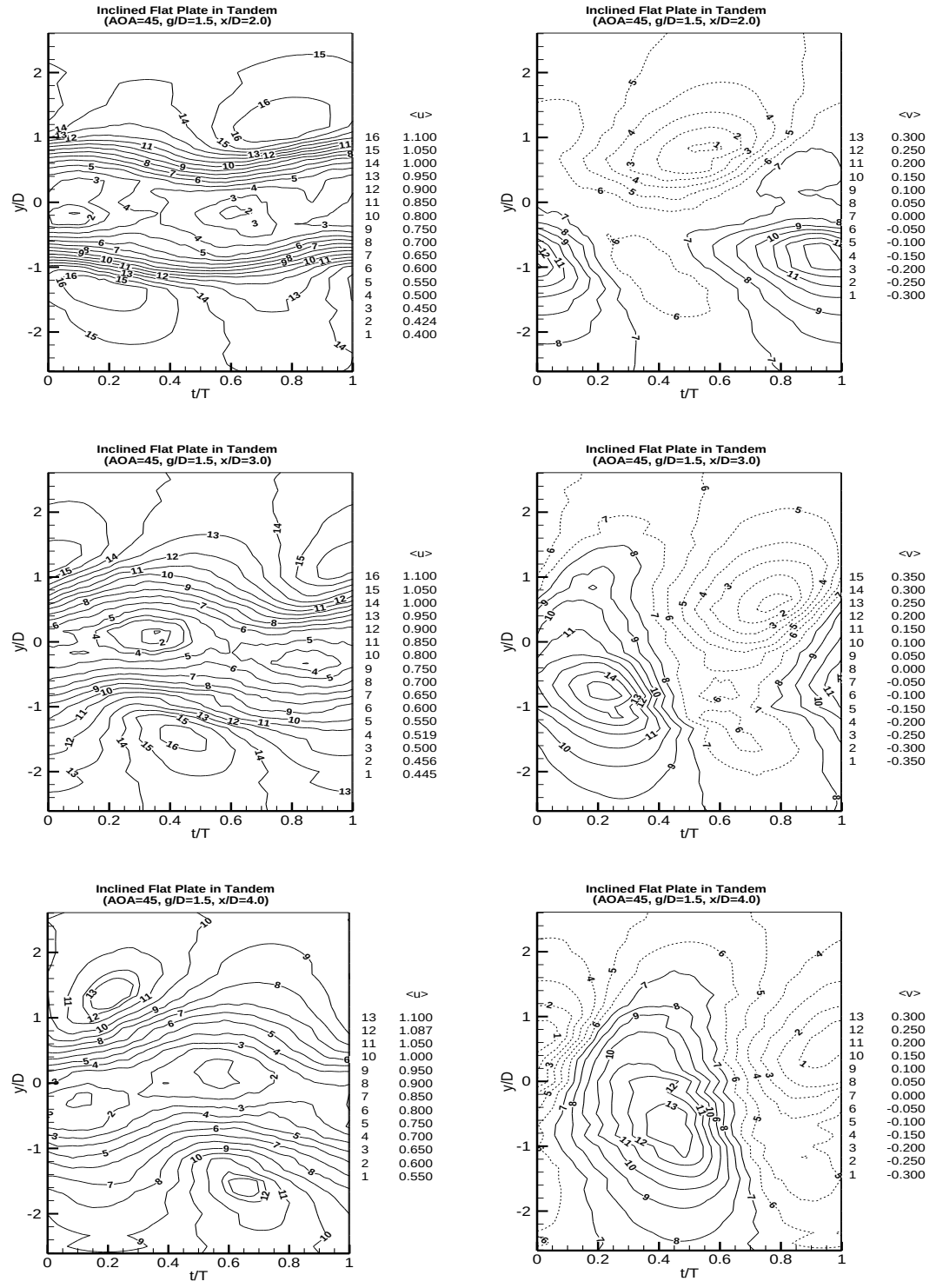

Figure 5.12. Stream wise and transverse velocity measured at various x/D downstream of two tandem inclined flat plates at g/D=1.5, α=45

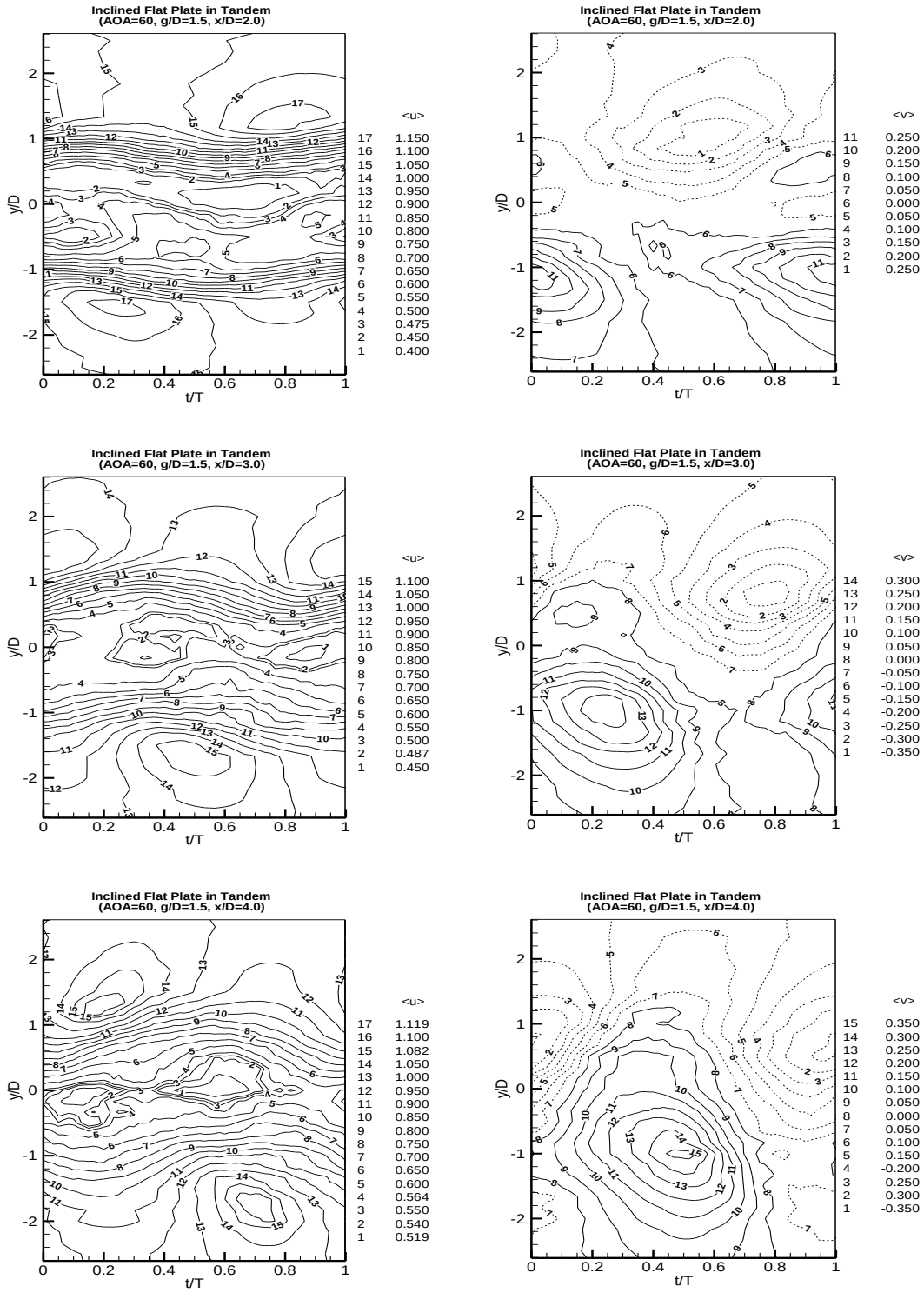

Figure 5.13. Stream wise and transverse velocity measured at various x/D downstream of two tandem inclined flat plates at g/D=1.5, α=60

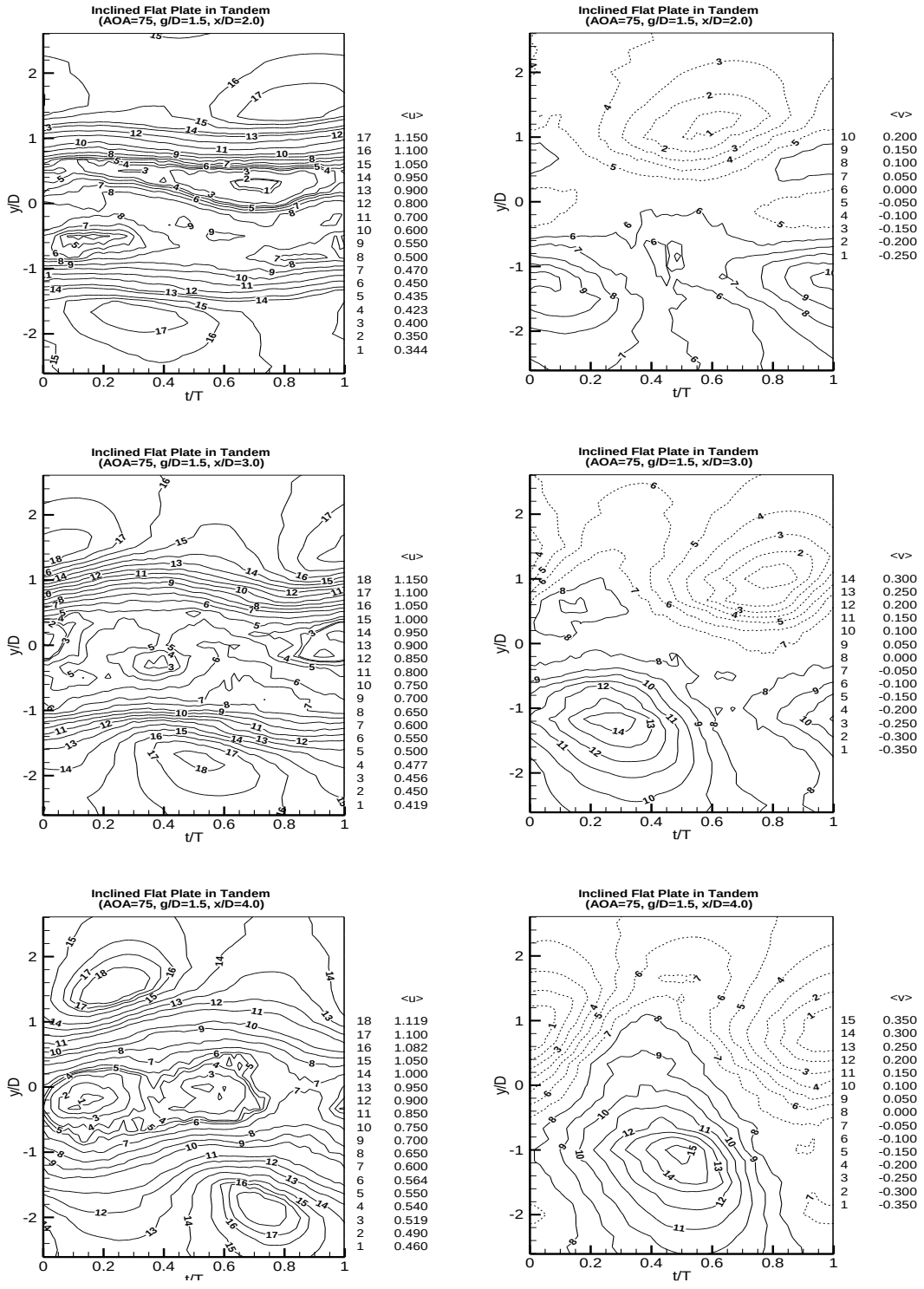

Figure 5.14. Stream wise and transverse velocity measured at various x/D downstream of two tandem inclined flat plates at g/D=1.5, α=75

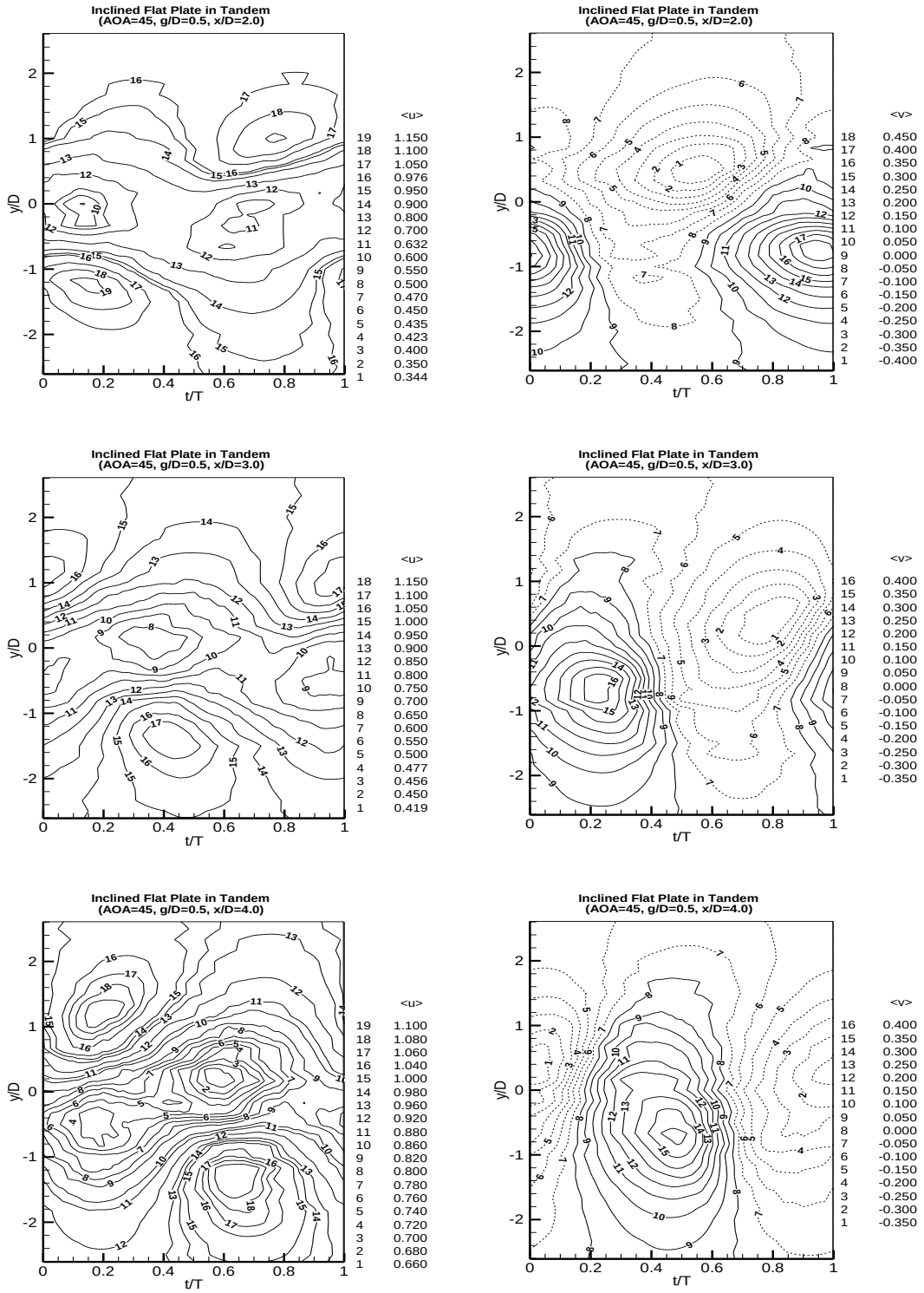

Figure 5.15. Stream wise and transverse velocity measured at various x/D downstream of two tandem inclined flat plates at g/D=0.5, α=45

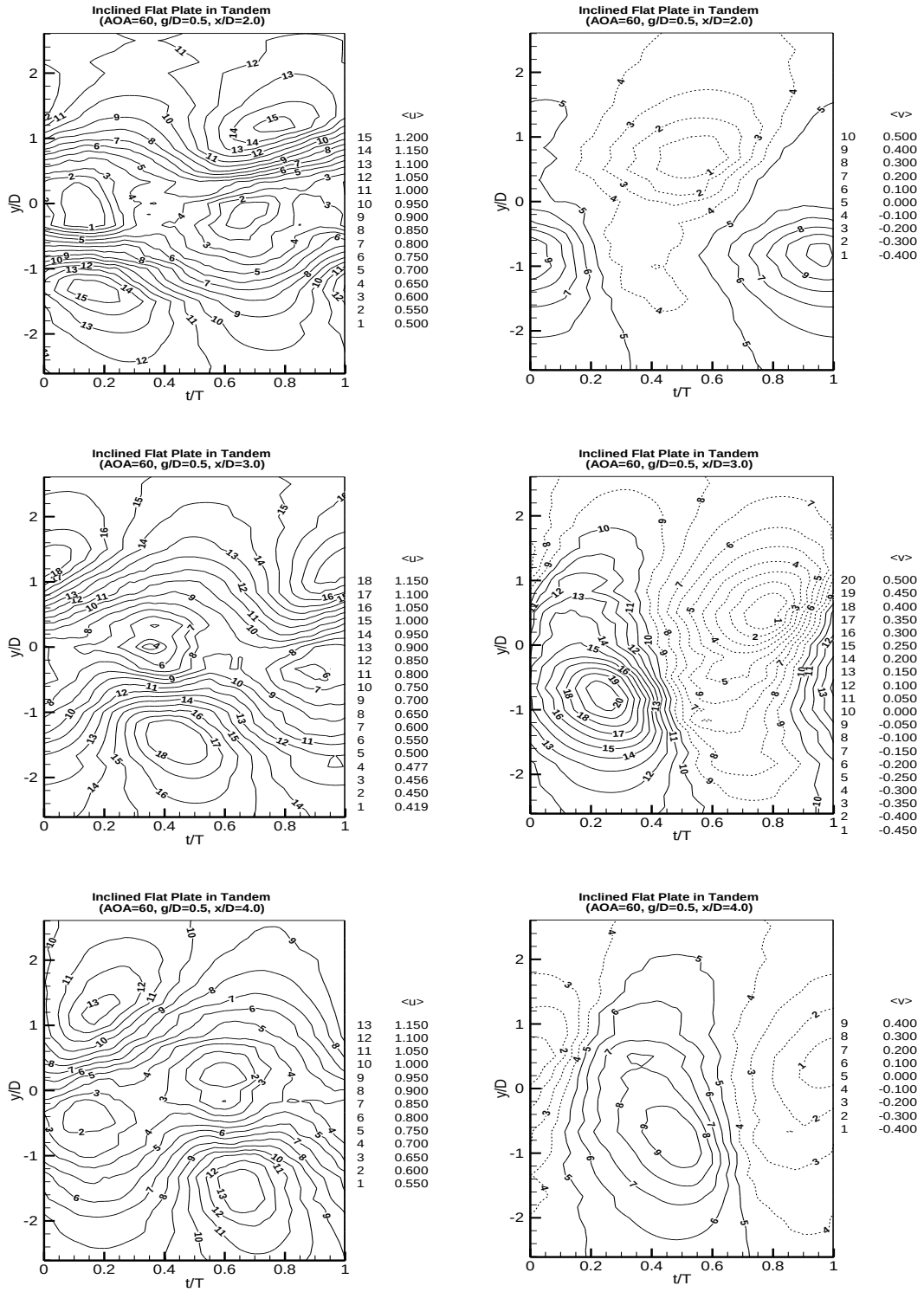

Figure 5.16. Stream wise and transverse velocity measured at various x/D downstream of two tandem inclined flat plates at g/D=0.5, α=60

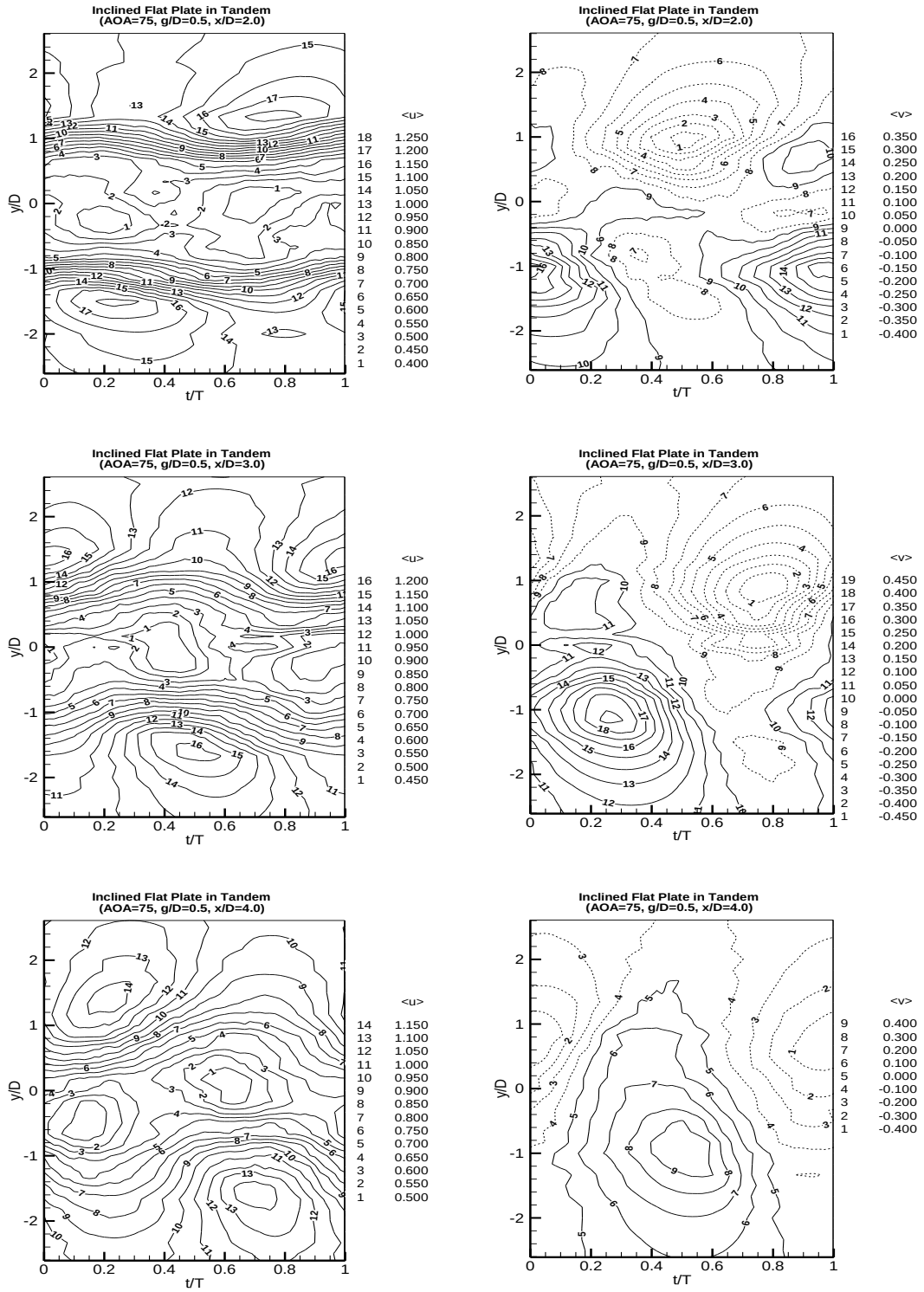

Figure 5.17. Stream wise and transverse velocity measured at various x/D downstream of two tandem inclined flat plates at g/D=0.5, α=75

5.4 Coherent flow structure

As a primary purpose of this study, the Vortex shedding phenomenon have been studied by employing triple decomposition technique rather than classical Reynolds decomposition to distinguish the incoherent turbulent flow fluctuation from coherent vortex shedding structure for a better understanding of this phenomena. Therefore, in this section extracted coherent vortex shed structure from incoherent turbulent fluctuations have been presented in figures 5.18 to 5.26. As it can be seen from the coherent stream wise and coherent transverse velocity contours, vortex shedding phenomenon is more clear and apparent than corresponding phase averaged contours. From the figures the existence of the peak of coherent structure along the edges behind the aft plate are clearly observable. Although the coherent transverse velocity exhibit similar pattern, however as the probe moves downstream the wake the coherent structure transverse direction develops and become as wide as the wake region.

Moreover, it was observed that for the case of tandem plates as the gap between the plates increases the coherent structure in stream wise direction decreases. Such observation is as a result of additional entrainment of the fluid flow into larger gap region between plates during the vortex formation.

Interestingly for the case of tandem plates at g/D=0.5, the coherent structure peaks increased as the angle of attack raised from 45 to 60 degrees. However, as the angle of attack increased to 75 the coherent structures decays.

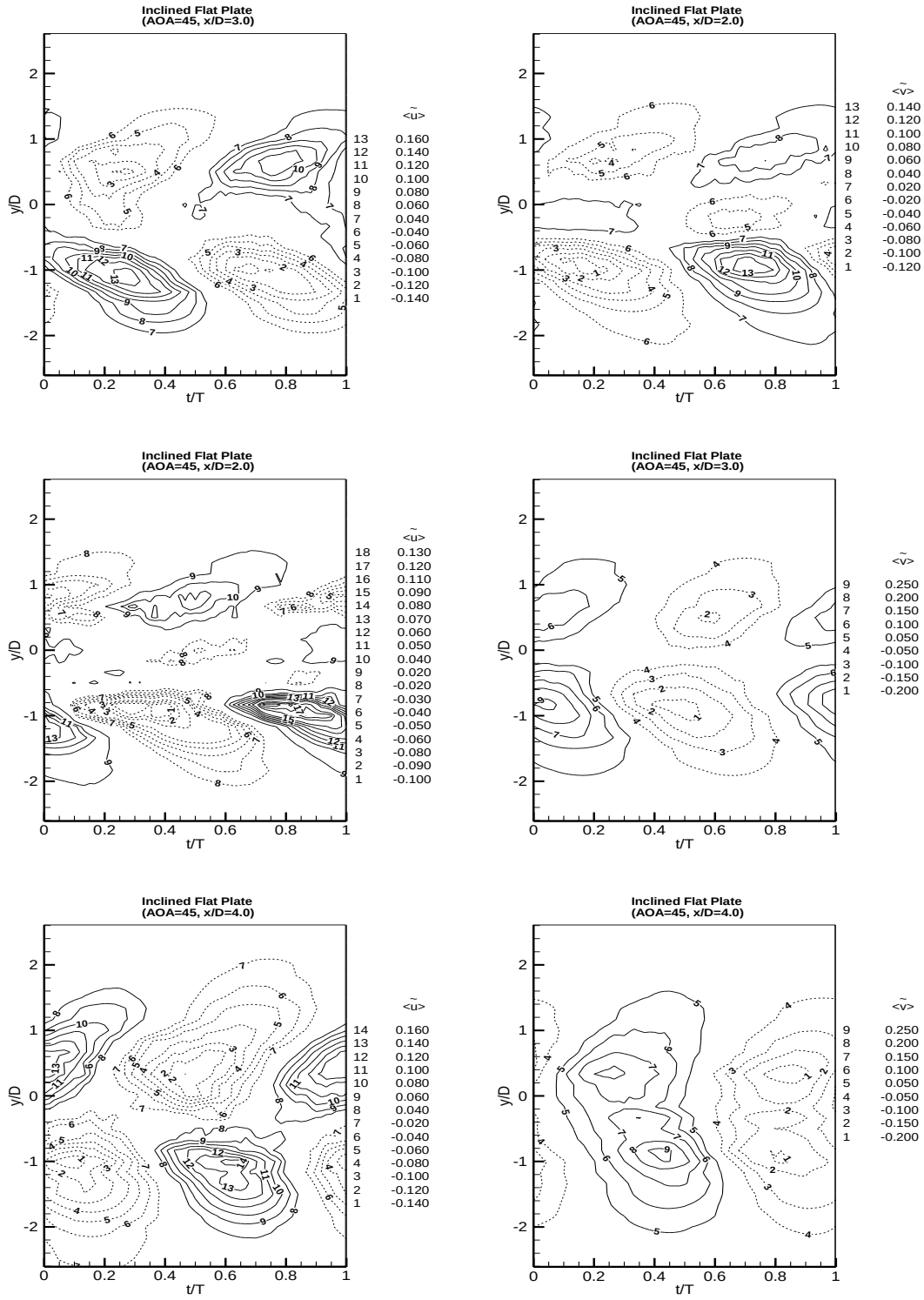

Figure 5.18. Coherent stream wise and coherent transverse velocity measured at various x/D downstream of single inclined flat plat at α=45

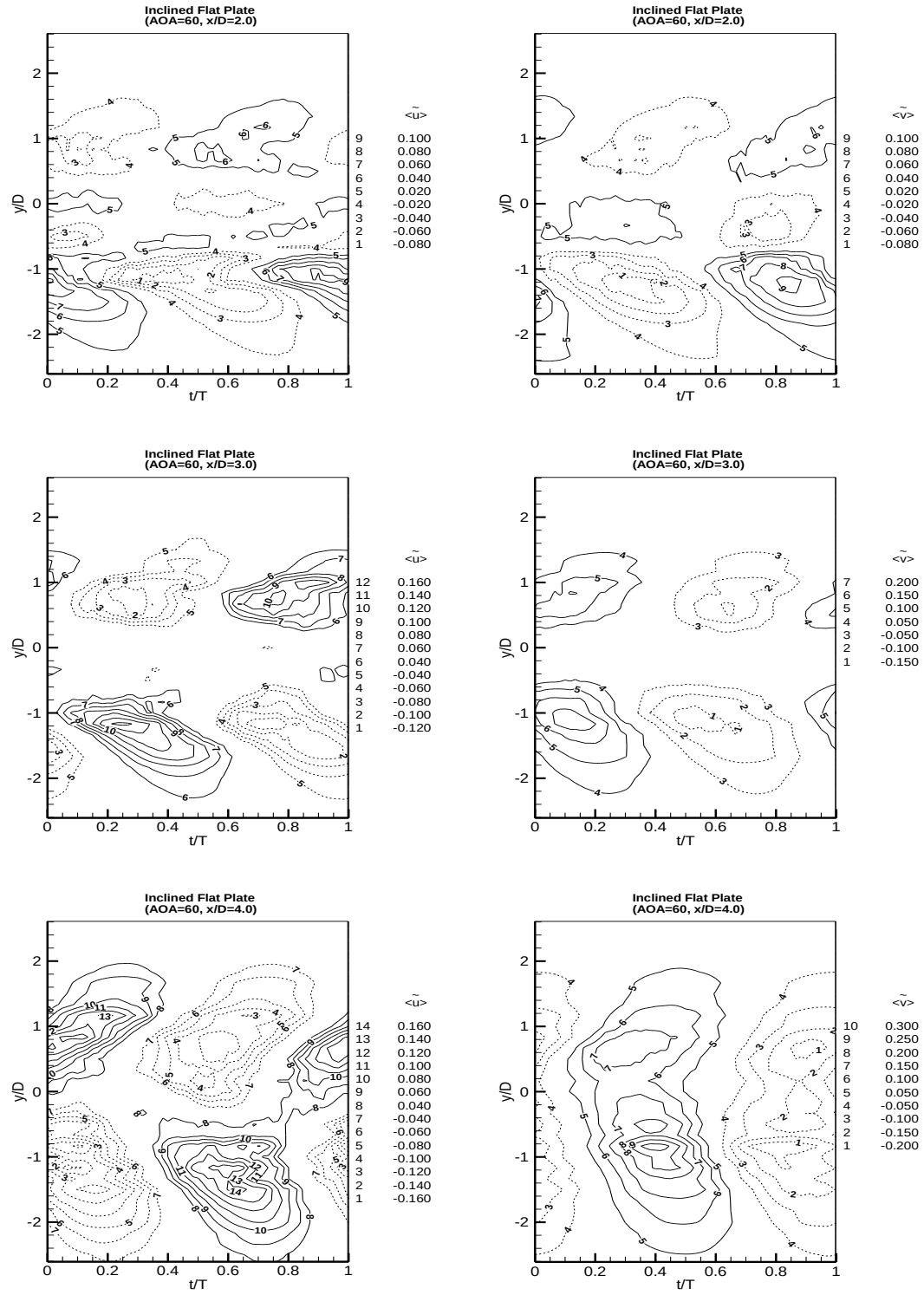

Figure 5.19. Coherent stream wise and coherent transverse velocity measured at various x/D downstream of single inclined flat plat at α=60

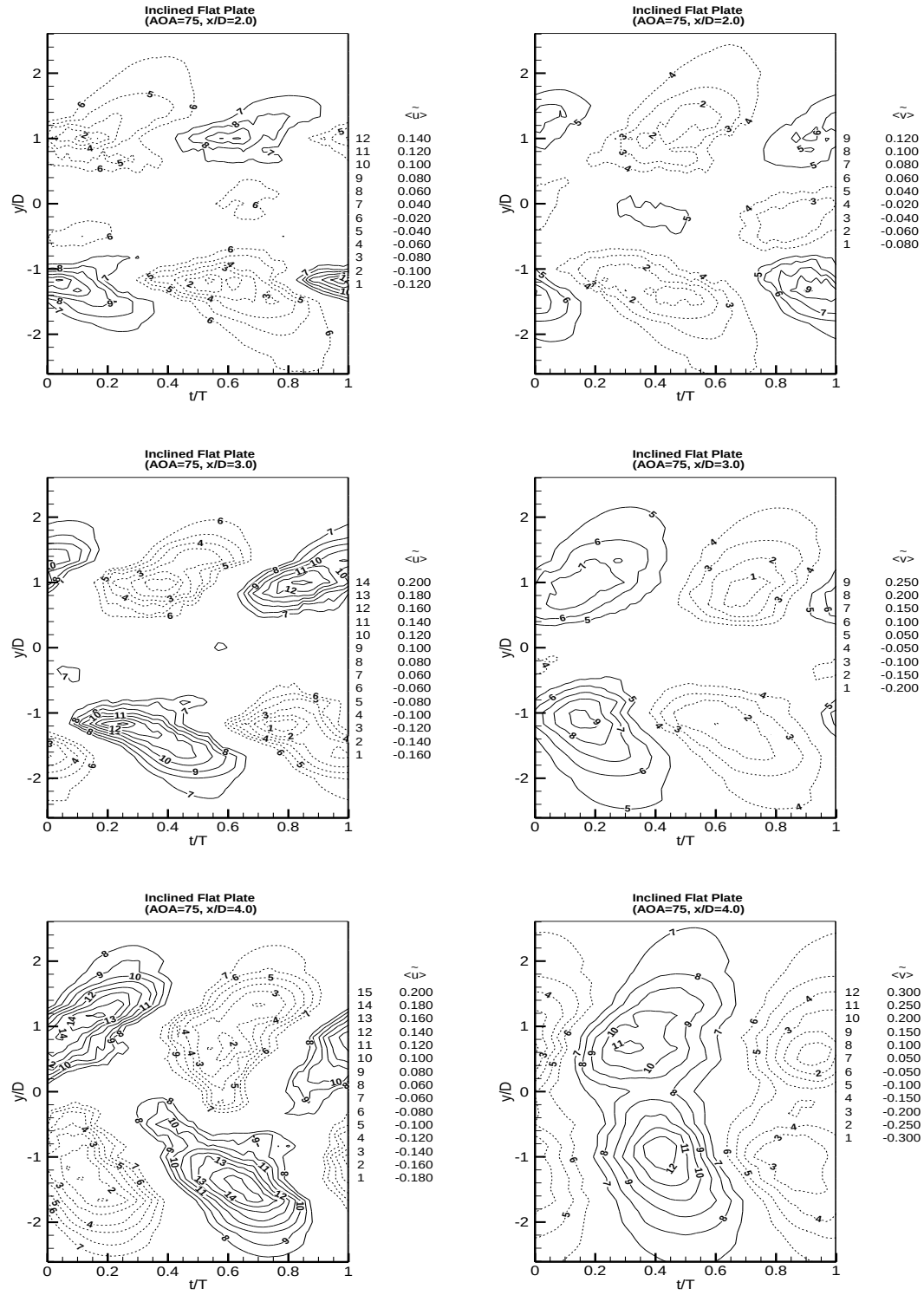

Figure 5.20. Coherent stream wise and coherent transverse velocity measured at various x/D downstream of single inclined flat plat at α=75

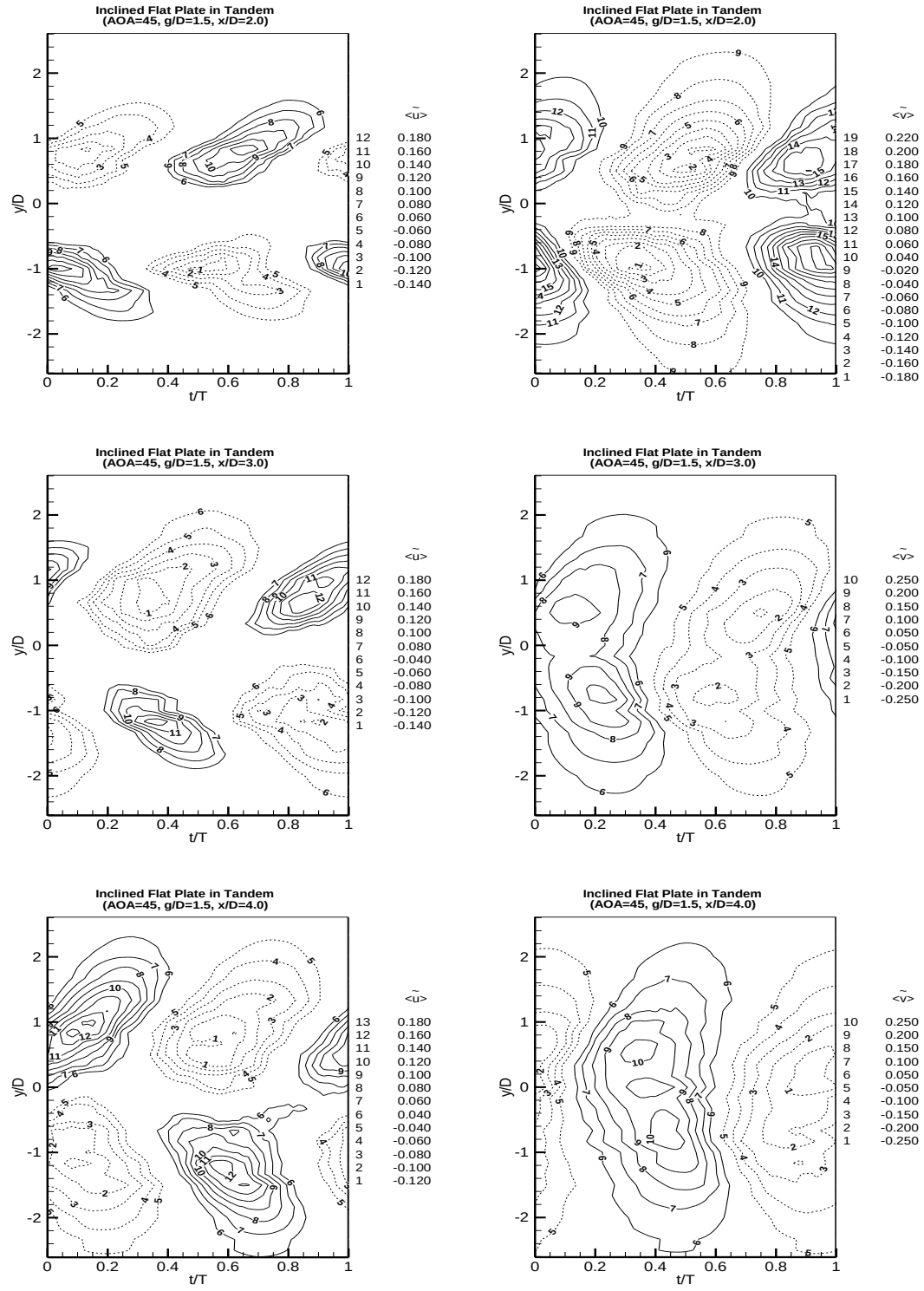

Figure 5.21. Coherent stream wise and coherent transverse velocity measured at various x/D downstream of two tandem inclined flat plates at g/D=1.5, α=45

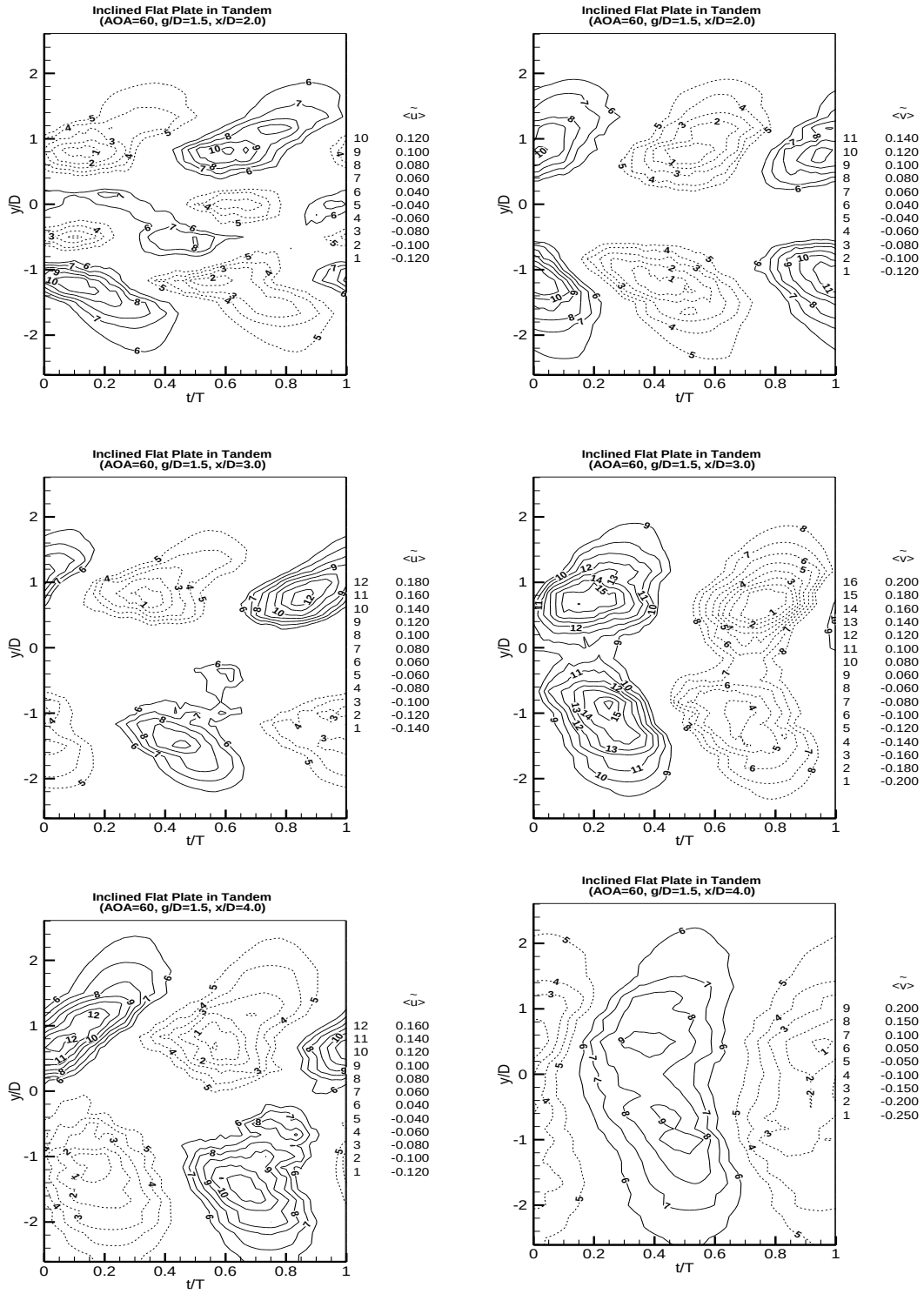

Figure 5.22. Coherent stream wise and coherent transverse velocity measured at various x/D downstream of two tandem inclined flat plates at g/D=1.5, α=60

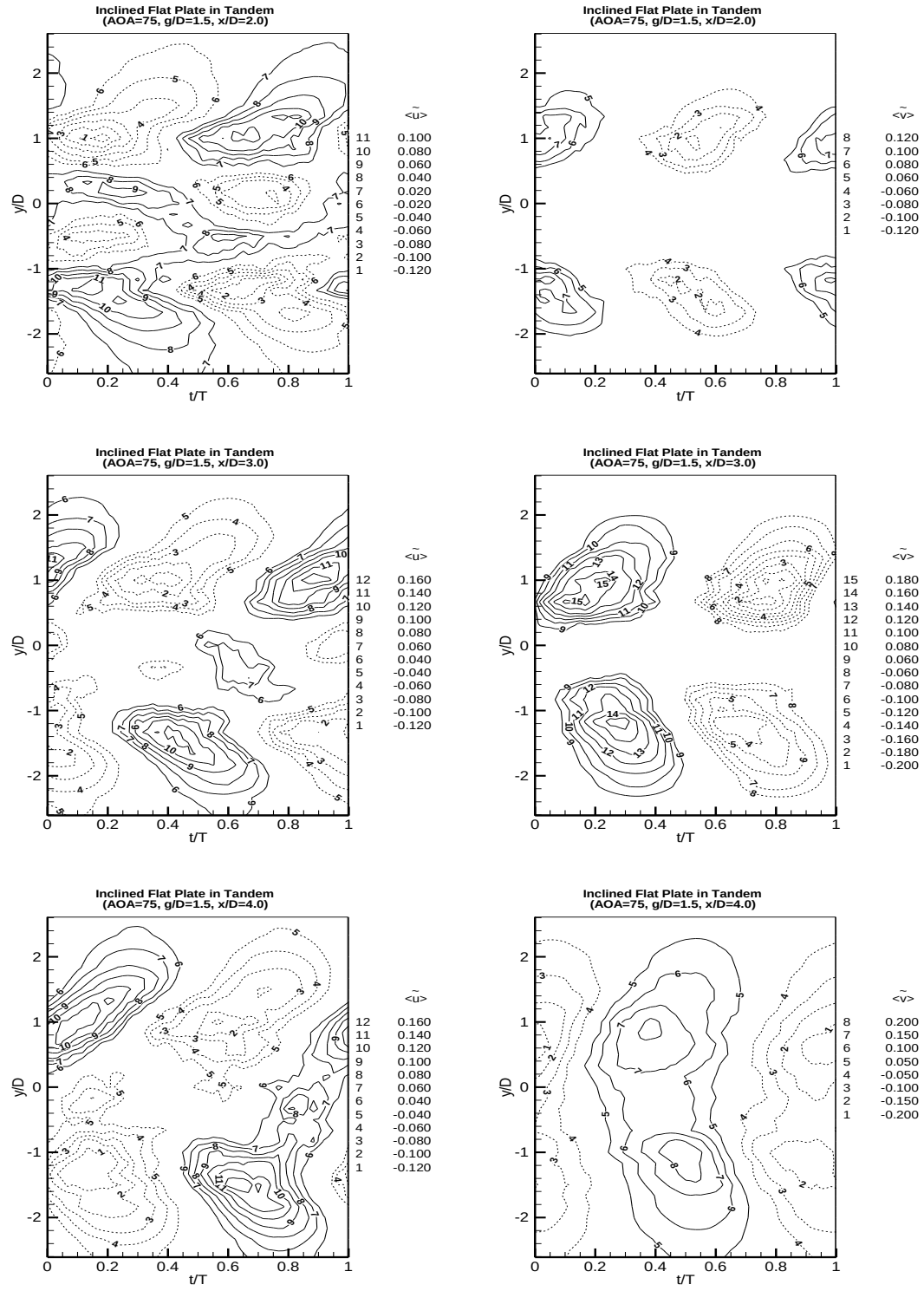

Figure 5.23. Coherent stream wise and coherent transverse velocity measured at various x/D downstream of two tandem inclined flat plates at g/D=1.5, α=75

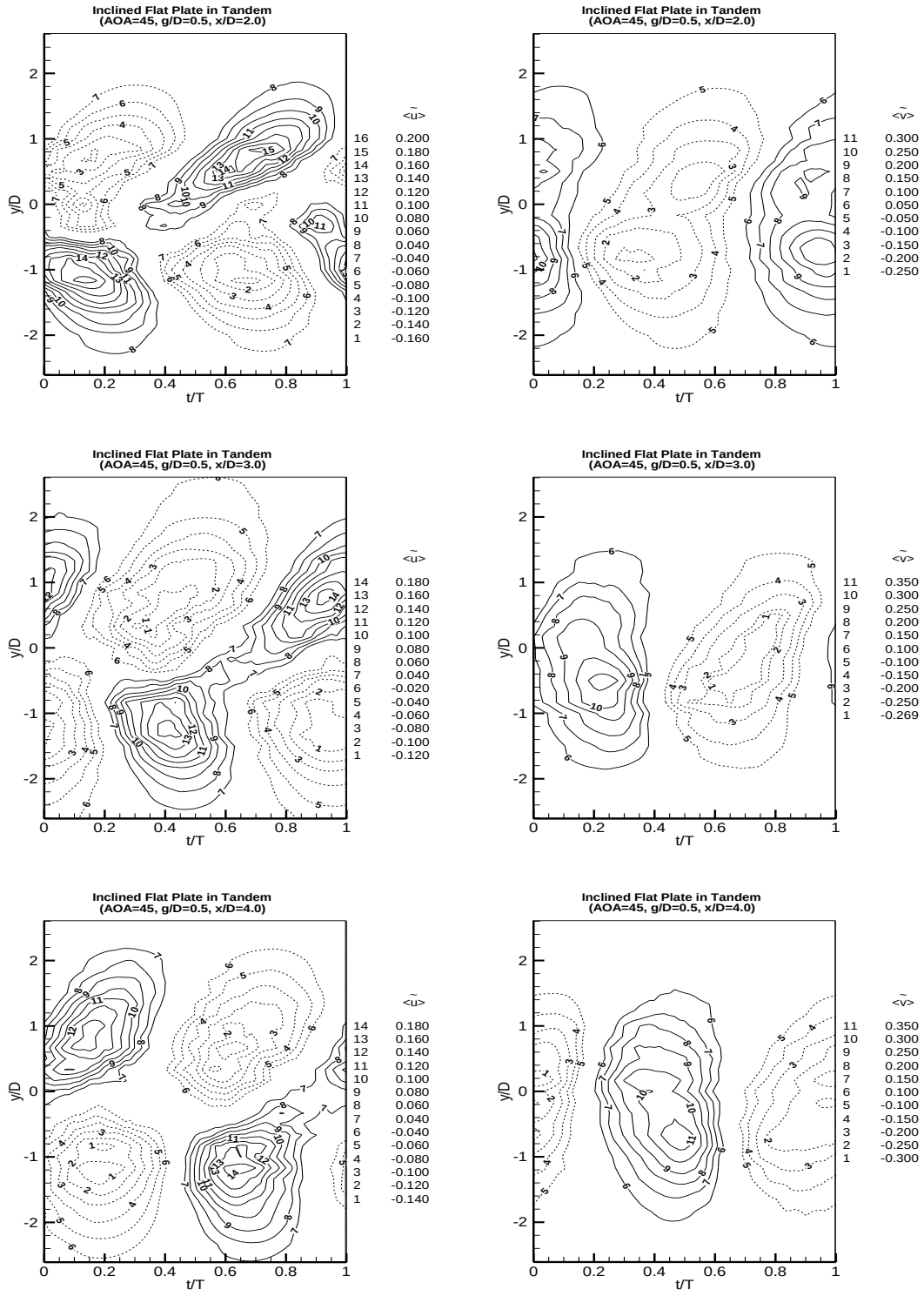

Figure 5.24. Coherent stream wise and coherent transverse velocity measured at various x/D downstream of two tandem inclined flat plates at g/D=0.5, α=45

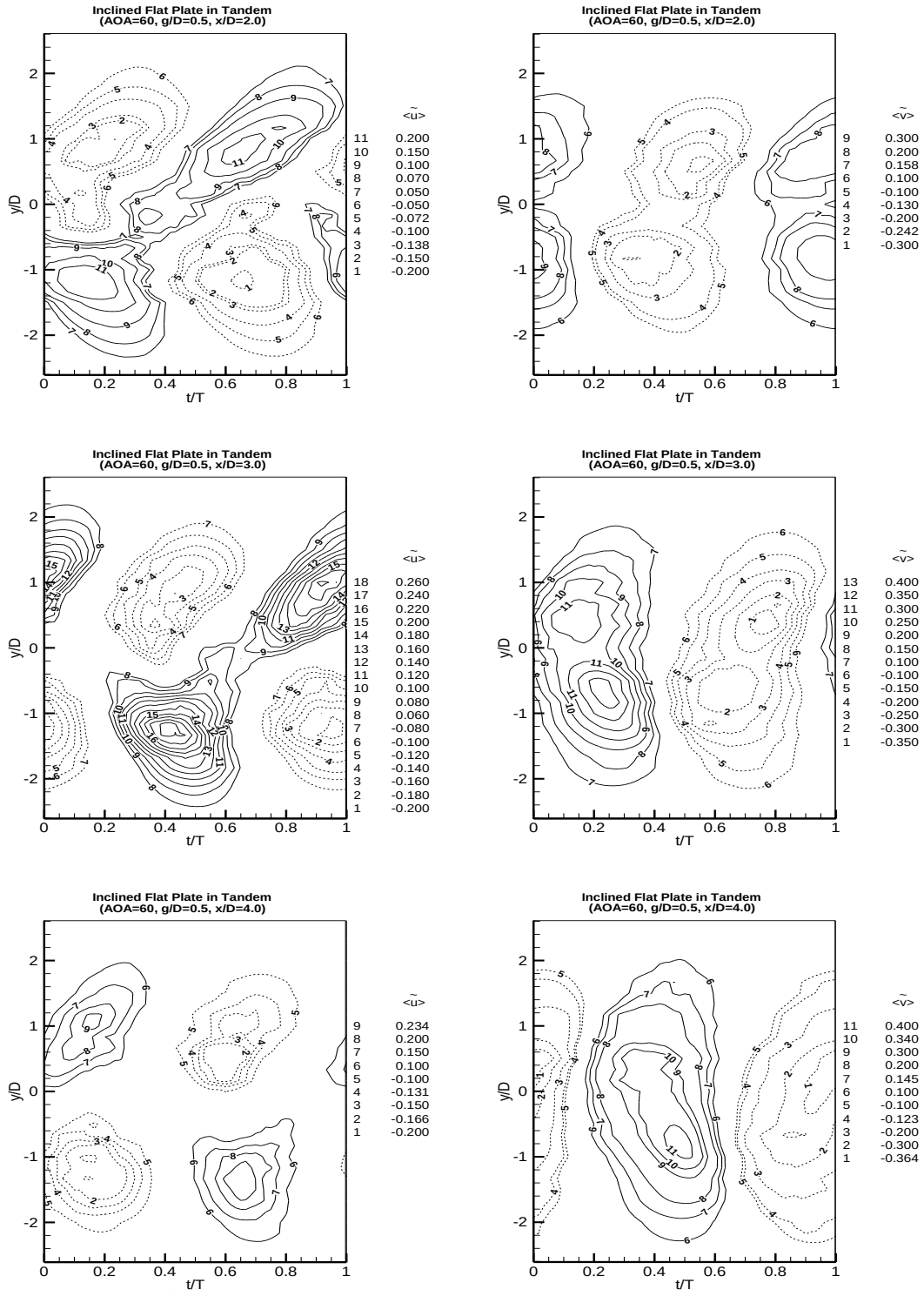

Figure 5.25. Coherent stream wise and coherent transverse velocity measured at various x/D downstream of two tandem inclined flat plates at g/D=0.5, α=60

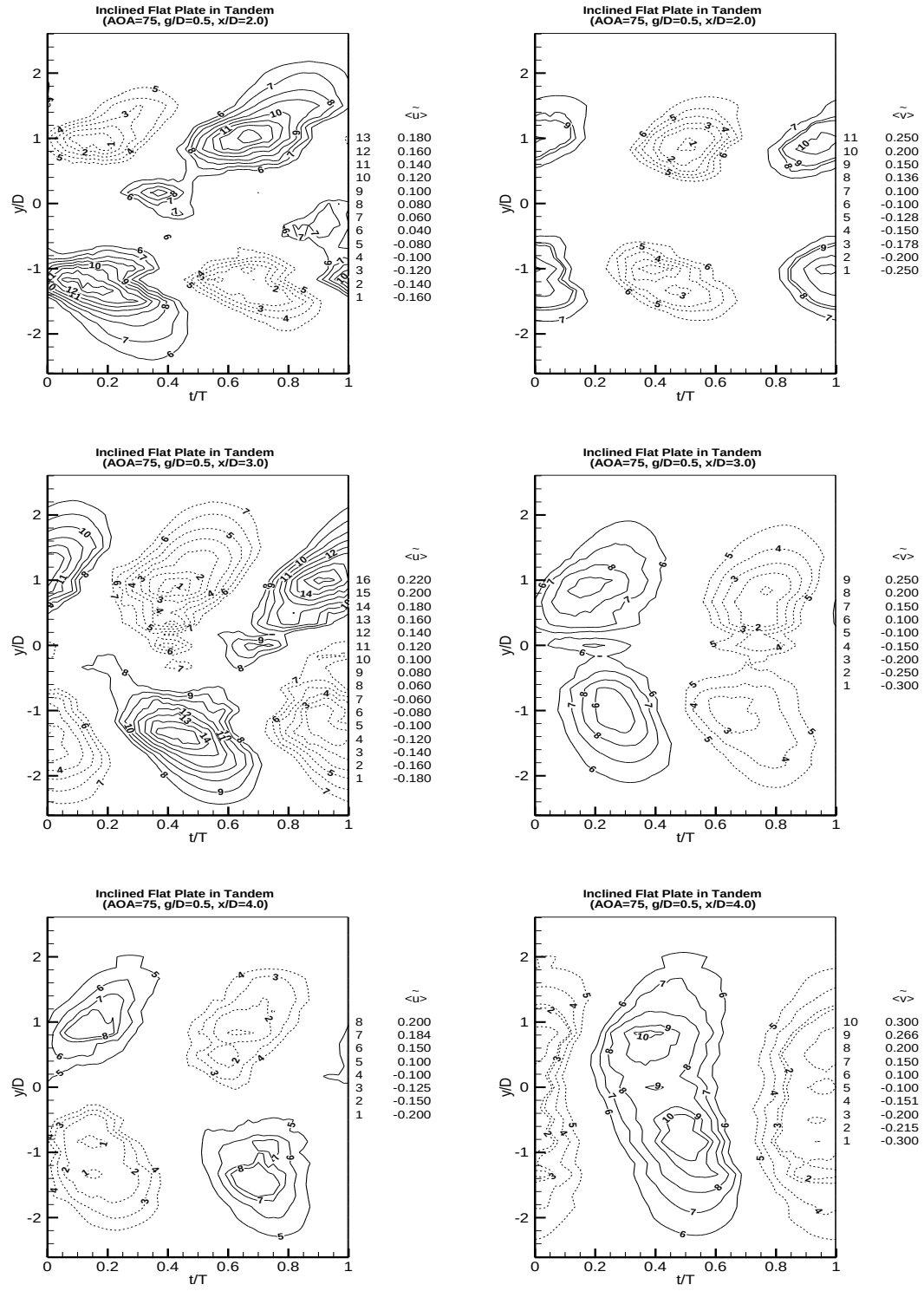

Figure 5.26. Coherent stream wise and coherent transverse velocity measured at various x/D downstream of two tandem inclined flat plates at g/D=0.5, α=75

5.5 Turbulent Kinetic Energy

As discussed triple decomposition distinguishes between coherent structure or vortex shedding phenomenon and incoherent structure of turbulent fluctuations. Therefore, it is possible to put the periodic shedding phenomenon a side and perform a detailed investigation on incoherent fluctuations. Incoherent turbulent kinetic energy production at three different normalized stream wise coordinate in the wake region of two tandem inclined plates have been illustrated in figures 5.27 to 5.29. Development of the Incoherent turbulent kinetic energy is clearly recognizable from the figures. It can be seen that in the wake region close to the downstream plate there is no apparent features of periodic flow. However farther in the downstream wake, the periodic features of flow develops and become more observable. As probe moves downstream in the wake from x/D= 2.0 to 4.0, the incoherent TKE production peaks increases gradually for all cases. However, comparison between g/D=0.5 and 1.5, reveals that the TKE peak production decreases for all measured x/D's in the wake region. As the gap ratio increases more fluid particle entrain into gap region during the shedding process. Therefore, such reduction in incoherent TKE production peak is observed.

In addition, the plotted contours of incoherent TKE production also demonstrated that the main turbulent kinetic energy production occurs in the region with the same width of the plates. Moreover, TKE peak production concentrated along the boundaries of the separated shear layer which corresponds to vortex shedding from the edges of the plates.

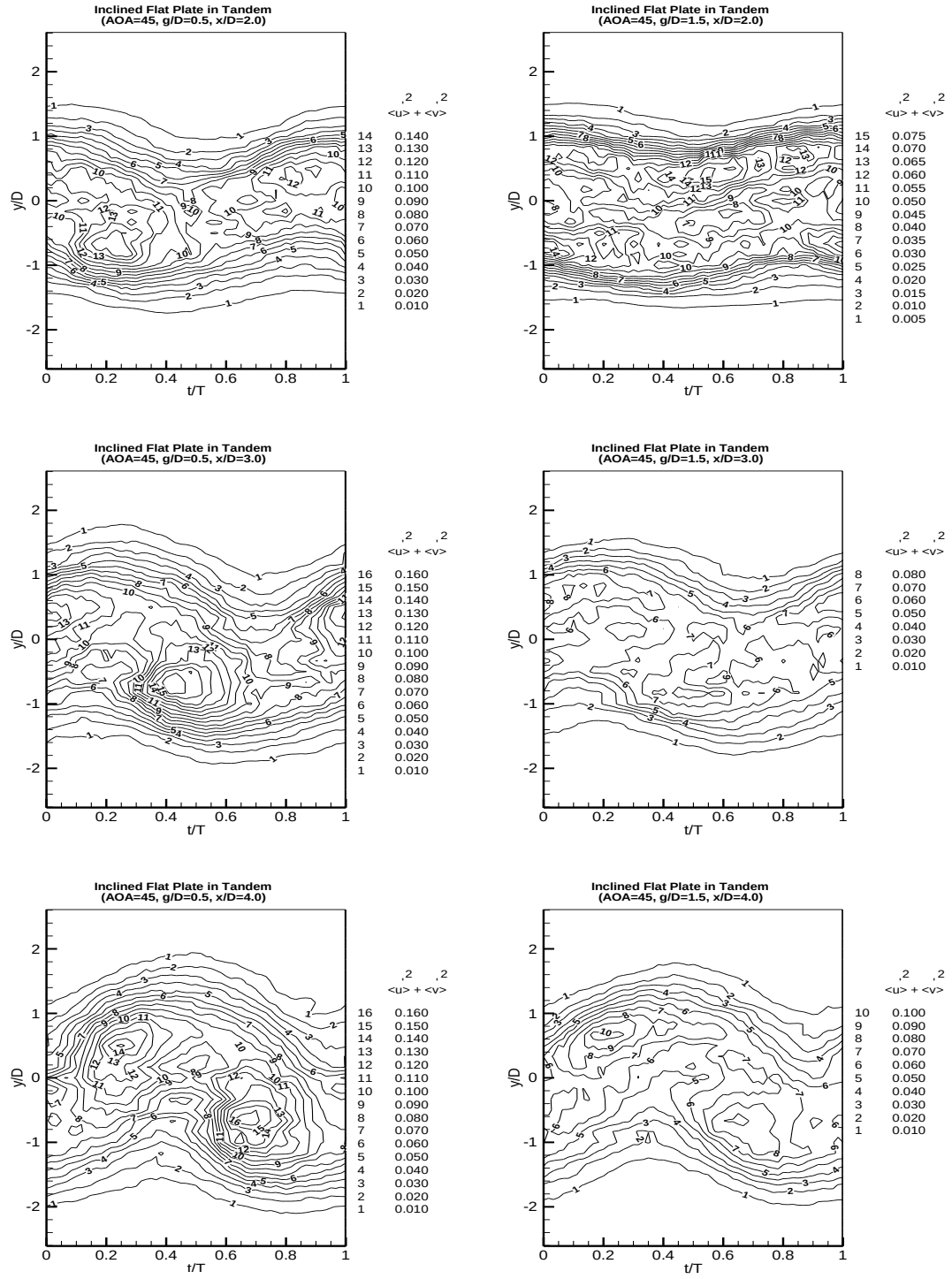

Figure 5.27. Incoherent Turbulent Kinetic Energy production measured at various x/D in the wake region of two tandem inclined flat plates at α=45

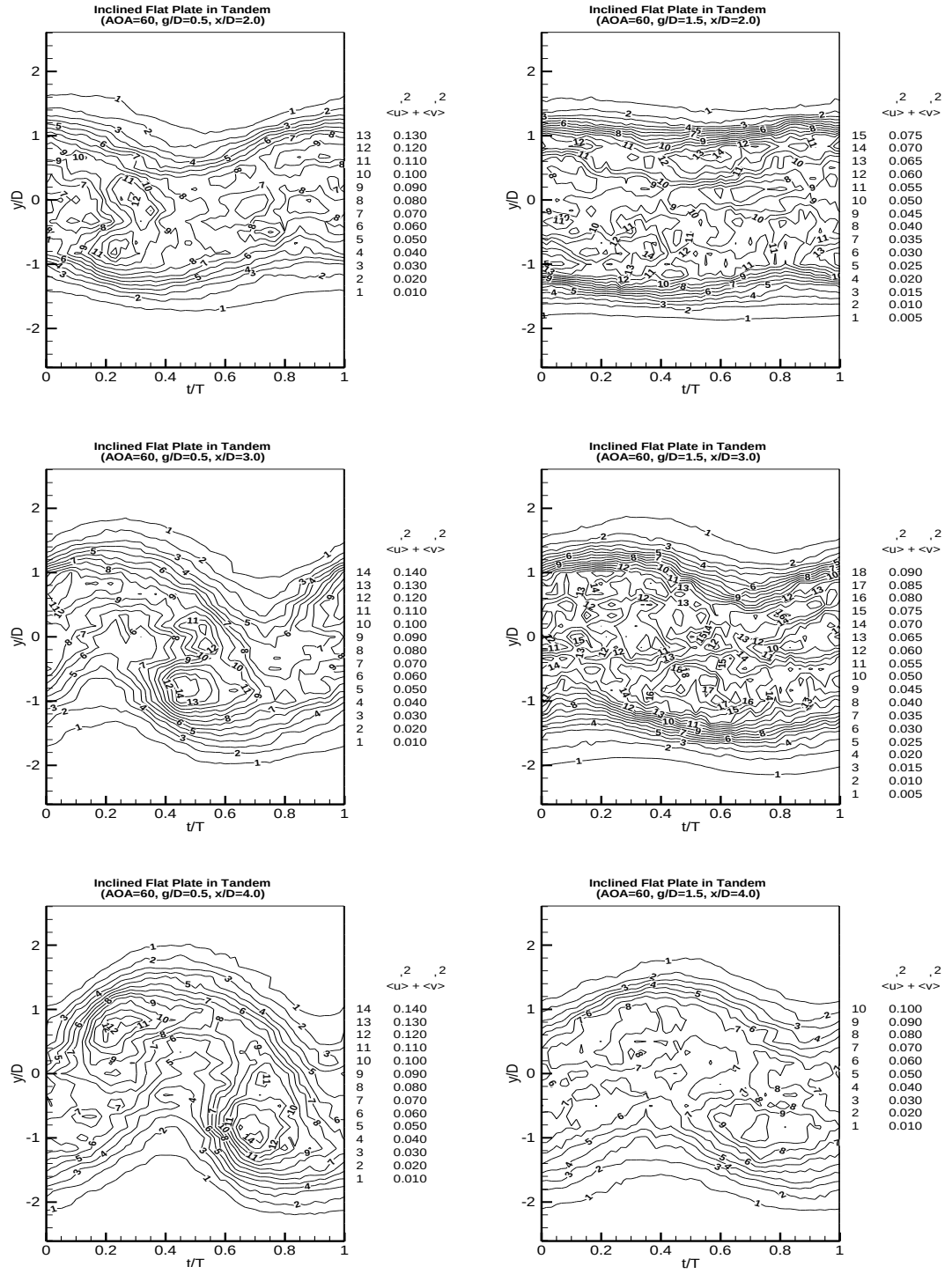

Figure 5.28. Incoherent Turbulent Kinetic Energy production measured at various x/D in the wake region of two tandem inclined flat plates at α=60

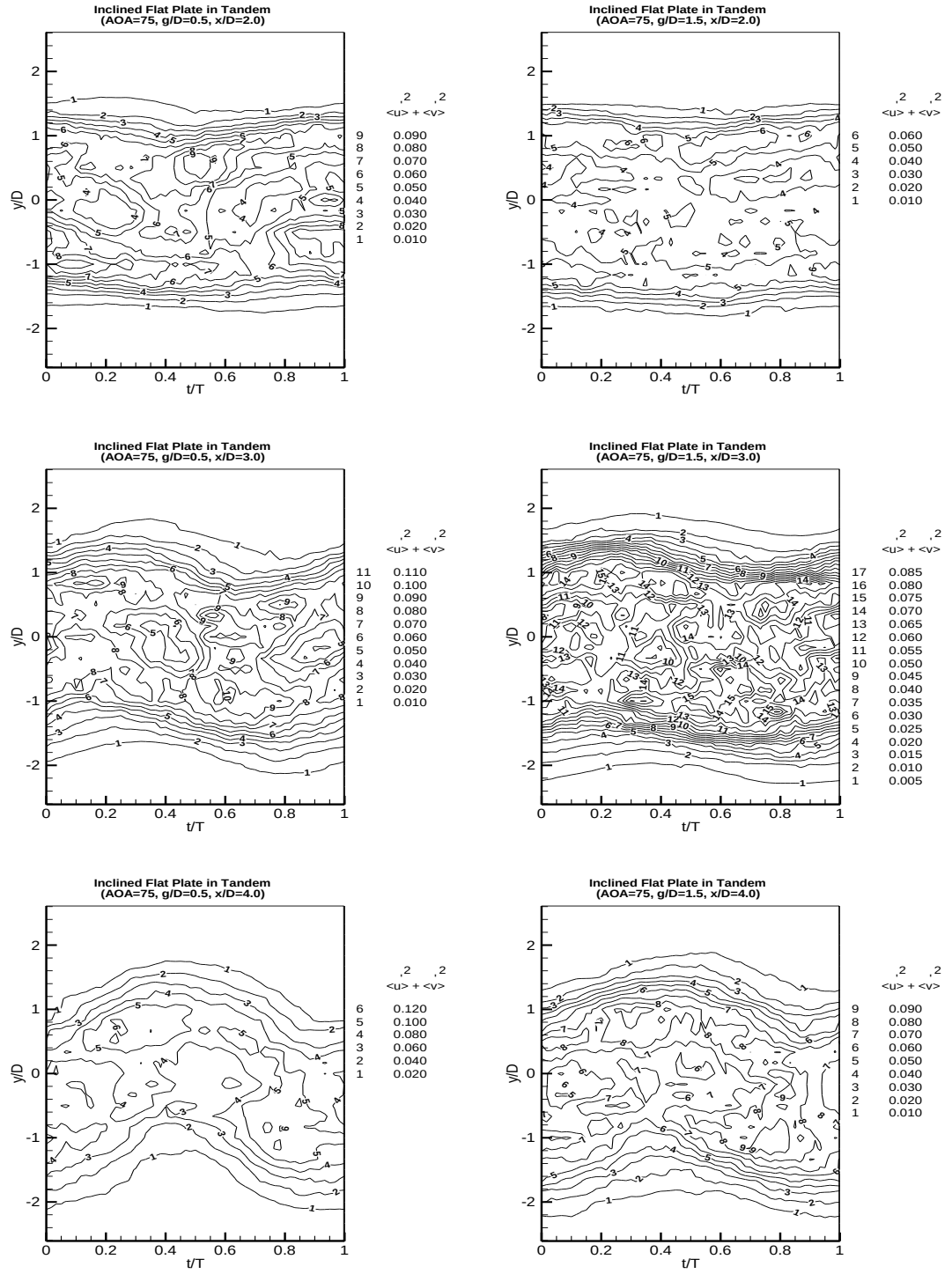

Figure 5.29. Incoherent Turbulent Kinetic Energy production measured at various x/D in the wake region of two tandem inclined flat plates at α=75

5.6 Time averaged properties

Quantifying development and decay of different properties in the downstream wake region are of great importance. Thus for a quantitative comparison between different tandem plates arrangement, time averaged stream wise and transverse velocity for various x/D's downstream the aft plate have been presented. Time averaged stream wise and transverse velocity profiles are depicted in figures 5.30 and 5.31.

It can be seen from the figures that while stream wise velocity profile shows symmetry along the centerline, transverse velocity profile shows anti-symmetric variation. Moreover, time averaged transverse velocity exhibits max positive and negative peaks approximately along the edges. These peaks can be an indication of rolled vortices from the edges of the plates. It can be seen that as the angle of attack increases these peaks occur at higher y/D.

It was also observed that while the time averaged stream wise velocity profiles recovers as the probe moves back downstream in the wake region, the time mean transverse velocity decays significantly. As the shear layers separated from the plates, the fluid flow subjected to momentum loss in the wake region. Therefore, time averaged streamwise velocity profile exhibit a drop in the wake region behind the plate. However, outside the wake it return to free stream value which is apparent from the figure. As the flow develops toward the downstream, the wake widen as the fluid entrained into the wake from the edges of plates periodically. Another sign of such entrainment process can be spotted from time averaged transverse velocity profile. At near the wake region exhibit high fluid entrainment toward the centerline. However, such process dissipated significantly beyond 4D in the downstream wake.

Geometries such as normal plate exhibit a symmetrical periodical train of vortices being shed alternately from the edges of the bodies in the wake region. Although these vortices rolled up in opposite direction, but they contain similar strength. As a result, the time mean flow over symmetrical bluff bodies exhibit zero mean lift and symmetric pattern along the wake centerline. In contrary, flow over asymmetrical geometry such as inclined flat plate exhibit asymmetrical flow structure and as a result none-zero mean lift generated on the flat plate. As it can be seen from the transverse velocity profile, the wake region behind the trailing edge exhibit higher momentum transfer towards the centerline than the leading edge. In addition, the time averaged transverse velocity along the wake centerline is also nonzero due to asymmetric nature of the inclined plates.

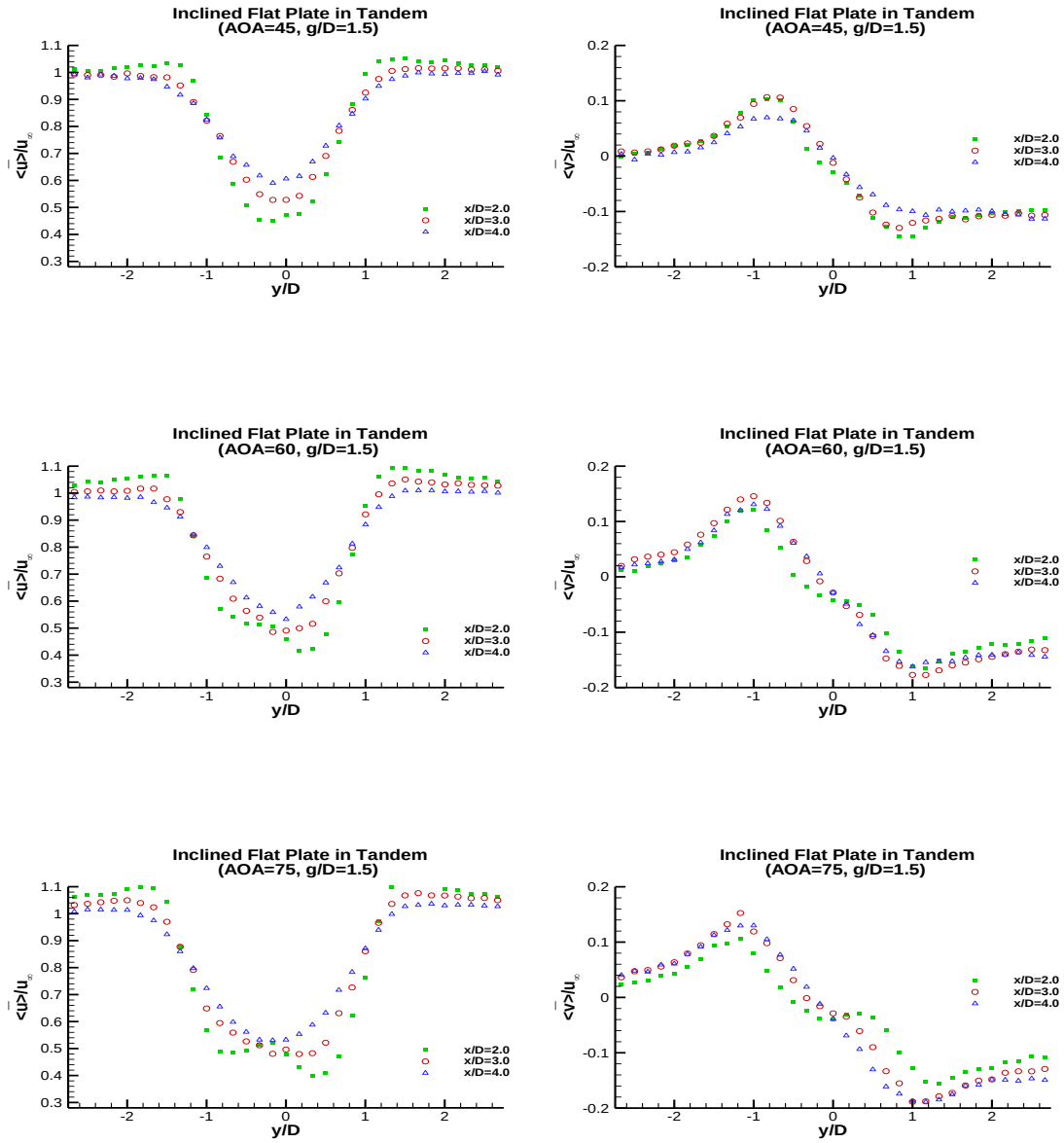

Figure 5.30. Comparison of variation of time averaged stream wise and traverse velocity measured at various x/D in the wake region of two tandem inclined flat plates for g/D=1.5

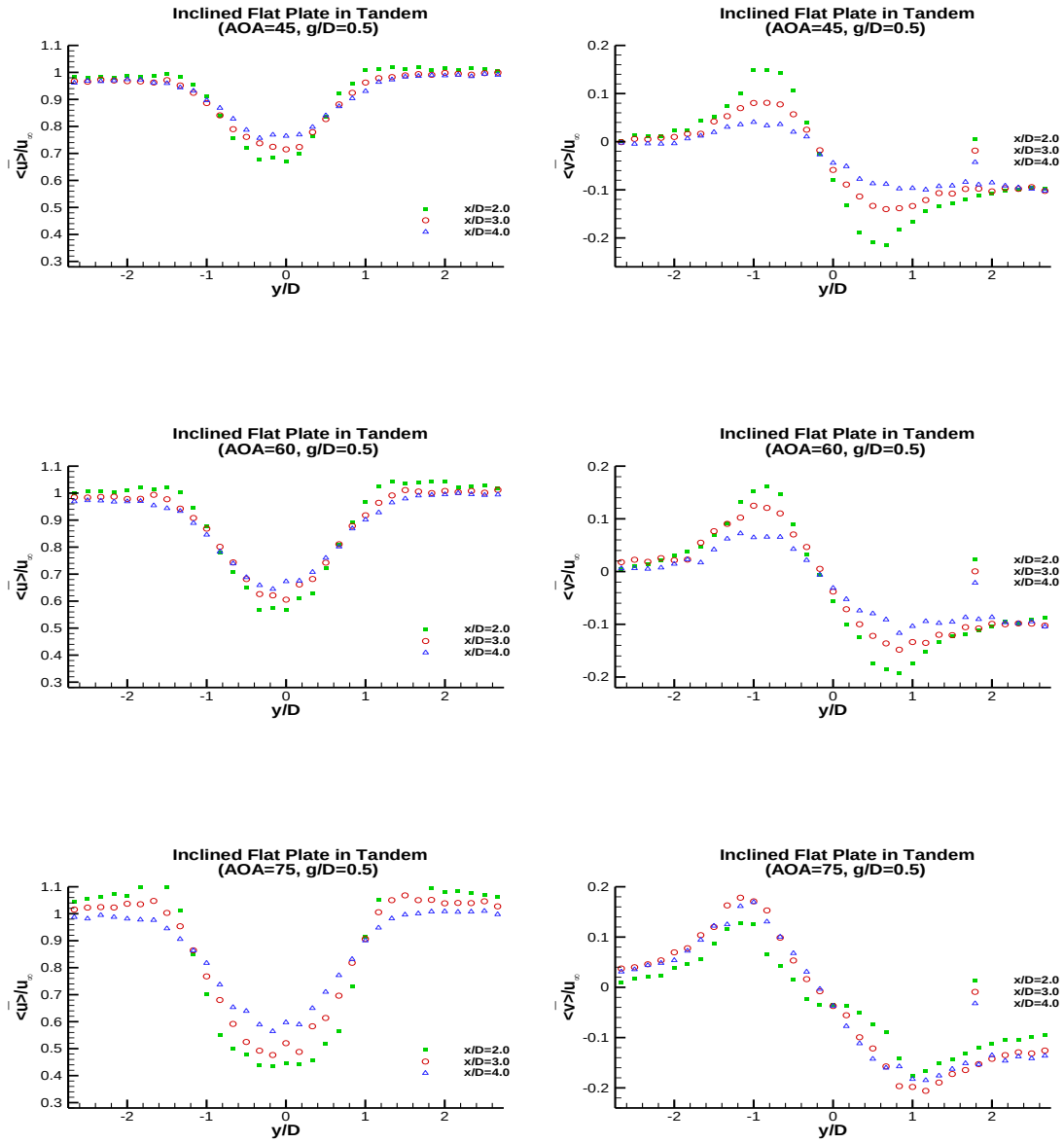

Figure 5.31. Comparison of variation of time averaged stream wise and traverse velocity measured at various x/D in the wake region of two tandem inclined flat plates for g/D=0.5

Chapter 6

CONCLUSION

6.1. Final Remarks

The aim of this study was to investigate vortex shedding and flow structures in the downstream wake region behind bluff bodies. This study tackled the problem of suppressing the vortex shedding by employing perforated surfaces and also interacting wakes of bluff bodies in tandem arrangement.

Therefore, first preliminary experiments have been conducted to study flow structure behind a square cylinder. Then perforated square cylinder with different perforation surfaces have been studied to investigate suitability and effectiveness of each perforation on suppression of vortex street in the wake region. The results were compared with results of the Turhal and Çuhadaroğlu (2010). The perforation employed together with a passive control method and the flow structure have been compared with the wake region behind the non-perforated square cylinder.

Moreover, interacting wakes of two inclined flat plates in tandem arrangement have been studied to probe the effects of gap ratio and angle of attack of the plates. The flow structures have been examined and presented in chapter 5 different for g/D and α, and the results were compared with the findings of J. M. Chen and Fang (1996); Lam (1996); Lam and Leung (2005); Lam and Wei (2010).

Square cylinder

1. The results of phase averaged time mean velocities and phase averaged fluctuations revealed a symmetrical flow pattern along the centerline.
2. Incoherent stresses reach the highest level as vortices are being shed.
3. During vortex formation from one edge of the square cylinder a maxima in incoherent stream wise normal stress was observed. However, the initiated shear layers from the opposite edge causes a maxima in transverse stress production.
4. 1/5 of period after a vortex is shed, significant momentum transfer towards the opposite shear layer was observed.
5. Turbulent kinetic energy production contours demonstrate that the main turbulent kinetic energy production occurs in the region with the same width of square cylinder.

Perforated square cylinder

6. It was observed that the perforated surfaces are effective only within effective width y/D= ±1.0, and up to 1.5D in the downstream wake.
7. Although previous studies reported that high injection through the rear surface is required to decreas the vortex shedding frequency, it was found that even for the case of this study with low entrainment flow rate, the shedding phenomenon have been affected significantly.
8. Multiple peaks have been observed in the spectra, implied the secondary vortex formation and suppression of the primary shedding due to entrainment of fluid through the perforated surfaces.

9. Phased averaged transverse velocity peaks lag behind Phased averaged stream wise velocity peaks with a phase shift equal ¼ of a cycle.
10. Asymmetric coherent flow structures behind perforated square cylinder have been observed.
11. Square cylinder with all-faces perforated, demonstrated the most significant reduction in the coherent structures compared with other perforation surfaces.

Inclined flat plate in tandem

1. Strouhal number decreases as the angle of attack increases.
2. Similarly, Strouhal number decreases as the gap between the plates increases
3. TKE peak production decreases as the gap ratio increases from g/D=0.5 and 1.5 due to more fluid particle entrain into gap region during the shedding process.
4. TKE peak production concentrated along the boundaries of the separated shear layer which corresponds to vortex shedding from the edges of the plates.
5. While stream wise velocity profile shows symmetry along the centerline, transverse velocity profile shows anti-symmetric variation.
6. Time averaged transverse velocity exhibits max positive and negative peaks approximately along the edges.
7. The wake region behind the trailing edge exhibit higher momentum transfer towards the centerline than the leading edge

6.2 Suggestions for future studies

Further experiments are required to investigate the suppression of vortex shedding downstream the perforated square cylinder. It is proposed to perform different experiments for square cylinders perforated with various holes in diameter. Therefore the effect of flow rate through the perforated can be investigated.

Further investigation on aerodynamic force of the various investigated configuration in this study is suggested. Such study is critical for bluff bodies in tandem arrangement where the gap between them act as key factor. Bluff bodies in close proximity act similar to a “single body” and hence vortices could not roll up inside the gap between the bodies, and the initiated shear layers from upstream body bypass this dead flow region and form vortices behind the downstream body. Whereas, for larger gap between the bodies vortices also roll up inside the gap and the vortex shedding phenomenon occurs independently from each body. As a result, the drag force is entirely influenced by such phenomenon and require a great attention.

In this study the velocity field have been measured at selected x/D downstream the wake where y/D varying. It is also suggested that experiments being performed with x/D varying finely in order to construct a grid of velocities. Hence the vorticity contours for the coherent structures can be also calculated via line integral techniques (Hussain (1986)).

Moreover, PIV measurements can be employed for further studies of the tandem inclined plates arrangements. PIV have capability of global flow field velocity measurement while hot wire anemometer (HWA) only provide point-wise

measurements. Therefore the gap region between the two plates can be also investigated for better insight to these problem.

REFERENCES

Alam, MD Mahbub, Moriya, M, Takai, K, & Sakamoto, H. (2002). Suppression of fluid forces acting on two square prisms in a tandem arrangement by passive control of flow. *Journal of Fluids and Structures, 16*(8), 1073-1092.

Auteri, F, Belan, M, Gibertini, G, & Grassi, D. (2008). Normal flat plates in tandem: An experimental investigation. *Journal of Wind Engineering and Industrial Aerodynamics, 96*(6), 872-879.

Auteri, Franco, Belan, Marco, Cassinelli, Carlo, & Gibertini, Giuseppe. (2009). Interacting Wakes of Two Normal Flat PlatesAn investigation based on phase averaging of LDA signals. *Journal of visualization, 12*(4), 307-321.

Baxendale, AJ, Grant, I, & Barnes, FH. (1985). The flow past two cylinders having different diameters. *Aeronautical Journal, 89*, 125-134.

Bearman, PW. (1971). An investigation of the forces on flat plates normal to a turbulent flow. *Journal of Fluid Mechanics, 46*(01), 177-198.

Bentley, JP, & Mudd, JW. (2003). Vortex shedding mechanisms in single and dual bluff bodies. *Flow Measurement and instrumentation, 14*(1), 23-31.

Bradshaw, Peter. (1996). *An Introduction to Turbulence and Its Measurement*: Pergamon Press.

Bradshaw, Peter. (2013). *An Introduction to Turbulence and Its Measurement: Thermodynamics and Fluid Mechanics Series*: Elsevier.

Brunn, H. H. (1995). Hot-wire anemometry: principles and signal analysis: Oxford University Press Inc.

Bruun, Hans H. (1996). Hot-wire anemometry: principles and signal analysis: IOP Publishing.

Cantwell, Brian, & Coles, Donald. (1983). An experimental study of entrainment and transport in the turbulent near wake of a circular cylinder. *Journal of fluid mechanics, 136*, 321-374.

Carassale, Luigi, Freda, Andrea, & Marrè-Brunenghi, Michela. (2014). Experimental investigation on the aerodynamic behavior of square cylinders with rounded corners. *Journal of Fluids and Structures, 44*, 195-204.

Chen, Jerry M, & Fang, Yuan-Cheng. (1996). Strouhal numbers of inclined flat plates. *Journal of wind engineering and industrial aerodynamics, 61*(2), 99-112.

Chen, Ye Jun, & Shao, Chuan Ping. (2013). Suppression of vortex shedding from a rectangular cylinder at low Reynolds numbers. *Journal of Fluids and Structures, 43*, 15-27.

Cowdrey, CF. (1962). A note on the use of end plates to prevent three-dimensional flow at the ends of bluff cylinders. *NPL Aero Report, 1025*.

Çuhadaroglu, Burhan. (2009). A numerical study on turbulent flow around a square cylinder with uniform injection or suction. *International Journal of Numerical Methods for Heat & Fluid Flow, 19*(6), 708-727.

Çuhadaroğlu, Burhan, Akansu, Yahya Erkan, & Turhal, Ahmet Ömür. (2007). An experimental study on the effects of uniform injection through one perforated surface of a square cylinder on some aerodynamic parameters. *Experimental Thermal and Fluid Science, 31*(8), 909-915.

Çuhadaroğlu, Burhan, & Turan, Osman. (2009). Numerical simulation of turbulent flow around a square cylinder with uniform injection or suction and heat transfer. *Numerical Heat Transfer, Part A: Applications, 55*(2), 163-184.

Deri, Enrico, Braza, Marianna, Cid, Emmanuel, Cazin, Sébastien, Michaelis, Dirk, & Degouet, Cédric. (2014). Investigation of the three-dimensional turbulent near-wake structure past a flat plate by tomographic PIV at high Reynolds number. *Journal of Fluids and Structures, 47*, 21-30.

Dianat, Golnaz. (2011). *Experimental and Numerical investigation of flow structures behind Bluff Bodies in Tandem Arrangement.* Eastern Mediterranean University (EMU).

Frisch, Uriel. (1995). *Turbulence: the legacy of AN Kolmogorov*: Cambridge university press.

Hacışevki, H, & Teimourian, A. (2015). Comparison of flow structures in the wake region of two similar normal flat plates in tandem and a square cylinder. *Experimental Thermal and Fluid Science, 69*, 169-177.

Hacışevki, H., & Teimourian, A. (2016). Interacting wakes of a narrow and a wide flat plate in tandem arrangement. *Fluid Dynamics Research, 48*(1), 015505.

Hacışevki, Hasan. (2001). *Vortex Shedding in Tandem Arrangement.* (Doctoral dissertation), Eastern Mediterranean University.

Hangan, H, & Vickery, BJ. (1999). Buffeting of two-dimensional bluff bodies. *Journal of Wind Engineering and Industrial Aerodynamics, 82*(1), 173-187.

Havel, B, Hangan, H, & Martinuzzi, R. (2001). Buffeting for 2D and 3D sharp-edged bluff bodies. *Journal of Wind Engineering and Industrial Aerodynamics, 89*(14), 1369-1381.

Hogan, James D, & Hall, Joseph W. (2010). The spanwise dependence of vortex-shedding from yawed circular cylinders. *Journal of Pressure Vessel Technology, 132*(3), 031301.

Hussain, AKM. (1986). Coherent structures and turbulence. *Journal of Fluid Mechanics, 173*, 303-356.

Igarashi, Tamotsu. (1981). Characteristics of the flow around two circular cylinders arranged in tandem: 1st report. *Bulletin of JSME, 24*(188), 323-331.

Igarashi, Tamotsu. (1984). Characteristics of the flow around two circular cylinders arranged in tandem: 2nd report, unique phenomenon at small spacing. *Bulletin of JSME, 27*(233), 2380-2387.

Igarashi, Tamotsu. (1997). Drag reduction of a square prism by flow control using a small rod. *Journal of Wind Engineering and Industrial Aerodynamics, 69*, 141-153.

Igarashi, Tamotsu, & Terachi, Nobuaki. (2002). Drag reduction of flat plate normal to airstream by flow control using a rod. *Journal of Wind Engineering and Industrial Aerodynamics, 90*(4–5), 359-376. doi: http://dx.doi.org/10.1016/S0167-6105(01)00198-2

Irwin, Peter A. (2008). Bluff body aerodynamics in wind engineering. *Journal of Wind Engineering and Industrial Aerodynamics, 96*(6), 701-712.

Jorgensen, FE. (1971). Directional sensitivity of wire and fiber-film probes. *DISA information, 11*(3), 1-7.

Kiya, M, & Matsumura, M. (1988). Incoherent turbulence structure in the near wake of a normal plate. *Journal of Fluid Mechanics, 190*, 343-356.

Knisely, Charles W. (1990). Strouhal numbers of rectangular cylinders at incidence: a review and new data. *Journal of Fluids and Structures, 4*(4), 371-393.

Lam, KM. (1996). Phase-locked eduction of vortex shedding in flow past an inclined flat plate. *Physics of Fluids (1994-present), 8*(5), 1159-1168.

Lam, KM, & Leung, MYH. (2005). Asymmetric vortex shedding flow past an inclined flat plate at high incidence. *European Journal of Mechanics-B/Fluids, 24*(1), 33-48.

Lam, KM, & Wei, CT. (2010). Numerical simulation of vortex shedding from an inclined flat plate. *Engineering Applications of Computational Fluid Mechanics, 4*(4), 569-579.

Leder, A. (1991). Dynamics of fluid mixing in separated flows. *Physics of Fluids A: Fluid Dynamics (1989-1993), 3*(7), 1741-1748.

Liu, Chia-Hung, & Chen, Jerry M. (2002). Observations of hysteresis in flow around two square cylinders in a tandem arrangement. *Journal of Wind Engineering and Industrial Aerodynamics, 90*(9), 1019-1050.

Malekzadeh, S, & Sohankar, A. (2012). Reduction of fluid forces and heat transfer on a square cylinder in a laminar flow regime using a control plate. *International Journal of Heat and Fluid Flow, 34*, 15-27.

Martinuzzi, Robert J, & Havel, Brian. (2004). Vortex shedding from two surface-mounted cubes in tandem. *International journal of heat and fluid flow, 25*(3), 364-372.

Mazharoğlu, Çetin, & Hacışevki, Hasan. (1999). Coherent and incoherent flow structures behind a normal flat plate. *Experimental thermal and fluid science, 19*(3), 160-167.

Najjar, FM, & Vanka, SP. (1995). Effects of intrinsic three-dimensionality on the drag characteristics of a normal flat plate. *Physics of Fluids (1994-present), 7*(10), 2516-2518.

Nakamura, Y. (1996). Vortex shedding from bluff bodies and a universal Strouhal number. *Journal of fluids and structures, 10*(2), 159-171.

Narasimhamurthy, Vagesh D, & Andersson, Helge I. (2009). Numerical simulation of the turbulent wake behind a normal flat plate. *International Journal of Heat and Fluid Flow, 30*(6), 1037-1043.

Norberg, C. (1993). Flow around rectangular cylinders: pressure forces and wake frequencies. *Journal of wind engineering and industrial aerodynamics, 49*(1), 187-196.

Okajima, Atsushi. (1982). Strouhal numbers of rectangular cylinders. *Journal of Fluid Mechanics, 123*, 379-398.

Perry, AE, & Steiner, TR. (1987). Large-scale vortex structures in turbulent wakes behind bluff bodies. Part 1. Vortex formation processes. *Journal of fluid mechanics, 174*, 233-270.

Pinarbasi, A, Pinar, E, Akilli, H, & Ince, E. (2015). Shallow water experiments of flow past two identical square cylinders in tandem. *European Journal of Mechanics-B/Fluids, 49*, 100-107.

Reynolds, WC, & Hussain, AKMF. (1972). The mechanics of an organized wave in turbulent shear flow. Part 3. Theoretical models and comparisons with experiments. *Journal of Fluid Mechanics, 54*(02), 263-288.

Saha, AK, Muralidhar, K, & Biswas, G. (2000). Experimental study of flow past a square cylinder at high Reynolds numbers. *Experiments in Fluids, 29*(6), 553-563.

Saha, Arun K. (2007). Far-wake characteristics of two-dimensional flow past a normal flat plate. *Physics of Fluids (1994-present), 19*(12), 128110.

Saha, Arun K. (2013). Unsteady flow past a finite square cylinder mounted on a wall at low Reynolds number. *Computers & Fluids, 88*, 599-615.

Sakamoto, H, Tan, K, Takeuchi, N, & Haniu, H. (1997). Suppression of fluid forces acting on a square prism by passive control. *Journal of Fluids Engineering, 119*(3), 506-511.

Snarski, Stephen R. (2004). Flow over yawed circular cylinders: Wall pressure spectra and flow regimes. *Physics of Fluids (1994-present), 16*(2), 344-359.

Sohankar, A, Khodadadi, M, & Rangraz, E. (2015). Control of fluid flow and heat transfer around a square cylinder by uniform suction and blowing at low Reynolds numbers. *Computers & Fluids, 109*, 155-167.

Sohankar, A, Mohagheghian, S, Dehghan, AA, & Manshadi, M Dehghan. (2015). A smoke visualization study of the flow over a square cylinder at incidence and tandem square cylinders. *Journal of Visualization, 18*(4), 687-703.

Steiner, TR, & Perry, AE. (1987). Large-scale vortex structures in turbulent wakes behind bluff bodies. Part 2. Far-wake structures. *Journal of Fluid Mechanics, 174*, 271-298.

Sumner, D. (2010). Two circular cylinders in cross-flow: a review. *Journal of Fluids and Structures, 26*(6), 849-899.

Sumner, D, Richards, MD, & Akosile, OO. (2008). Strouhal number data for two staggered circular cylinders. *Journal of Wind Engineering and Industrial Aerodynamics, 96*(6), 859-871.

Sumner, David. (2004). Closely spaced circular cylinders in cross-flow and a universal wake number. *Journal of fluids engineering, 126*(2), 245-249.

Szepessy, S, & Bearman, PW. (1992). Aspect ratio and end plate effects on vortex shedding from a circular cylinder. *Journal of Fluid Mechanics, 234*, 191-217.

Tennekes, Hendrik, & Lumley, John Leask. (1972). *A first course in turbulence*: MIT press.

Turhal, Ahmet Ömür, & Çuhadaroğlu, Burhan. (2010). The effects of surface injection through a perforated square cylinder on some aerodynamic parameters. *Experimental Thermal and Fluid Science, 34*(6), 725-735.

Tutu, Narinder K, & Chevray, Rene. (1975). Cross-wire anemometry in high intensity turbulence. *Journal of Fluid Mechanics, 71*(04), 785-800.

Wu, SJ, MIAU, Jiun-Jih, Hu, CC, & Chou, JH. (2005). On low-frequency modulations and three-dimensionality in vortex shedding behind a normal plate. *Journal of Fluid Mechanics, 526*, 117-146.

Yang, Dan, Pettersen, Bjørnar, Andersson, Helge I, & Narasimhamurthy, Vagesh D. (2012). Vortex shedding in flow past an inclined flat plate at high incidencea). *Physics of Fluids (1994-present), 24*(8), 084103.

Yunus, A Cengel, & Cimbala, John M. (2006). Fluid mechanics: fundamentals and applications. *International Edition, McGraw Hill Publication*, 185-201.

Zdravkovich, M. M. (1987). The effects of interference between circular cylinders in cross flow††An earlier version as originally presented as an invited paper,

entitled "Forces on pipe clusters", at the International Symposium on Separated Flow around Marine Structures, Norwegian Institute of Technology, Trondheim, Norway, 26-28 June 1985. *Journal of Fluids and Structures, 1*(2), 239-261. doi: 10.1016/S0889-9746(87)90355-0

Zdravkovich, MM. (1969). Smoke observations of the formation of a Karman vortex street. *Journal of Fluid Mechanics, 37*(03), 491-496.

Zdravkovich, MM. (1972). Smoke observations of wakes of tandem cylinders at low Reynolds numbers. *Aeronautical Journal, 76*, 108-114.

Zdravkovich, MM. (1977). REVIEW—Review of flow interference between two circular cylinders in various arrangements. *Journal of Fluids Engineering, 99*(4), 618-633.

Zdravkovich, MM. (1987). The effects of interference between circular cylinders in cross flow. *Journal of Fluids and Structures, 1*(2), 239-261.

Zdravkovich, MM. (1988). Review of interference-induced oscillations in flow past two parallel circular cylinders in various arrangements. *Journal of Wind Engineering and Industrial Aerodynamics, 28*(1), 183-199.

Zdravkovich, MM. (1996). Different modes of vortex shedding: an overview. *Journal of fluids and Structures, 10*(5), 427-437.

Zdravkovich, MM. (1997). Flow around Circular Cylinders; Vol. I Fundamentals. *Journal of Fluid Mechanics*, *350*(1), 377-378.

Zhang, H, & Melbourne, WH. (1992). Interference between two circular cylinders in tandem in turbulent flow. *Journal of Wind Engineering and Industrial Aerodynamics, 41*(1), 589-600.

APPENDIX

Convertor1 Program

```
c
**********************************************************************
*
c       CONVERTING ACQUIRED VELOCITY DATA TO MATLAB MATRIX
FORMAT
c
**********************************************************************
*


      parameter (ii=10240)
      dimension t1(ii),t2(ii),u(ii),v(ii),uref(ii),ufilt(ii),ur(ii)
      character ic1,ic2,ic3,ic4,ic5,ic6
      character*29 file2
      character*24 file3
      character*32 file1


      print *,' Data Amalgamation for Ensemble Phase Averaging '
      print *,' '
      print *,'       Exp No  =?'
      read *,iexp
      call number(iexp,ic5,ic6)


      print *,'       ix= ?'
      read *,ix


      print *,'  Enter first grid no   iymin ?'
      read *,iymin
      print *,'  Enter last grid no   iymax  ?'
      read *,iymax
      print *,'Enter number of ensembles ?'
      read *,iens
```

```
  call number(ix,ic1,ic2)

  print *,'Enter no of removed cycles  scycle=?'
  read *,scycle
  print *,'Enter U infinity (m/s)?'
  read *,uinf
  imax=ii-1
  print *,' '
  print *,' Number of data samples is selected as =',imax

  do ir=iymin,iens*iymax
 print *,' '
 print *,'   ir=  ',ir
 print *,' '

 call number(ir,ic3,ic4)
file1='c:\f32\ensprgs\data\e'//ic5//ic6//'x'//ic1//ic2//ic3//ic4//
+'.dat'

   file2='c:\matlab\filter\e'//ic5//ic6//'x'//ic1//ic2//ic3//ic4//
+'.flt'
  file3='c:\flowpt\data\'//ic5//ic6//'x'//ic1//ic2//'.w'//ic3//ic4
open(1,file=file1)
open(2,file=file2)
open(3,file=file3)
do i=1,imax+1
if(i.eq.1)then
read(2,*)ddelay1,ddelay2,freq
else
read(2,*)t2(i),uref(i),ufilt(i)
read(3,*)t1(i-1),u(i-1),v(i-1),ur(i-1)
```

```
  end if
  end do




  write(1,11)scycle,uinf,freq,ddelay1,ddelay2
  do i=2,imax+1
  write(1,10)t1(i-1),uref(i),ufilt(i),u(i-1),v(i-1)
  end do
  close(2)
  end do
10 format(f7.4,1x,f7.3,1x,f7.3,1x,f7.3,1x,f7.3)
11 format(f4.1,1x,f5.2,1x,f6.2,1x,f8.5,1x,f8.5)
  stop
  end


  subroutine number(input,io1,io2)
  character io1,io2

   if(input.lt.10)then
   io1=48
   io2=input+48
   else if(input.ge.10.and.input.lt.20)then
   io1=49
   io2=input+38
   else if(input.ge.20.and.input.lt.30)then
   io1=50
   io2=input+28
```

```
else if(input.ge.30.and.input.lt.40)then
io1=51
io2=input+18
 else if(input.ge.40.and.input.lt.50)then
io1=52
io2=input+8
else if(input.ge.50.and.input.lt.60)then
io1=53
io2=input-2
else if(input.ge.60.and.input.lt.70)then
io1=54
io2=input-12
 else if(input.ge.70.and.input.lt.80)then
io1=55
io2=input-22
 else if(input.ge.80.and.input.lt.90)then
io1=56
io2=input-32
else if(input.ge.90.and.input.lt.100)then
io1=57
io2=input-42
end if

return
end
```

Convertor2 Program

```
c
**********************************************************************
*
c     BLENDING FILTERED AND UNFILTERED VELOCITY DATA FOR
FURTHER                c     ANALYSIS
c
**********************************************************************
*


      parameter (ii=10240)
      dimension t1(ii),t2(ii),u(ii),v(ii),uref(ii),ufilt(ii),ur(ii)
      character ic1,ic2,ic3,ic4,ic5,ic6
      character*29 file2
      character*24 file3
      character*32 file1


      print *,' Data Amalgamation for Ensemble Phase Averaging '
      print *,' '
      print *,'      Exp No  =?'
      read *,iexp
      call number(iexp,ic5,ic6)


      print *,'      ix= ?'
      read *,ix


      print *,'  Enter first grid no   iymin ?'
      read *,iymin
      print *,'  Enter last grid no   iymax  ?'
      read *,iymax
      print *,'Enter number of ensembles ?'
      read *,iens
```

```
  call number(ix,ic1,ic2)

  print *,'Enter no of removed cycles  scycle=?'
  read *,scycle
  print *,'Enter U infinity (m/s)?'
  read *,uinf
  imax=ii-1
  print *,' '
  print *,' Number of data samples is selected as =',imax

  do ir=iymin,iens*iymax
 print *,' '
 print *,'   ir=  ',ir
 print *,' '

 call number(ir,ic3,ic4)
file1='c:\f32\ensprgs\data\e'//ic5//ic6//'x'//ic1//ic2//ic3//ic4//
+'.dat'

   file2='c:\matlab\filter\e'//ic5//ic6//'x'//ic1//ic2//ic3//ic4//
+'.flt'
  file3='c:\flowpt\data\'//ic5//ic6//'x'//ic1//ic2//'.w'//ic3//ic4
open(1,file=file1)
open(2,file=file2)
open(3,file=file3)
do i=1,imax+1
if(i.eq.1)then
read(2,*)ddelay1,ddelay2,freq
else
read(2,*)t2(i),uref(i),ufilt(i)
read(3,*)t1(i-1),u(i-1),v(i-1),ur(i-1)
```

```
  end if
  end do




  write(1,11)scycle,uinf,freq,ddelay1,ddelay2
  do i=2,imax+1
  write(1,10)t1(i-1),uref(i),ufilt(i),u(i-1),v(i-1)
  end do
  close(2)
  end do
10 format(f7.4,1x,f7.3,1x,f7.3,1x,f7.3,1x,f7.3)
11 format(f4.1,1x,f5.2,1x,f6.2,1x,f8.5,1x,f8.5)
  stop
  end


  subroutine number(input,io1,io2)
  character io1,io2

   if(input.lt.10)then
   io1=48
   io2=input+48
   else if(input.ge.10.and.input.lt.20)then
   io1=49
   io2=input+38
   else if(input.ge.20.and.input.lt.30)then
   io1=50
   io2=input+28
```

```
else if(input.ge.30.and.input.lt.40)then
io1=51
io2=input+18
 else if(input.ge.40.and.input.lt.50)then
io1=52
io2=input+8
else if(input.ge.50.and.input.lt.60)then
io1=53
io2=input-2
else if(input.ge.60.and.input.lt.70)then
io1=54
io2=input-12
 else if(input.ge.70.and.input.lt.80)then
io1=55
io2=input-22
 else if(input.ge.80.and.input.lt.90)then
io1=56
io2=input-32
else if(input.ge.90.and.input.lt.100)then
io1=57
io2=input-42
end if

return
end
```

Ensemble Program

```
c
**********************************************************************
*
c       CALCULATION OF ENSEMBLE-PHASE AVERAGED STATISTICAL
PROPERTIES
c                              AND DERIVATIVE OF STRESSES
c
**********************************************************************
*


      character ic1,ic2,ic3,ic4,ic5,ic6
      character*30 file4,file6
      character*31 file2,file3,file5,file7
      character*32 file1
      character*25 file8,file9
      parameter (ii=10239,jj=1000,nr=99,nn=61,kk=18,ll=10)
      dimension uph(kk,nr,nn),vph(kk,nr,nn),uphav(kk,nr,nn),t(ii),
     +  cohstr(kk,nr,nn),vphav(kk,nr,nn),ucoh(kk,nr,nn),vcoh(kk,nr,nn),
     +  udas(kk,nr,nn),vdas(kk,nr,nn),udassq(kk,nr,nn),vdassq(kk,nr,nn),
     +  stress(kk,nr,nn),sumudas(kk,nr,nn),sumvdas(kk,nr,nn),ufilt(ii),
     +  sumusq(kk,nr,nn),sumvsq(kk,nr,nn),sumstres(kk,nr,nn),u(ii),
     +  avudas(kk,nr,nn),avvdas(kk,nr,nn),avusq(kk,nr,nn),per(jj),
     +  avvsq(kk,nr,nn),avstress(kk,nr,nn),sumuph(kk,nr,nn),uref(ii),
     +  sumvph(kk,nr,nn),tref(jj),tfilt(jj),delay(jj),avucoh(kk,nr),
     +  avvcoh(kk,nr),avsqu(kk,nr),avsqv(kk,nr),avcostrs(kk,nr),v(ii),
     +  udasav(kk,nr),vdasav(kk,nr),avusqr(kk,nr),avvsqr(kk,nr),
     +  avstres(kk,nr),uuphav(kk,nr,nn),vvphav(kk,nr,nn),vort(kk,nr,ll),
     +  avuphav(kk,nr),avvphav(kk,nr),uav(kk,nr),vav(kk,nr)


      print *,' '
      print *,'     CALCULATION OF COHERENT and INCOHERENT
PROPERTIES'
```

```
print *,' '
print *,'       Exp No  =?'
read *,iexp
call number(iexp,ic5,ic6)
print *,'  Enter number of ensembles ?'
read *,iens

print *,'  Enter first grid no for analysis    iymin= ? '
read *,iymin
print *,'  Enter last grid no  for analysis    iymax= ?'
read *,iymax
print *,'  Enter first grid no for analysis    ixmin= ?'
read *,ixmin
print *,'  Enter last grid no for analysis     ixmax= ?'
read *,ixmax
print *,' '
print *,'  DOMAIN maximum y-grid iymaxx ?'
read *,iymaxx
print *,'  DOMAIN maximum x-grid ixmaxx ?'
read *,ixmaxx
print *,' '
print *,'Enter starting X/d for the domain xstart (e.g 4.0 )'
read *,xstart
print *,' '
xlength=160
ylength=137.2
dwidth=25.
print *,'Domain is',xlength,' X ',ylength,'Y '
print *,' '
print *,' '
print *,' '
```

```
if(iens.eq.1)then
irstrt=iymin*iens
else
irstrt=(iymin*iens)-(iens-1)
end if
dx=xlength/((ixmaxx-1)*1000)
dy=ylength/((iymaxx-1)*1000)

do ix=ixmin,ixmax
inftot=0
uinftot=0.
 do ir=irstrt,iens*iymax
sumudas(ix,ir,1)=0.
sumvdas(ix,ir,1)=0.
sumusq(ix,ir,1)=0.
sumvsq(ix,ir,1)=0.
sumstres(ix,ir,1)=0.
ucohtot=0.
vcohtot=0.
totusq=0.
totvsq=0.
totcostr=0.
suphav=0.
svphav=0.
udastot=0.
vdastot=0.
usqrtot=0.
vsqrtot=0.
stresstot=0.
sumref=0.
```

```
      sumfilt=0.
      sumdelay=0.
      n=0.
      ut=0.
      vt=0.
      jcount=0
      call number(ix,ic1,ic2)
      call number(ir,ic3,ic4)
     file1='c:\f32\ensprgs\data\e'//ic5//ic6//'x'//ic1//ic2//ic3//ic4/
    +/'.dat'
     open(1,file=file1)
     read(1,*) scycle,uinf,freq,ddelay1,ddelay2


      halfper=0.5/freq
      uinftot=uinftot+uinf
      inftot=inftot+1
        do i=1,ii
        read(1,*)t(i),uref(i),ufilt(i),u(i),v(i)
        u(i)=u(i)/uinf
        v(i)=v(i)/uinf

c
**********************************************************************
**
c       start averaging after (scycle=2-5) cycles
c
**********************************************************************
**


         if(t(i).gt.(scycle*2*halfper))then
```

```
        sumref=uref(i)+sumref
        sumfilt=ufilt(i)+sumfilt
        n=n+1
        if(n.eq.1)istart0=i
        end if
        end do
      avuref=sumref/(ii-istart0)
      avufilt=sumfilt/(ii-istart0)
        do i=1,ii
        uref(i)=uref(i)-avuref
        ufilt(i)=ufilt(i)-avufilt
        end do

c
*************************************************************************
*
c      Determination of phase delay
c
*************************************************************************
*

      n1=1
        do i=istart0,ii-1
        if(uref(i).lt.0.and.uref(i+1).gt.0.or.
     +   uref(i).gt.0.and.uref(i+1).lt.0)then
        tref(n1)=((uref(i)*(t(i)-t(i+1)))/(uref(i+1)-uref(i)))+t(i)
        n1max=n1
        n1=n1+1
        end if
        end do

      n2=1
```

```
      do i=istart0,ii-1
      if(ufilt(i).lt.0.and.ufilt(i+1).gt.0.or.
     +  ufilt(i).gt.0.and.ufilt(i+1).lt.0)then
      tfilt(n2)=((ufilt(i)*(t(i)-t(i+1)))/(ufilt(i+1)-ufilt(i)))+
     +  t(i)
      if(n2.le.2.and.ufilt(i).lt.0.and.ufilt(i+1).gt.0.)then
      if(n2.eq.1)jcount=1
      if(n2.eq.2)jcount=2
      istart=i
      end if
      n2max=n2
      n2=n2+1
      iend=i+1
      end if
      end do

     n=1
      do n1=2,n1max
       do n2=2,n2max
       dif1=abs(((tfilt(n2)-tref(n1))-ddelay2)/ddelay2)
       dif2=abs(((tfilt(n2)-tfilt(n2-1))/halfper)-1)
       dif3=abs(((tref(n1)-tref(n1-1))/halfper)-1)
       if(dif2.lt.0.25.and.dif3.lt.0.25.and.dif1.lt.0.25)then
       delay(n)=tfilt(n2)-tref(n1)
c        if(delay(n).gt.0.)then
       sumdelay=sumdelay+delay(n)
       n=n+1
c        end if
       end if
       end do
      end do
```

```
      if(n.gt.1)then
      avdelay2=sumdelay/(n-1)
      else
      avdelay2=ddelay2
      end if
      if(n.eq.1)then
      print *,'*WARNING*(phase delay loop never used)'
      print *,'CHECK INPUT DELAY OR DATA'
      end if
      if(n.gt.1.and.n.lt.30)then
      print *,' '
      print *,'WARNING* phase delay loop was used only',n,' times '
      end if



c
**********************************************************************
*
c     Determination of periods
c
**********************************************************************
*


      if(jcount.eq.1)then
      if(mod(n2max,2).gt.0)then
      ncycle=(n2max-1)/2
      else
      ncycle=(n2max-2)/2
      end if
      end if
      if(jcount.eq.2)then
      if(mod(n2max,2).gt.0)then
```

```
  ncycle=((n2max-1)/2)-1
  else
  ncycle=(n2max/2)-1
  end if
  end if
  do j=1,ncycle
  if(jcount.eq.1)then
    per(j)=tfilt(2*j+1)-tfilt(2*j-1)
  else if(jcount.eq.2)then
     if(j.eq.1)then
     per(1)=tfilt(4)-tfilt(2)
     else
     per(j)=tfilt(2*j+2)-tfilt(2*j)
     end if
   else
   print *,'jcount ne 1 or 2 '
   end if
  end do

  icount=icount+1
  if(iens.eq.1)iy=ir
  if(iens.gt.1.and.icount.le.iens)then
  iy=(ir+(iens-1))/iens
  end if
  if(icount.eq.iens)icount=0
 print *,' '
 print *,'       ix          iy          ir          n      avd
+elay2          ncycle '
 print *,ix,iy,ir,n,avdelay2,ncycle
```

```
c
**********************************************************************
*
c       Calculation of u average and v average
c
**********************************************************************
*



c     temporarily set ddelay1=0.0002
        do i=1,ii
        ddelay1=0.
        t(i)=t(i)+ddelay1+avdelay2
        end do
        do i=istart,iend
        ut=ut+u(i)
        vt=vt+v(i)
        end do
       uav(ix,ir)=ut/(iend-istart)
       vav(ix,ir)=vt/(iend-istart)


c
**********************************************************************
*
c       Phase averaging and coherent properties at selected phase points
c
**********************************************************************
*


       itmax=61
        do it=1,itmax
        uphh=0.
        vphh=0.
```

```
ncount=0
 do j=1,ncycle
 if(jcount.eq.1)then
 time=(((it-1)*1.)/(itmax-1))*per(j)+tfilt((2*j)-1)
 else
 time=(((it-1)*1.)/(itmax-1))*per(j)+tfilt(2*j)
 end if

  do i=istart-10,iend
  if(t(i).lt.time.and.t(i+1).gt.time)then
  ncount=ncount+1
  uph(ix,ir,it)=(u(i)+u(i+1))/2
  vph(ix,ir,it)=(v(i)+v(i+1))/2
  sumuph(ix,ir,it)=uph(ix,ir,it)+uphh
  sumvph(ix,ir,it)=vph(ix,ir,it)+vphh
  uphh=sumuph(ix,ir,it)
  vphh=sumvph(ix,ir,it)
  end if
  end do
 end do
 uphav(ix,ir,it)=sumuph(ix,ir,it)/ncount
 vphav(ix,ir,it)=sumvph(ix,ir,it)/ncount
 ucoh(ix,ir,it)=uphav(ix,ir,it)-uav(ix,ir)
 vcoh(ix,ir,it)=vphav(ix,ir,it)-vav(ix,ir)
 uuphav(ix,ir,it)=uinf*uphav(ix,ir,it)
 vvphav(ix,ir,it)=uinf*vphav(ix,ir,it)
 cohstr(ix,ir,it)=ucoh(ix,ir,it)*vcoh(ix,ir,it)
 ucohtot=ucoh(ix,ir,it)+ucohtot
 vcohtot=vcoh(ix,ir,it)+vcohtot
 totusq=ucoh(ix,ir,it)**2+totusq
 totvsq=vcoh(ix,ir,it)**2+totvsq
```

```
          totcostr=cohstr(ix,ir,it)+totcostr
          suphav=uphav(ix,ir,it)+suphav
          svphav=vphav(ix,ir,it)+svphav
         end do

c
*************************************************************************
*
c       Averaged coherent properties
c
*************************************************************************
*
        avuphav(ix,ir)=suphav/itmax
        avvphav(ix,ir)=svphav/itmax
        avucoh(ix,ir)=ucohtot/itmax
        avvcoh(ix,ir)=vcohtot/itmax
        avsqu(ix,ir)=totusq/itmax
        avsqv(ix,ir)=totvsq/itmax
        avcostrs(ix,ir)=totcostr/itmax

c
*************************************************************************
*
c       Incoherent statistical properties
c
*************************************************************************
*

         do it=1,itmax
         ncount=0
          do j=1,ncycle
          if(jcount.eq.1)then
          time=(((it-1)*1.)/(itmax-1))*per(j)+tfilt((2*j)-1)
```

```
          else
          time=(((it-1)*1.)/(itmax-1))*per(j)+tfilt(2*j)
          end if
           do i=istart-10,iend
           if(t(i).lt.time.and.t(i+1).gt.time)then
           ncount=ncount+1
           udas(ix,ir,it)=(u(i)+u(i+1))/2-uphav(ix,ir,it)
           vdas(ix,ir,it)=(v(i)+v(i+1))/2-vphav(ix,ir,it)
           udassq(ix,ir,it)=udas(ix,ir,it)**2
           vdassq(ix,ir,it)=vdas(ix,ir,it)**2
           stress(ix,ir,it)=udas(ix,ir,it)*vdas(ix,ir,it)
           end if
           end do
          sumudas(ix,ir,it)=sumudas(ix,ir,it)+udas(ix,ir,it)
          sumvdas(ix,ir,it)=sumvdas(ix,ir,it)+vdas(ix,ir,it)
          sumusq(ix,ir,it)=sumusq(ix,ir,it)+udassq(ix,ir,it)
          sumvsq(ix,ir,it)=sumvsq(ix,ir,it)+vdassq(ix,ir,it)
          sumstres(ix,ir,it)=sumstres(ix,ir,it)+stress(ix,ir,it)
          end do

c
**********************************************************************
c       average over total periods
c
**********************************************************************

         avudas(ix,ir,it)=sumudas(ix,ir,it)/ncount
         avvdas(ix,ir,it)=sumvdas(ix,ir,it)/ncount
         avusq(ix,ir,it)=sumusq(ix,ir,it)/ncount
         avvsq(ix,ir,it)=sumvsq(ix,ir,it)/ncount
         avstress(ix,ir,it)=sumstres(ix,ir,it)/ncount
```

```
        end do


c
**********************************************************************
c       average over one cycle
c
**********************************************************************

        do it=1,itmax
        udastot=avudas(ix,ir,it)+udastot
        vdastot=avvdas(ix,ir,it)+vdastot
        usqrtot=avusq(ix,ir,it)+usqrtot
        vsqrtot=avvsq(ix,ir,it)+vsqrtot
        stresstot=avstress(ix,ir,it)+stresstot
        end do
        udasav(ix,ir)=udastot/itmax
        vdasav(ix,ir)=vdastot/itmax
        avusqr(ix,ir)=usqrtot/itmax
        avvsqr(ix,ir)=vsqrtot/itmax
        avstres(ix,ir)=stresstot/itmax
        end do
        close(1)
       uinfav=uinftot/inftot
       print *,'uinfav=',uinfav
       end do


c
**********************************************************************
****
c      Ensemble Averaging
```

```
c
**********************************************************************
****


      do ix=ixmin,ixmax
      do iy=iymin,iymax
      if(iens.eq.1)then
      irstrt=iy*iens
      else
      irstrt=(iy*iens)-(iens-1)
      end if

      do it=1,itmax

      s1=0.
      s2=0.
      s3=0.
      s4=0.
      s5=0.
      s6=0.
      s7=0.
      s8=0.
      s9=0.
      s10=0.
      s11=0.
      s12=0.
      s13=0.
      s14=0.
      s15=0.
      s16=0.
```

```
s17=0.


 do ir=irstrt,iy*iens

 uphav(ix,iy,it)=uphav(ix,ir,it)/iens+s1
 s1=uphav(ix,iy,it)
 vphav(ix,iy,it)=vphav(ix,ir,it)/iens+s2
 s2=vphav(ix,iy,it)
 ucoh(ix,iy,it)=ucoh(ix,ir,it)/iens+s3
 s3=ucoh(ix,iy,it)
 vcoh(ix,iy,it)=vcoh(ix,ir,it)/iens+s4
 s4=vcoh(ix,iy,it)
 uuphav(ix,iy,it)=uuphav(ix,ir,it)/iens+s5
 s5=uuphav(ix,iy,it)
 vvphav(ix,iy,it)=vvphav(ix,ir,it)/iens+s6
 s6=vvphav(ix,iy,it)
 cohstr(ix,iy,it)=cohstr(ix,ir,it)/iens+s7
 s7=cohstr(ix,iy,it)
 udas(ix,iy,it)=udas(ix,ir,it)/iens+s8
 s8=udas(ix,iy,it)
 vdas(ix,iy,it)=vdas(ix,ir,it)/iens+s9
 s9=vdas(ix,iy,it)
 udassq(ix,iy,it)=udassq(ix,ir,it)/iens+s10
 s10=udassq(ix,iy,it)
 vdassq(ix,iy,it)=vdassq(ix,ir,it)/iens+s11
 s11=vdassq(ix,iy,it)
 stress(ix,iy,it)=stress(ix,ir,it)/iens+s12
 s12=stress(ix,iy,it)
 avudas(ix,iy,it)=avudas(ix,ir,it)/iens+s13
 s13=avudas(ix,iy,it)
```

```
  avvdas(ix,iy,it)=avvdas(ix,ir,it)/iens+s14
  s14=avvdas(ix,iy,it)
  avusq(ix,iy,it)=avusq(ix,ir,it)/iens+s15
  s15=avusq(ix,iy,it)
  avvsq(ix,iy,it)=avvsq(ix,ir,it)/iens+s16
  s16=avvsq(ix,iy,it)
  avstress(ix,iy,it)=avstress(ix,ir,it)/iens+s17
  s17=avstress(ix,iy,it)

  end do
end do
end do
end do


  do ix=ixmin,ixmax
  do iy=iymin,iymax

if(iens.eq.1)then
irstrt=iy*iens
else
irstrt=(iy*iens)-(iens-1)
end if

s18=0.
s19=0.
s20=0.
s21=0.
s22=0.
s23=0.
s24=0.
```

```
s25=0.
s26=0.
s27=0.
s28=0.
s29=0.
s30=0.
s31=0.
 do ir=irstrt,iy*iens

 avuphav(ix,iy)=avuphav(ix,ir)/iens+s18
 s18=avuphav(ix,iy)
 avvphav(ix,iy)=avvphav(ix,ir)/iens+s19
 s19=avvphav(ix,iy)
 avucoh(ix,iy)=avucoh(ix,ir)/iens+s20
 s20=avucoh(ix,iy)
 avvcoh(ix,iy)=avvcoh(ix,ir)/iens+s21
 s21=avvcoh(ix,iy)
 avsqu(ix,iy)=avsqu(ix,ir)/iens+s22
 s22=avsqu(ix,iy)
 avsqv(ix,iy)=avsqv(ix,ir)/iens+s23
 s23=avsqv(ix,iy)
 avcostrs(ix,iy)=avcostrs(ix,ir)/iens+s24
 s24=avcostrs(ix,iy)
 udasav(ix,iy)=udasav(ix,ir)/iens+s25
 s25=udasav(ix,iy)
 vdasav(ix,iy)=vdasav(ix,ir)/iens+s26
 s26=vdasav(ix,iy)
 avusqr(ix,iy)=avusqr(ix,ir)/iens+s27
 s27=avusqr(ix,iy)
 avvsqr(ix,iy)=avvsqr(ix,ir)/iens+s28
 s28=avvsqr(ix,iy)
```

```
          avstres(ix,iy)=avstres(ix,ir)/iens+s29
          s29=avstres(ix,iy)
          uav(ix,iy)=uav(ix,ir)/iens+s30
          s30=uav(ix,iy)
          vav(ix,iy)=vav(ix,ir)/iens+s31
          s31=vav(ix,iy)

c    print *,iy,ir,avstres(ix,ir),avsqu(ix,ir),avsqv(ix,ir),
c     +      avusqr(ix,ir)
          end do
          end do
          end do



c
**********************************************************************
c       Results
c
**********************************************************************


         do ix=ixmin,ixmax
         call number(ix,ic1,ic2)



        file2='c:\paper2\ensdata\cod'//ic5//ic6//'x'//ic1//ic2//'.dat'
        file3='c:\paper2\ensdata\avd'//ic5//ic6//'x'//ic1//ic2//'.dat'
        file4='c:\paper2\ensdata\3dd'//ic5//ic6//'x'//ic1//ic2//'.dat'
        file5='c:\paper2\ensdata\vec'//ic5//ic6//'x'//ic1//ic2//'.dat'
        file6='c:\paper2\ensdata\ave'//ic5//ic6//'x'//ic1//ic2//'.dat'
        file7='c:\paper2\ensdata\vor'//ic5//ic6//'x'//ic1//ic2//'.dat'
        file8='c:\gle\ensdata\'//ic5//ic6//'x'//ic1//ic2//'ad.dat'
```

```
      file9='c:\gle\ensdata\'//ic5//ic6//'x'//ic1//ic2//'bd.dat'
      open(2,file=file2)
      open(3,file=file3)
      open(4,file=file4)
      open(5,file=file5)
      open(6,file=file6)
      open(7,file=file7)
      open(8,file=file8)
      open(9,file=file9)
      write(2,20)ix
      write(2,21)
      write(2,22)ix,iymax,itmax
       do it=1,itmax
c       phase=(it*1./(itmax-1))-(0.5+(1./(itmax-1)))
       dd=0.005
       phase=(it-1)*1./(itmax-1)
       do iy=iymin,iymax
       y=(iy-((iymaxx+1)/2))*dy*1000./dwidth
       e1=avusq(ix,iy,it)+avvsq(ix,iy,it)
       e2=(ucoh(ix,iy,it)**2)+(vcoh(ix,iy,it)**2)
       e3=(ucoh(ix,iy,it)**2)
       e4=(vcoh(ix,iy,it)**2)
       e5=(cohstr(ix,iy+1,it)-cohstr(ix,iy,it))/dd
       e6=(avstress(ix,iy+1,it)-avstress(ix,iy,it))/dd
      write(2,*)phase,y,it,iy,uphav(ix,iy,it),vphav(ix,iy,it),
     +   ucoh(ix,iy,it),vcoh(ix,iy,it),cohstr(ix,iy,it),
     +   avusq(ix,iy,it),avvsq(ix,iy,it),avstress(ix,iy,it),
     +   e1,e2,e3,e4,e5,e6

      end do
      end do
```

```
      close(2)

      write(3,30)ix
      write(3,31)
      write(3,32)ix,iymax
      do iy=iymin,iymax
       y=(iy-((iymaxx+1)/2))*dy*1000./dwidth
       write(3,*)y,iy,avuphav(ix,iy),avvphav(ix,iy),avucoh(ix,iy),
     +  avvcoh(ix,iy),avsqu(ix,iy),avsqv(ix,iy),avcostrs(ix,iy),
     +  avusqr(ix,iy),avvsqr(ix,iy),avstres(ix,iy)

       write(8,80)y,avuphav(ix,iy),avvphav(ix,iy),avsqu(ix,iy),
     +   avsqv(ix,iy),uav(ix,iy)
       write(9,90)y,avcostrs(ix,iy),avusqr(ix,iy),avvsqr(ix,iy),
     +   avstres(ix,iy),vav(ix,iy)
      end do
      close(3)
      close(8)
      close(9)
      write(4,40)ix
      write(4,41)
      do it=1,itmax,2
c      phase=(it*1./(itmax-1))-(0.5+(1./(itmax-1)))
       phase=(it-1)*1./(itmax-1)
      write(4,42)ix,it,iymax
      do iy=iymin,iymax
       y=(iy-((iymaxx+1)/2))*dy*1000./dwidth
       e1=avusq(ix,iy,it)+avvsq(ix,iy,it)
       e2=(ucoh(ix,iy,it)**2)+(vcoh(ix,iy,it)**2)
       e3=(ucoh(ix,iy,it)**2)
       e4=(vcoh(ix,iy,it)**2)
```

```
      e5=(cohstr(ix,iy+1,it)-cohstr(ix,iy,it))/dd
      e6=(avstress(ix,iy+1,it)-avstress(ix,iy,it))/dd
     write(4,*)phase,y,it,iy,uphav(ix,iy,it),vphav(ix,iy,it),
    +   ucoh(ix,iy,it),
    +  vcoh(ix,iy,it),cohstr(ix,iy,it),avusq(ix,iy,it),
    +  avvsq(ix,iy,it),avstress(ix,iy,it),e1,e2,udas(ix,iy,it),
    +  vdas(ix,iy,it),e3,e4,e5,e6
     end do
     end do
     close(4)

     end do

     write(5,50)
     write(5,51)
     write(7,70)
     write(7,71)
     itt=0
     ncount=0
100   ncount=ncount+1
     if(ncount.eq.1)then
     itt=1
     else if(ncount.eq.2)then
     itt=((itmax-1)/4)+1
     else if(ncount.eq.3)then
     itt=((itmax-1)/2)+1
     else if(ncount.eq.4)then
     itt=((itmax-1)*3/4)+1
     else
     itt=itmax
     end if
```

```
      if(ncount.gt.5)go to 101
      write(5,52)itt,iymax
      do ix=ixmin,ixmax
      do iy=iymin,iymax
       y=(iy-((iymaxx+1)/2))*dy*1000./dwidth
       x=(ix*dx*1000./dwidth)+xstart
       e1=avusq(ix,iy,itt)+avvsq(ix,iy,itt)
       e2=(ucoh(ix,iy,itt)**2)+(vcoh(ix,iy,itt)**2)
      write(5,*)x,y,ix,iy,uphav(ix,iy,itt),vphav(ix,iy,itt),
     +  ucoh(ix,iy,itt),vcoh(ix,iy,itt),cohstr(ix,iy,itt),
     +  avusq(ix,iy,itt),avvsq(ix,iy,itt),avstress(ix,iy,itt),e1,e2
      end do
      end do
      if(ixmax.lt.2.or.iymax.lt.2.or.ixmin.eq.ixmax.
     +  or.iymin.eq.iymax)go to 100

      write(7,72)itt,iymax-1,ixmax-1
      do i=ixmin,ixmax-1
      do j=iymin,iymax-1
       yy=((iy+0.5)-((iymaxx+1)/2))*dy*1000./dwidth
       xx=((ix+0.5)*dx*1000./dwidth)+xstart
      vort(i,j,itt)=((((((uuphav(i+1,j,itt)-uuphav(i,j,itt))/2)+
     +  uuphav(i,j,itt))-(((uuphav(i+1,j+1,itt)-uuphav(i,j+1,itt))/2)+
     +  uuphav(i,j+1,itt)))*dx)-(((((vvphav(i,j+1,itt)-vvphav(i,j,itt))
     +  /2)+vvphav(i,j,itt))+(((vvphav(i+1,j+1,itt)-vvphav(i+1,j,itt))/
     +  2)+vvphav(i+1,j,itt)))*dy))*(1./(2*dx*dy))*
     +  ((dwidth/1000)/uinfav)
      write(7,*)xx,yy,i,j,vort(i,j,itt)
      end do
      end do
```

```
101    close(5)
       close(7)

       write(6,60)
       write(6,61)
       do ix=ixmin,ixmax
       write(6,62)ix,iymax
       do iy=iymin,iymax
        y=(iy-((iymaxx+1)/2))*dy*1000./dwidth
       write(6,*)y,iy,avucoh(ix,iy),avvcoh(ix,iy),avsqu(ix,iy),
     +   avsqv(ix,iy),avcostrs(ix,iy),avusqr(ix,iy),
     +   avvsqr(ix,iy),avstres(ix,iy)
       end do
       end do
       close(6)



 20    format('TITLE = "Contour properties at X=',i2,' "')
 21    format('VARIABLES = "P", "Y" , "IT" , "IY" , "V1", "V2", "V3",
     +"V4", "V5", "V6", "V7", "V8" , "V20" , "V21" , "V22" , "V23" , "
     +V24" , "V25"')
 22    format('ZONE T="x(',i2,')',"',',1x,'I=',i2,', J=',i2,', F=POINT
     +')
 30    format('TITLE = "Averaged properties at X=',i2,' "')
 31    format('VARIABLES = "Y", "IY" , "V18", "V19", "V9", "V10", "V11
     +", "V12", "V13", "V14", "V15", "V16"')
 32    format('ZONE T="x(',i2,')',"',',1x,'I=',i2,', F=POINT')
 40    format('TITLE = "3-D properties at X=',i2,' "')
 41    format('VARIABLES = "P", "Y" , "IT" , "IY" , "V1", "V2", "V3",
     +"V4", "V5", "V6", "V7", "V8" , "V20" , "V21" ,"V22" , "V23" , "V24
```

```
 +" , "V25" , "V26"')
42    format('ZONE T="x(',i2,'),t(',i2,')",',1x,'I=',i2,', F=POINT')
50    format('TITLE = "Coherent & Incoherent Data in X-Y Domain"')
51    format('VARIABLES = "X", "Y", "IX" , "IY" , "V1", "V2", "V3", "
 +V4", "V5", "V6", "V7", "V8" , "V20", "V21"')
52    format('ZONE T="t(',i2,')","',',1x,'I=',i2,', F=POINT')
60    format('TITLE = "Averaged properties in X-Y Domain"')
61    format('VARIABLES = "Y", "IY" , "V9", "V10", "V11", "V12", "V13
 +", "V14", "V15", "V16"')
62    format('ZONE T="x(',i2,')","',',1x,'I=',i2,', F=POINT')
70    format('TITLE = "Vorticity Data in X-Y Domain"')
71    format('VARIABLES = "xx" , "yy" , "i", "j", "V17"')
72    format('ZONE T="t(',i2,')","',',1x,'I=',i2,', J=',i2,', F=POINT
 +')
80    format(f5.2,1x,f9.6,1x,f9.6,1x,f9.6,1x,f9.6,1x,f7.4)
90    format(f5.2,1x,f9.6,1x,f9.6,1x,f9.6,1x,f9.6,1x,f9.6,1x,f7.4)
      if(iymin.ne.ixmin.or.iymax.ne.ixmax)then
      print *,' '
      print *,' '
      print *,'WARNING;Data for x-y plotting is not of same dimension
 +s'
     end if
     stop
     end


  subroutine number(input,io1,io2)
  character io1,io2

     if(input.lt.10)then
     io1=48
```

```
io2=input+48
else if(input.ge.10.and.input.lt.20)then
io1=49
io2=input+38
else if(input.ge.20.and.input.lt.30)then
io1=50
io2=input+28
else if(input.ge.30.and.input.lt.40)then
io1=51
io2=input+18
 else if(input.ge.40.and.input.lt.50)then
io1=52
io2=input+8
else if(input.ge.50.and.input.lt.60)then
io1=53
io2=input-2
else if(input.ge.60.and.input.lt.70)then
io1=54
io2=input-12
 else if(input.ge.70.and.input.lt.80)then
io1=55
io2=input-22
 else if(input.ge.80.and.input.lt.90)then
io1=56
io2=input-32
else if(input.ge.90.and.input.lt.100)then
io1=57
io2=input-42
end if
     return
end
```